2012

Study on permanent magnet transverse flux machine

Oleksandr Dobzhanskyi
Louisiana State University and Agricultural and Mechanical College

STUDY ON PERMANENT MAGNET TRANSVERSE FLUX MACHINE

A Dissertation
Submitted to the Graduate Faculty of the
Louisiana State University and
Agricultural and Mechanical College
in partial fulfillment of the
requirements for the degree of
Doctor of Philosophy
in
The Department of Electrical & Computer Engineering

by
Dobzhanskyi Oleksandr
Master of Electrical Engineering, Louisiana State University, 2010; Master of Industrial Engineering, Kiev National University of Construction and Architecture, 2007; Bachelor in Industrial Engineering, Kiev National University of Construction and Architecture, 2006
May 2012

ACNOWLEGEMENTS

I would like to thank my advisor prof. E. Mendrela for guiding me through my work so that my dissertation would be a contribution to Electrical Engineering as a science. His encouragement and ability to motivate inspired me for becoming a professional in Power area.

I am thankful to profs. S. Mehraeen, R. Vaidyanathan and L. Czarnecki for their corrections and suggestions.

TABLE OF CONTENTS

LIST OF TABLES

LIST OF FIGURES

ABSTRACT

As known, permanent magnet (PM) machines exhibit higher efficiency, higher reliability and higher energy than electrically excited machines. Among PM machines transverse flux (PMTF) machines offer higher power to volume ratio than other types of PM machines. That is why there is a great interest of researches towards PMTF machines. For the last 50 years more than a hundred different topologies have been introduced in this class of electric machines.

This dissertation is concentrated mainly on the newest PMTF machine topology proposed and patented by Jacek F. Gieras in March 4, 2010. Such a topology (topology of 2010) is an object of this dissertation. A prototype that was built with 3D Finite Element Method (FEM) modeling of PMTF generator proves that the generator that was built on the basis of topology of 2010 has several significant disadvantages among which the greatest impact have high leakage flux losses.

Applying FEM modeling, various steps to improve machine performance have been undertaken. Results obtained from modeling show, that keeping the same diameter and lengths of the machine as well as number of turns of the winding, output power of the machine can be two times higher and the negative flux linkage that is established by "inactive" PMs significantly reduced. This was achieved by introducing magnetic shunts to the stator structure. These shunts also reduce cogging torque.

Modifications include changing machine stator structure, slot shape, and implementation of magnetic shunts which play a vital role in preventing flux leakage losses and reducing cogging torque. During modifications a big attention was paid to simplifying a manufacturing process. Modifications do not complicate machine design and count all aspects which may arise when manufacturing.

Modified version of the PMTF machine was built by Polish manufacturer "Komel" for University of Nevada-Reno. This project was supported by National Science Foundation. The prototype results prove that the magnetic shunts block almost 70% of negative magnetic flux coming from inactive magnets. The induced voltage of the machine calculated using 3D FEM model is the same what was obtained during prototype laboratory test. However, the laboratory test also shows that if magnetic shunts are made of pure iron, generator has significant power losses. These power losses are caused by eddy currents induced on the magnetic shunts. To prevent eddy currents flowing on the magnetic shunts' surface, instead of pure iron, laminated steel or magnetic powder has to be selected as a material for shunts.

Combining the ideas of topologies [1-3] a new version of PMTF machine is introduced in this dissertation. Its electromechanical parameters are calculated. Three different designs of PMTF generator are compared in terms of output power to volume ratio.

CHAPTER 1: INTRODUCTION

1.1 Overview of the Dissertation

Highly efficient Permanent Magnet Transverse Flux (PMTF) machines have been under careful attention of researches. In the past years there are many papers written on these machines [6-22]. Most of them intended to improve their construction in order to get better performance when they operate as wind generators. This dissertation focuses on a PMTF machine as a generator also.

The various PMTF constructions of PMTF machines are proposed not only to improve the machine performance but also to make a manufacturing process easier. In some papers [15] authors discus various shapes of magnetic poles, such as: C-core, E-core and claw pole. Another paper [16] introduces a ring-shape PMTF machine which does not use a shaft to transfer the torque and to support both the rotor and the stator. It is achieved by applying a direct drive turbine to the stator. Many authors in their papers [20] discuss different types of the machine are studied: machine with surface mounted magnets which are described in [21] and others with flux-concentration described in [22]. The aim of this study is to find out which group of PMTF machines gives better performance and lower cost.

Research towards improvement of PMTF machine performance led to new PMTF machine patents. Taking into account all disadvantages of PMTF machines patented in the past new efficient and simpler in structure machines appear from year to year. For example, a construction patented in 1997 [2] looks more complex from the manufacturing point of view, where the rotor requires to be set up not only with the core and PMs but also with elements which hold the magnets. A year later another topology [3] which makes the reference to the topology of 1997, is introduced where there is no problem with magnet attachments, but some complexity in combining outer and inner stator in one machine.

The diagram representing all patented PMTF machine topologies in the USA after 1965 is shown in Fig. 1.1.

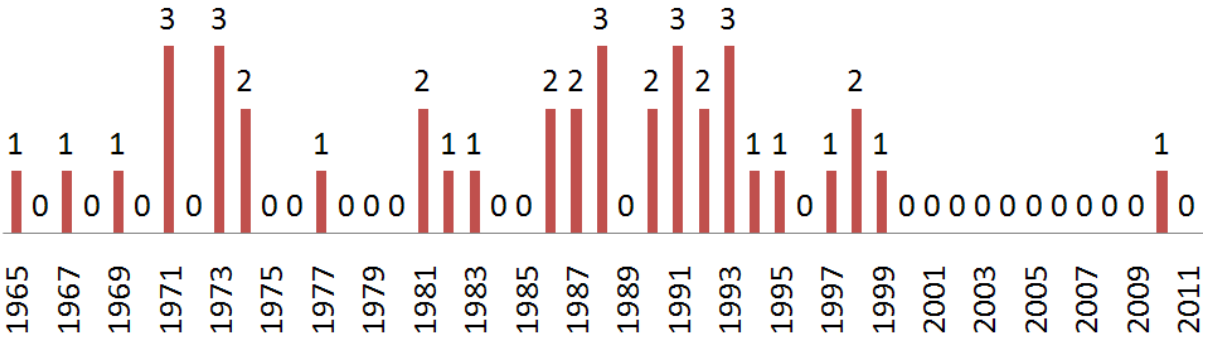

Fig. 1.1 USA Patents on Transverse Flux Machines

The digit on each chart corresponds to a number of patents introduced at the particular year. It can be concluded from the diagram that the peak of researchers' attention to PMTF machines is within 1986 to 1999 years. After 1999 prior to 2010 no new topologies were introduced in the literature. Topology that appears in 2010 (topology of 2010) proves, that the interest of researches to PMTF machines still exists and there is still a space for new ideas.

This dissertation is directed on the study and improvement of the newest patented version of PMTF machine (topology of 2010). This work makes the reference to a PMTF machine prototype which was built according to the topology of 2010. A thorough analysis of the electromechanical parameters of the machine was carried out and the results were compared with ones obtained from the measurements carried out on the physical model. This comparison allowed detecting the disadvantages of the topology of 2010. Based on these observations some modifications were done towards improving machine performance. After description of the machine design and its principle of operation, the main objectives for this dissertation are listed.

PMTF Machine Topology of 2010

The topology of 2010 design is schematically shown in Fig. 1.2 where one half of PMTF is shown as a longitudinal cross-section. PMTF machine consists of three outer stator assemblies *12a, 12b, 12c* (one for each of three phases: A, B, C) and corresponding to them rotor assemblies *14a*, *14b*, *14c*. Each stator assembly includes toroidal or ring coil *16*, and the U-shaped magnetic poles *18* made of laminated steel [1].

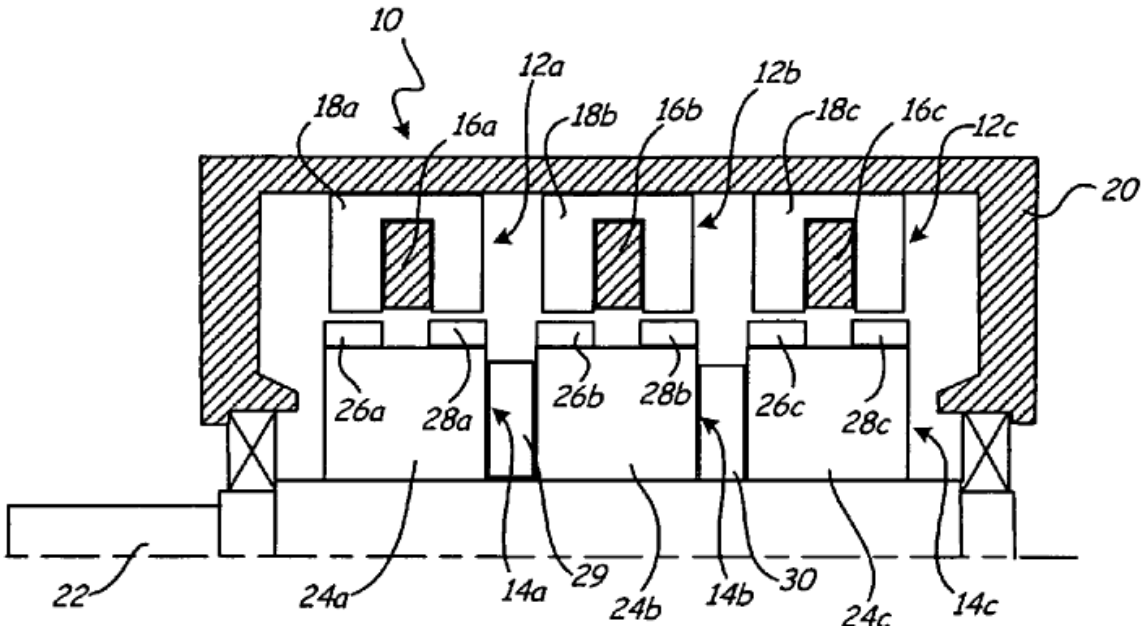

Fig. 1.2 Cross-section of a three-phase PMTF machine [1]

Rotor assembly *14* is affixed to a shaft *22*, and includes cylindrical ferromagnetic core *24* and permanent magnets *26* and *28*. Rotor and stator assemblies are distributed circumferentially around the shaft *22* [1].

Each phase of the three phase electric machine shown in Fig. 1.2 operates in the same way. Accordingly, the operation of the three-phase electric machine is described with respect to a single phase of the machine defined by stator assembly *12a* and rotor assembly *14a*. When the machine is

operating as a generator, permanent magnets *26a* and *28a* are caused to rotate by rotating shaft *22* to create a an alternating magnetic field. Hence, magnetic flux Φ circulates in alternating direction through U-shaped magnetic circuit *18a* (Fig. 1.3). In particular, magnetic flux circulates from a first pole "S" through the top portion of U-shaped magnetic pole *18a*. Next, down through a second pole "N". An alternating current (AC) voltage is generated in ring coil *16a* in response to the circulating magnetic flux [1].

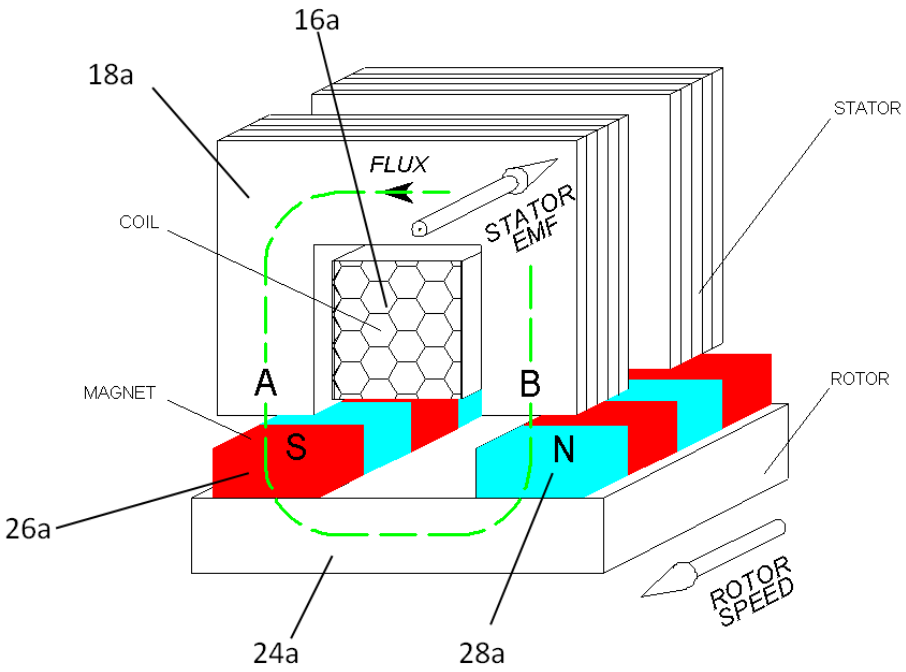

Fig. 1.3 Magnetic flux circulating through U-shaped stator magnetic circuit [29]

Based on the desired 2 KW output power value, dimensions of the machine were calculated and prototype of the generator was built. The results obtained from testing the prototype showed significant differences between the calculations and measurements taken from the real model [29]. The prototype output power was 65% lower than expected value.

Main objectives of this dissertation directed to improving the PMTF machine performance are listed below.

1.2 Objectives of the Dissertation

1. To study the latest proposed version of PMTF machine in order to find out the deficiencies which it faces.
2. To propose and design the improved version of PMTF machine and optimize its construction.
3. To determine the performance of the improved version of PMTF machine in steady-state and dynamic conditions.
4. To design a new topology of PMTF machine with high output power to volume ratio and analyze it in steady-state and dynamic conditions.

1.3 How the Objectives Were Accomplished

- **Objective 1.** To find out the deficiency of the newest version of PMTF machine, it was modeled using 3D FEM and the results were compared with those obtained from the experimental test carried out on the physical model of the generator.
- **Objective 2.** To accomplish the Objective 2, a few modified versions of the machine were proposed and designed applying 3D FEM software: Maxwell 12v. To ensure that the designed and optimized PMTF machine was not overheated, the heat transfer model was built and the temperature analysis was done.
- **Objective 3.** To determine the PMTF machine performance in steady-state, the equivalent circuit was applied. The analysis of generator dynamics was done using Matlab/Simulink software.

- **Objective 4.** Based on the review of previous PMTF machine topologies a new design which offers higher output power to volume ration was designed. Its performance was analyzed and compared with previous topologies.

1.4 Tasks of the Dissertation

1. To analyze flux linkage of the stator winding of the topology of 2010 in order to determine flux leakage losses in the machine using 3D FEM modeling.
2. To propose modifications to the stator and rotor structure in order to improve machine performance.
3. To optimize machine construction with aim to get high efficiency and power to volume ratio.
4. To determine the machine performance in steady-state and dynamic conditions.
5. To analyze the temperature of the machine in order to avoid its overheating.
6. To propose the gearless wind power generating system.
7. To design a new topology of the PMTF machine based on the combination of the ideas represented in patents [1-3]. To determine its performance and compare with the results obtained from the modified version of the topology of 2010.

1.5 Outline of the Dissertation

1. Chapter 2 discusses the software used in the dissertation for machine thorough analysis. Software is based on both field and circuit theories.
2. Chapter 3 represents the object of the dissertation (topology of 2010) and its design parameters. In this chapter a prototype and 3D FEM model of the machine are introduced.

3. Chapter 4 deals with thorough analysis of the machine magnetic flux distribution and flux leakage problems. Different ways to improve machine performance are described and analyzed.
4. Chapter 5 represents a 1kW PMTF machine which is studied in steady-state and dynamic conditions. Temperature analysis is done too.
5. Chapter 6 is dedicated to a new configuration of the PMTF machine with double armature.
6. Chapter 7 contains conclusions and future scope of study.

CHAPTER 2: DESCRIPTION OF THE SOFTWARE USED IN THE DISSERTATION

2.1 Field and Circuit Theories in Analyzing Electric Machines

Electrical and electromechanical devices can be described using two theoretical approaches:

- field theory;

- circuit theory.

Applying the field theory, a particular device is described mathematically in space and time domain and the particular mathematical model reminds the physical object despite simplifying assumptions are applied.

In the circuit theory a particular device is represented by the electric circuit with all passive and active elements, and the mathematical model is analyzed in time domain only. The passive elements (resistance, inductance and capacitance) are usually determined using a field theory or are found out experimentally.

The field theory applied to magnetic elements of the machine structure allows including the local nonlinearity. This cannot be done using circuit theory. However, the disadvantage of the field theory is of using very complex algebra and in general, to find the solution of mathematical expressions is a time consuming procedure.

A practical approach to solve a problem of electromechanical devices like electric machines is to apply the field theory in designing the particular object, and then, using the circuit theory, machine performance is analyzed under variable load and supply conditions. The circuit parameters are determined first using a field theory.

2.1.1 Field Theory Software

The equations derived in field theory can be solved analytically or applying numerical methods. The analytical methods do not allow taking elements of magnetic circuit like teeth in stator and rotor.

Thus, the local saturation of magnetic circuit should be ignored. This deficiency does not have numerical methods. That is why they are commonly used nowadays. One of these widely used methods is Finite Element Method (FEM).

2.1.2 Maxwell's Equations for Magnetostatic Problems [24]

In this dissertation FEM is used to solve magnetostatic problems. These are problems in which the magnetic field is time-invariant. "*In this case, the field intensity (H) and flux density (B) must obey the following Maxwell's equation:*

$$\nabla \times H = J \tag{2.1}$$

$$\nabla \cdot B = 0 \tag{2.2}$$

where J is a current density.

Constitutive relationship between B and H for each material:

$$B = \mu \cdot H \tag{2.3}$$

If a material is nonlinear, the permeability μ is a function of B:

$$\mu = \frac{B}{H(B)} \tag{2.4}$$

FEM is used to find a field that satisfies Eqns. (2.1 – 2.3) via a magnetic vector potential approach. Flux density is written in terms of the vector potential A, as:

$$B = \nabla \times A \tag{2.5}$$

This definition of B always satisfies Eqn. (2.2). When substituted into Eqns. (2.1) can be rewritten as:

$$\nabla \times \frac{1}{\mu\, B} \nabla \times A = J \tag{2.6}$$

For a linear isotropic material, Eqn. (3.6) reduces to:

$$-\frac{1}{\mu}\nabla^2 \cdot A = J \qquad (2.7)$$

FEM retains the form of (2.6), so that magnetostatic problems with a nonlinear B-H relationship can be solved.

In the general 3D case, A is a vector with three components. However, in the 2D planar and aximmetric cases, two of these three components are zero, leaving just the component in the "out of the page" direction.

The advantage of using the vector potential formulation is that all the conditions to be satisfied have been combined into a single equation. If A is found, B and H can then be deduced by differentiating A. The form of Eqn. (2.6) is an elliptic partial differential equation, and it arises in the study of many different types of engineering phenomena".

2.1.3 Finite Element Method [23]

"*The Finite Element Method (FEM) has been developed into a key, indispensable technology in the modeling and simulation of advanced engineering systems in various fields like housing, transportation, communications, and so on. The FEM was first used to solve problems of stress analysis, and has since been applied to many other problems like thermal analysis, fluid flow analysis, piezoelectric analysis, and others. Basically, the analyst seeks to determine the distribution of some field variable like the displacement in stress analysis, the temperature or heat flux in thermal analysis, the electrical charge in electrical analysis, and so on. The FEM is a numerical method seeking an approximated solution of the distribution of field variables in the problem domain into several elements*".

In this dissertation FEM is used to solve magnetostatic problems. In magnetostatic problems the magnetic field is time-invariant.

"*The behavior of a phenomenon in a system depends upon the geometry or domain of the system, the property of the material or medium, and the boundary, initial and loading conditions.*

The procedure of computational modeling using FEM consists of four steps:

- *Modeling of the geometry;*
- *Meshing (discretization);*
- *Specification of material property;*
- *Specification of boundary, initial and loading conditions*".

Modeling of the geometry [23]

"*Real structures, components or domains are in general very complex, and have to be reduced to a manageable geometry. Curved parts of the geometry and its boundary can be modeled using curves and curved surfaces. However, it should be noted that the geometry is eventually represented by piecewise straight lines of flat surfaces, if linear elements are used. The accuracy of representation of the curved parts is controlled by the number of elements used. It is obvious that with more elements, the representation of the curved parts by straight edges would be smoother and more accurate. Unfortunately, the more elements, the longer is the computational time that is required. Hence, due to the constraints on computational hardware and software, it is always necessary to limit the number of element*".

Meshing [23]

"*Meshing is performed to descretize the geometry created into small pieces called elements or cells. The solution for an engineering problem can be very complex and if the problem domain is divided (meshed) into small elements or cells using a set of grids or nodes, the solution within an element can be approximated very easily using simple functions such as polynomials. Thus, the solutions for all of the elements form the solution of the whole problem domain. Mesh generation is a*

very important task of the pre-process. It can be a very time consuming task to the analyst, and usually an experienced analyst will produce a more credible mesh for a complex problem. The domains have to be meshed properly into elements of specific shapes such as triangles and quadrilaterals". Triangle mesh of the PM synchronous machine is shown in Fig. 2.1.

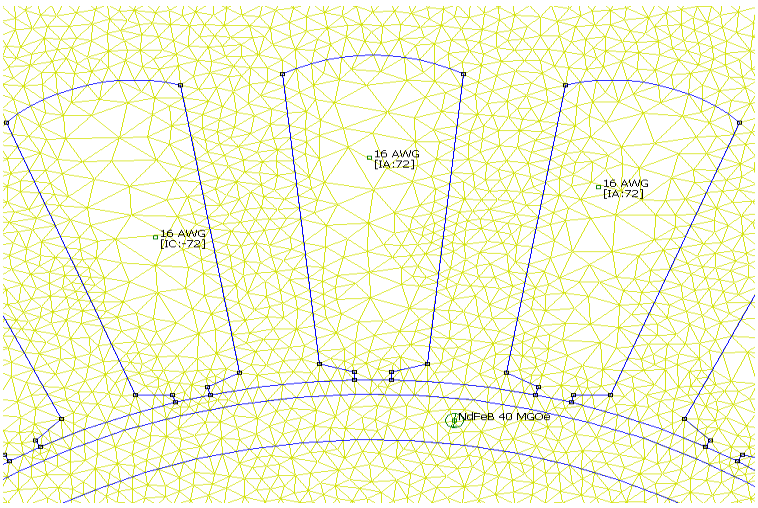

Fig. 2.1 Triangle mesh in FEM

Property of material or medium [23]

"*Many engineering systems consist of more than one material. Property of materials can be defined either for a group of elements or each individual element, if needed. For different phenomena to be simulated, different sets of material properties are required. For, example, Youg's modulus and shear modulus are required for the stress analysis of solids and structures whereas the thermal conductivity coefficient will be required for a thermal analysis. Input of material's properties into a pre-processor is usually straightforward. All the analyst needs to do is select material properties and specify either to which region of the geometry or which elements the data applies*".

Boundary, initial and loading conditions [23]

"*Boundary, initial and loading conditions play a decisive role on solving the simulation. To input these conditions is usually done using commercial pre-processor, and it is often interfaced with graphics. Users can specify these conditions either to the geometrical identities (points, lines or curves, surfaces, and volumes) or to the elements or grid*".

2.1.4 Commercial FEM programs Used in the Dissertation

There are many commercially used FEM programs. Three programs are used in this dissertation: FEMM 4.0 [24], Maxwell 12v [25] and ePhysics 12v [26].

- **FEMM 4.0** [24]

"*FEMM 4.0 is a set of programs for solving low frequency electromagnetic problems of two-dimensional planar and axisymmetric domains. The program currently addresses linear/nonlinear magnetostatic problems, linear/nonlinear time harmonic magnetic problems, linear electrostatic problems, and steady-state heat flow problems [24]*.

FEMM is divided into three parts:

• Interactive shell (femm.exe):

This program is a Multiple Document Interface pre-processor and a post-processor for the various types of problems solved by FEMM. It contains a CAD like interface for laying out the geometry of the problem to be solved and for defining material properties and boundary conditions. Autocad DXF files can be imported to facilitate the analysis of existing geometries. Field solutions can be displayed in the form of contour and density plots. The program also allows the user to inspect the field at arbitrary points, as well as evaluate a number of different integrals and plot various quantities of interest along user-defined contours.

• *Triangle.exe:*

Triangle breaks down the solution region into a large number of triangles, a vital part of the finite element process

• *Solvers:*

- *fkern.exe - for magnetics;*
- *belasolv - for electrostatics;*
- *hsolv - for heat flow problems;*
- *csolv - for current flow problems. Each solver takes a set of data files that describe problem and solves the relevant partial differential equations to obtain values for the desired field throughout the solution domain.*

The Lua scripting language is integrated into the interactive shell".

FEMM 4.0 was used in this dissertation mainly to study the magnetic field and flux linkage behavior in the generator with and without shunts.

- **Maxwell 12v** [25]

"*Maxwell 12v is an interactive software package that uses finite element method to solve three-dimensional (3D) electrostatic, magnetostatic, eddy current and transient problems. It is used to compute:*

• *Static electric fields, forces, torques, and capacitances caused by voltage distributions and charges.*

• *Static magnetic fields, forces, torques, and inductances caused by DC currents, static external magnetic fields, and permanent magnets.*

• *Time-varying magnetic fields, forces, torques, and impedances caused by AC currents and oscillating external magnetic fields.*

• *Transient magnetic fields caused by electrical sources and permanent magnets*".

Maxwell 12v is a key software used for calculation of electromagnetic parameters of the considered transverse flux generator.

- **ePhysics 12v** [24, 26]

"*ePhysics is an interactive software package for analyzing thermal and structural deformation and stress. ePhysics is designed to work in standalone mode or coupled with Maxwell electromagnetic or High-Frequency Solution Sequences (HFSS). Using ePhysics 12v the following can be computed:*

• *Temperature and heat flow vector distributions.*

• *Average temperature, hot spot temperature, and cold spot temperature.*

• *Displacement, von Mises stress, principal stresses, and traction.*

• *RMS measure of stress, maximum von Mises stress, and maximum principal stress.*

In general, finite element based field solvers enable to simulate thermal and structural fields in practically any type of device. It is expected to draw the structure and specify all relevant material characteristics, boundary conditions and sources. ePhysics 12v then generates the necessary field solutions and computes the requested quantities of interest. It can be viewed and analyzed the fields in the device using the software's post-processing features".

"*The heat flow problems address by ePhysics 12v are essentially steady-state heat conduction problems. These problems are represented by a temperature gradient, G (analogous to the field intensity, E for electrostatic problems), and heat flux density, F (analogous to electric flux density, D, for electrostatic problems).*

The heat flux density must obey Gauss' Law, which says that the heat flux out of any closed volume is equal to the heat generation within the volume. Analogous to the electrostatic problem, this law is represented in differential form as:

$$\nabla \cdot F = q \qquad (2.8)$$

where q represents volume heat generation.

Temperature gradient and heat flux density are also related to one another via the constitutive relationship:

$$F = kG \qquad (2.9)$$

where k is the thermal conductivity. Thermal conductivity is often a weak function of temperature. FEM allows for the variation of conductivity as an arbitrary function of temperature.

Ultimately, one is generally interested in discerning the temperature, T, rather than the heat flux density or temperature gradient. Temperature is related to the temperature gradient, G, by [49]:

$$G = -\nabla \cdot T \qquad (2.10)$$

Substituting (2.10) into Gauss' Law and applying the constitutive relationship yields the second order partial differential equation:

$$-\nabla \cdot (k\nabla T)T = q \qquad (2.11)$$

ePhysics solves (2.9) for temperature T over a user-defined domain with user-defined heat sources and boundary conditions".

ePhysics 12v is used in the dissertation for temperature analysis of the generator.

2.1.5 Circuit Theory Software

- **Matlab and Simulink 2010** [28]

"*MATLAB® is a high-level language and interactive environment that enables to perform computationally intensive tasks faster than with traditional programming languages such as C, C++, and Fortran.*

Simulink® is an environment for multidomain simulation and Model-Based Design for dynamic and embedded systems. It provides an interactive graphical environment and a customizable set of block libraries that let you design, simulate, implement, and test a variety of time-varying systems, including communications, controls, signal processing, video processing, and image processing".

Dynamic and steady-state analysis of the generator is done using Matlab and Simulink.

CHAPTER 3: PMTF MACHINE CONSTRUCTION AND DESIGN PARAMETERS

3.1 Description of the Machine Prototype and 3D FEM Model

The prototype of the PMTF generator that is the object of study in this chapter was designed by the University of Nevada, Reno in cooperation with National Wind Technology Center (Fig. 3.1). The machine was designed accordingly to the topology of 2010 which has been discussed in Chapter 1. The stator consists of three rings, each of them for different phase. The rotor, placed inside of the stator, has also three ferromagnetic rings attached to the rotor shaft. Two rows of PMs are glued to each of the cylinders.

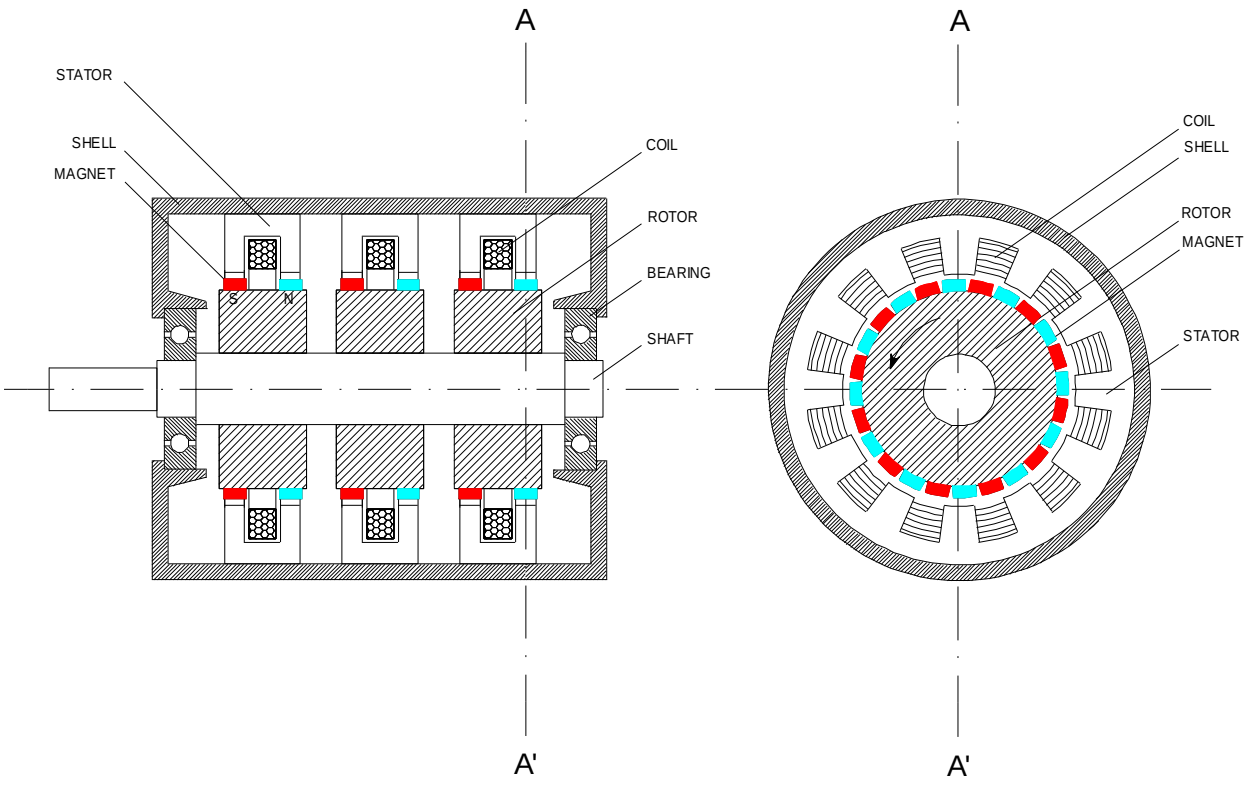

Figure 3.1 Scheme of PMTF machines designed according to the topology of 2010 [29]

The prototype of the generator is shown in Fig. 3.2.

a)

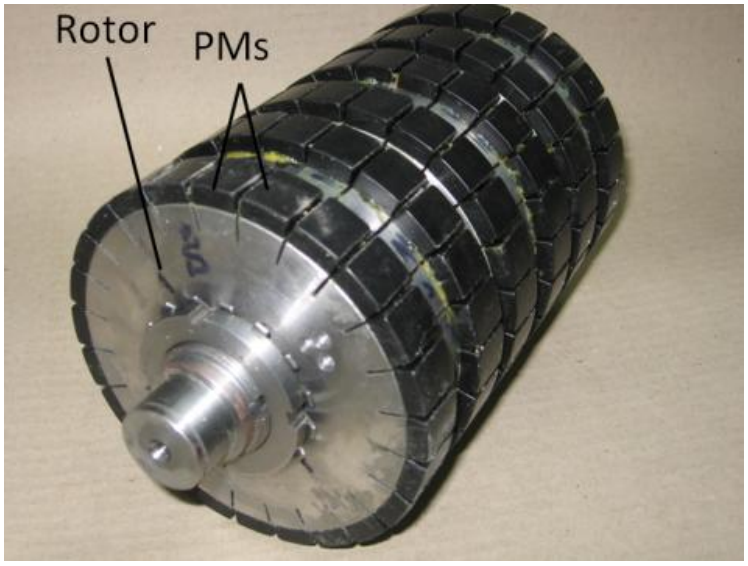

b)

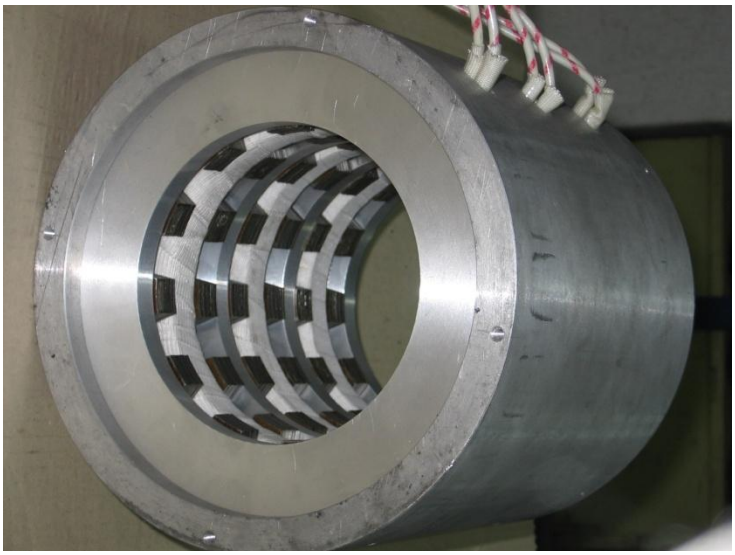

Figure 3.2 PMTF machine prototype: a) rotor, b) stator [29]

For analyzing the generator performance its 3D FEM model was built.

Since all three parts of the generator do not influence one another magnetically the analysis of the generator operation can be carried out for a single phase. The structure of one machine phase is shown schematically in Fig. 3.3.

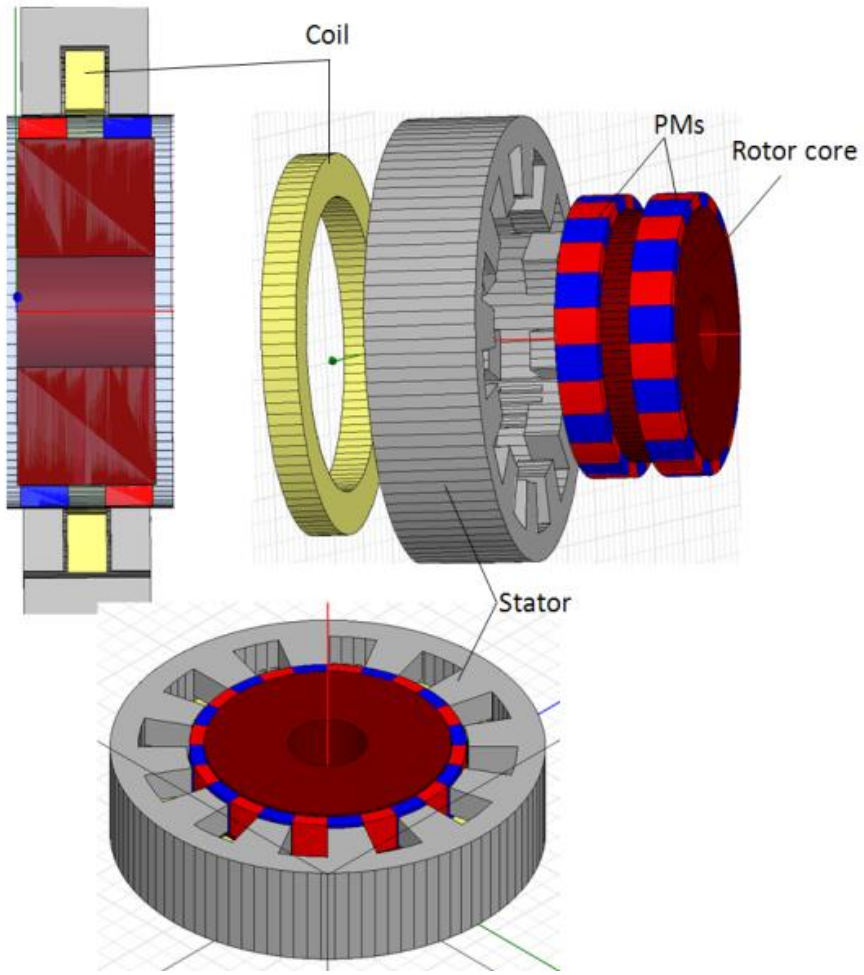

Figure 3.3 Machine structure for one phase

The stator core has 12 U-shape poles made of laminated steel. The stator winding has a form of O-ring and is placed inside of the core poles. The rotor ring, made of solid iron, has two rows of PMs with 24 magnets in each row. The dimensions of the stator and rotor parts shown in Fig. 3.4 are

enclosed in Table 3.1. The design parameters of the machine for a single phase are enclosed in Table 3.2.

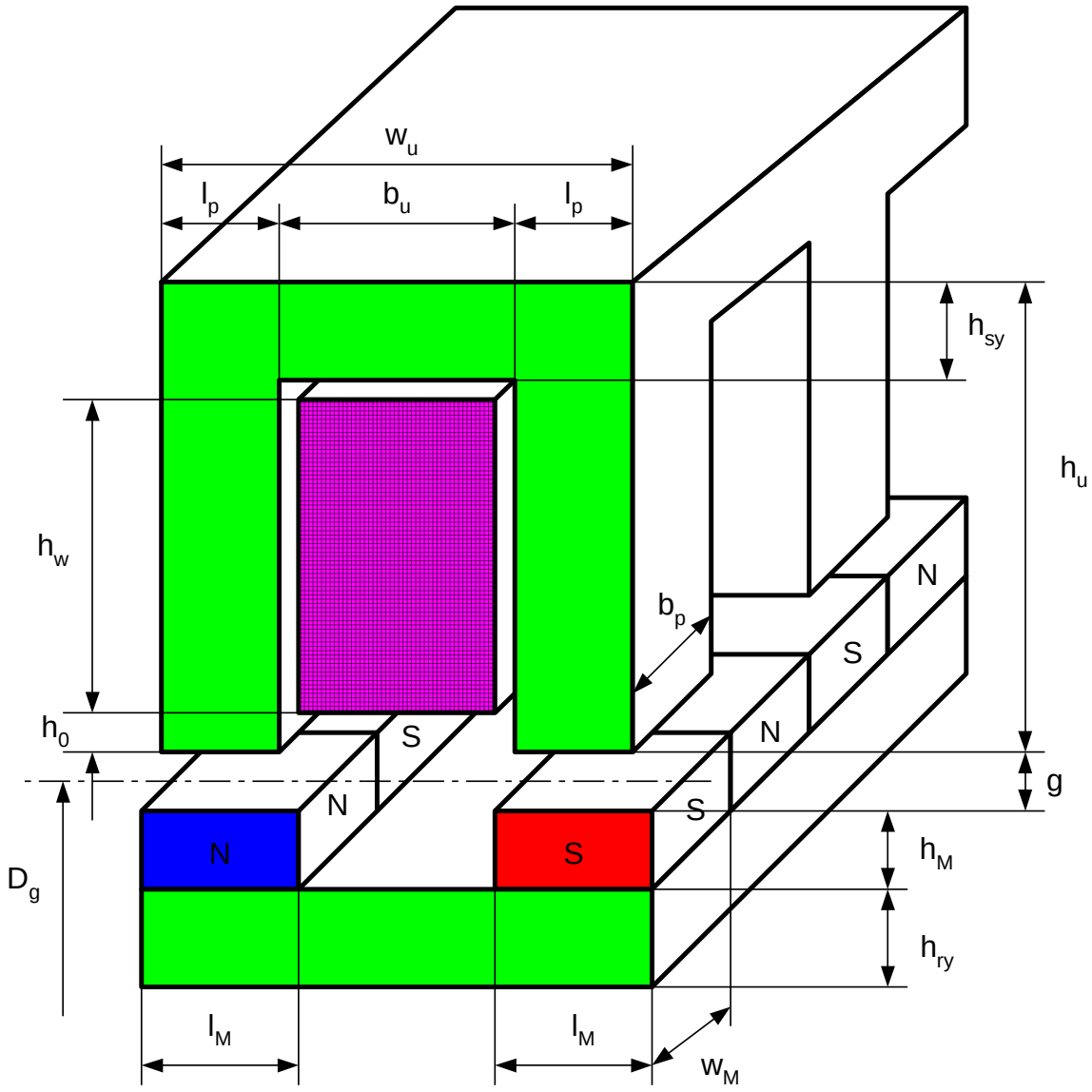

Figure 3.4 Machine dimensions [29]

Table 3.1 Dimensions of the generator parts

PARAMETER	DIMENSIONS
Pole pitch	τ = 16 mm
Dimensions of the permanent magnet	h_M = 6.2 mm, l_M = 17 mm, w_M = 13.4 mm
Permanent magnets	NdFeB with $B_r \geq 1.25$ T
Average diameter of the air gap	D_g = 120 mm
Rotor outer diameter	D_{rot} = 119 mm
Stator inner diameter	$D_{st,in}$= 121 mm
Circumferential width of the stator pole	b_p = 14 mm
Axial length of the stator pole	l_p = 15 mm
Distance between stator poles	b_u = 17 mm
Axial width of the stator core per phase	w_u = 47 mm
Axial width of the rotor core per phase	49 mm
Height of the stator coil	h_w = 17 mm
Axial width of the stator coil	approx. 17 mm
Height of the stator core (poles + yoke)	h_u = 33 mm
Height of the stator yoke	h_{sy} = 13 mm
Height of the rotor yoke	h_{ry} = 36.1 mm
Height of unfilled stator slot	h_o = 1 mm

Table 3.2 Design parameters for a single phase structure of the generator

STATOR	
Winding:	
- Number of coils	1
- Number of turns per coil	28
- Wire	AWG12 (square)
- Winding fill factor, k_{fill}	0.7
Magnetic Core:	
- Number of magnetic core poles	p = 12
- Air-gap length	g=1.5 mm
ROTOR	
- Number of rotor poles	p=24
Permanent magnets:	
- Type	NdFeB 35
- Relative permeability, μ	1.09967 H/m
- Bulk conductivity, γ	625000 S/m
- Residual flux density, B_r	1.2 T
- Thickness (radial lengths)	6 mm

The magnetic flux set by the PMs during the rotation is closed through the stator poles in axially oriented plane. When the rotor rotates its magnets change their polarity with respect to the stator pole inducing voltage in the stator winding with frequency: $f = pn/120$, where p is the number of poles on the rotor circumference and n is the rotor speed in rpm.

To obtain a phase shift between phase voltages permanent magnets of each phase must be displaced by 120 electrical degrees (20 mechanical degrees). The magnet axial layout is shown in Fig. 3.5 [29].

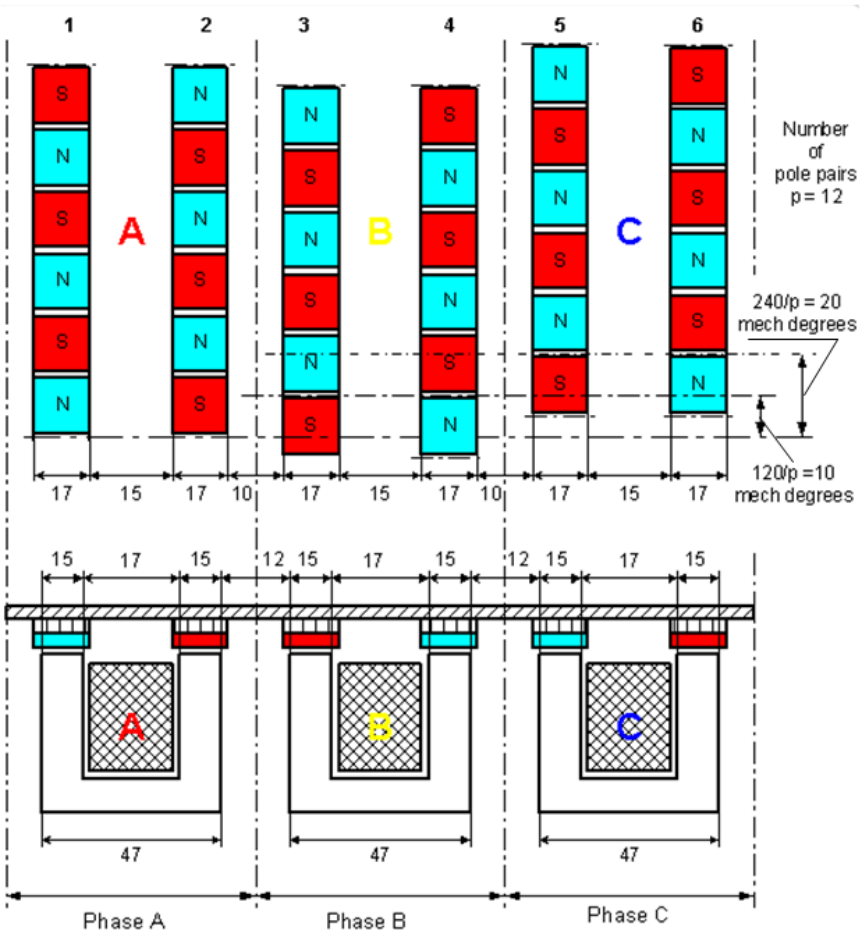

Figure 3.5 PM axial layout for 3-phase machine structure [29]

3.2 Electromechanical Parameters of the Generator

The estimated electromechanical parameters of the generator which were calculated and presented in the report [29] are shown in Table 3.3. These parameters however do not match the results obtained from the test carried on generator prototype which also are enclosed in Table 3.3.

Table 3.3 Estimated electromechanical parameters of the generator

Electromechanical parameters	Estimated	Measured (prototype)	Calculated (3D FEM model)
No load phase voltage amplitude $[V]$	48.3	16.1	16
Speed [rpm]	600	600	600
Output power [W]	2090	750	800

The output power and no-load voltage obtained during the test at 600 rpm are nearly three times lower. Similar differences occurred also for the entire range of speeds from 0 to 1200 rpm what is illustrated by the characteristics shown in Figs. 3.6 and 3.7.

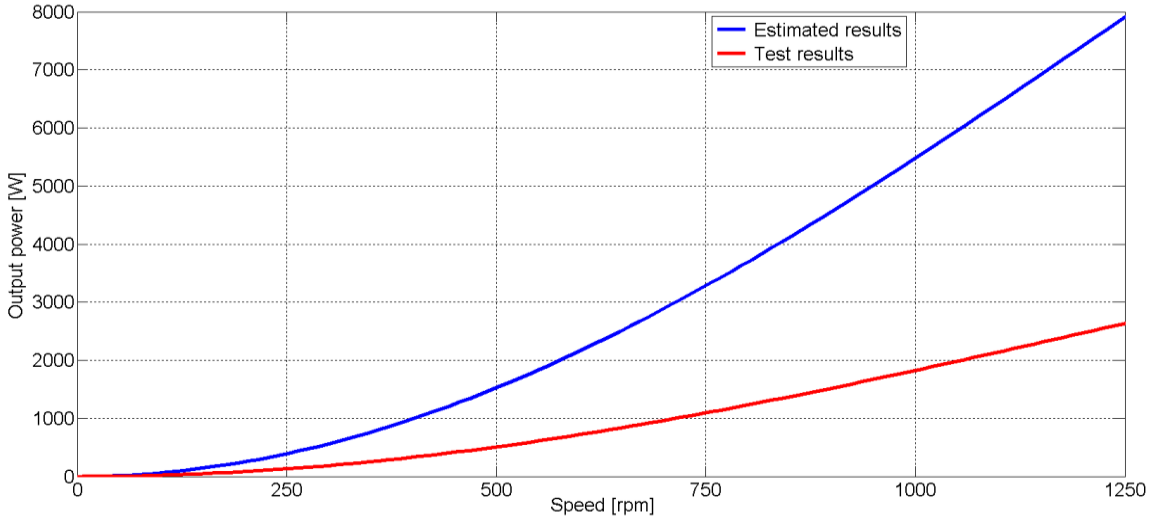

Figure 3.6 Output power of the generator

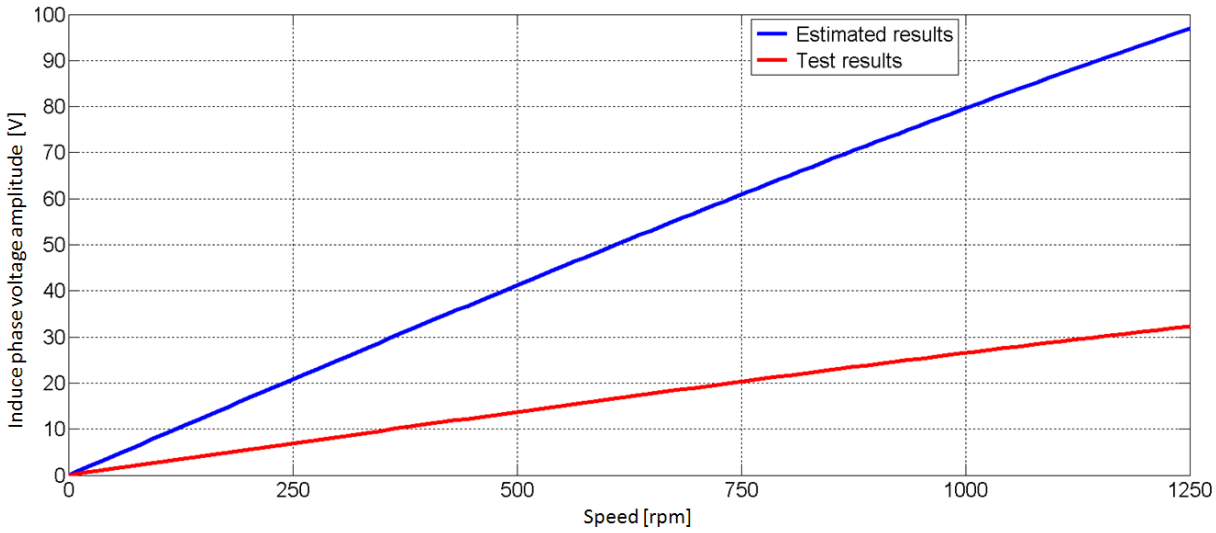

Figure 3.7 Induced voltage of the generator

To find out the cause of these differences a 2D FEM generator model was built. In this model only one stator pole with rotor active magnets was considered. The flux density distribution obtained from the model simulation is shown in Fig. 3.8.

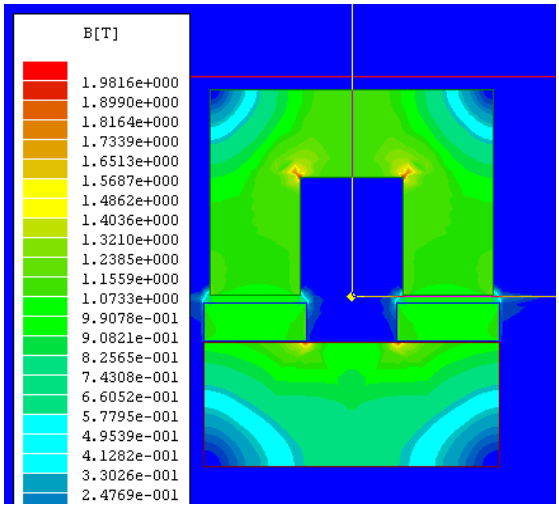

Figure 3.8 Magnetic flux density of the machine [29]

The flux linkage relevant to this flux density is 0.08 Wb per stator pol. This, multiplied by angular frequency ω and by the number of stator poles N_{st} of a single phase according to the equation:

$$V_{ph} = 2\pi f N_{st} \lambda_{pole} \tag{3.1}$$

gives 49 V.

These results indicate that the estimated value of induced voltage enclosed in the report were obtained from 2D FEM modeling in which no influence of non-active magnets was assumed.

To find out what is the cause that the voltage induced by the active rotor magnets is lower, further test and 3D FEM modeling were performed.

CHAPTER 4: MAGNETIC FLUX ANALYSIS AND IMPROVEMENT OF THE GENERATOR PERFORMANCE

4.1 Magnetic Flux Distribution Determination

To determine the magnetic flux distribution in the stator core three search coils made of 10 turns were applied [29]. Fig. 4.1 shows the places where the search coils were mounted.

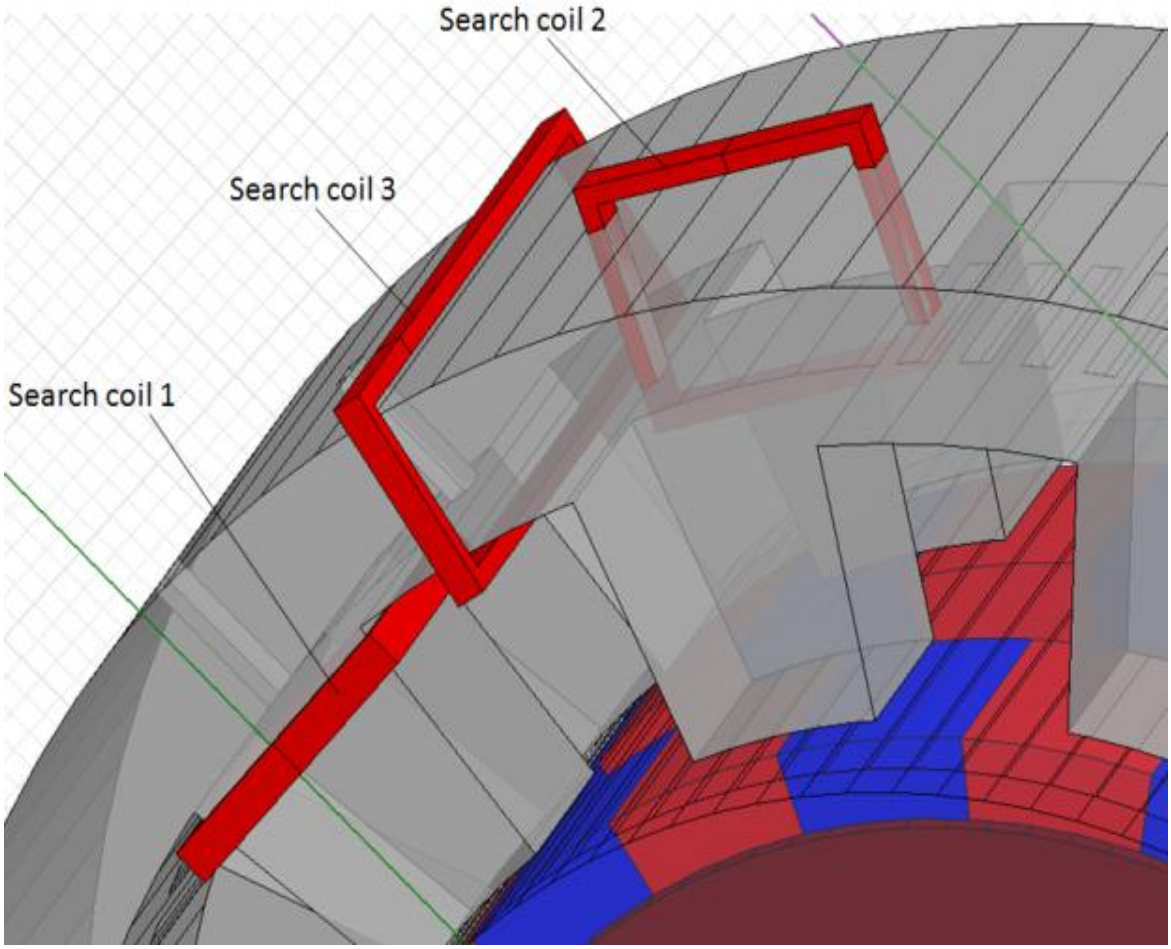

Figure 4.1 Search coils mounted on the stator

The coil 1 senses the flux linking the phase winding. Coil 2 senses the axial stator pole flux, and the coil 3 senses the circumferential flux passing between stator poles. The voltages induced in the search coils taken from the prototype test [29] and calculated in 3D FEM are shown in Fig. 4.2.

Comparing both test and simulation results no significant discrepancies occurred. This justifies the correctness of 3D FEM modeling.

Voltage induced in coil 3 implies that relatively large magnetic flux passes circumferentially which does not contribute to the induction of phase voltage. The distribution of this flux in the stator yoke is shown in Fig. 4.3

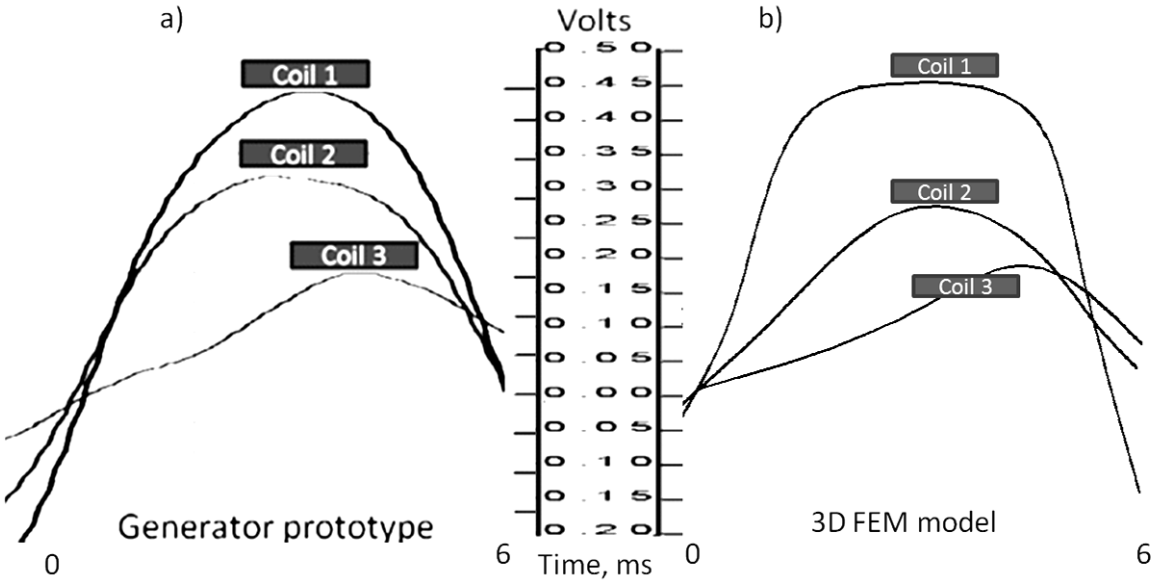

Figure 4.2 Induced voltages in the search coils: a) test results [29], b) simulation results

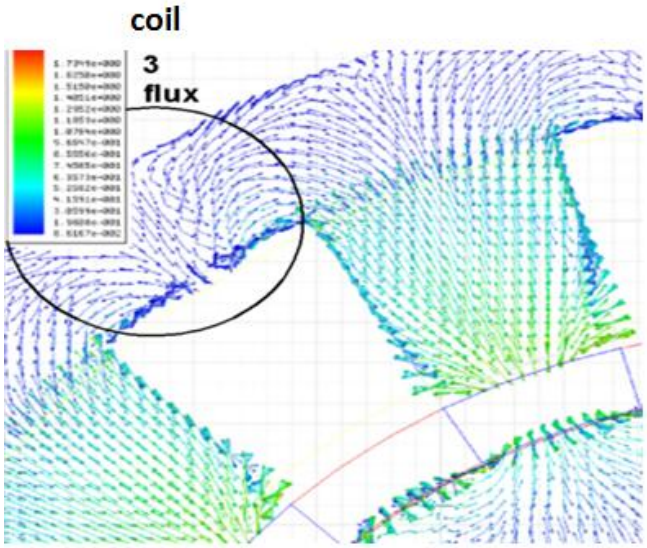

Figure 4.3 Magnetic flux in the stator yoke

To eliminate this flux the stator core was modified to the version shown in Fig. 4.4. The induced phase voltage calculated for the new version is shown in Fig. 4.5 a. The amplitude of this voltage is 7.5% higher than that induced in the original version which is shown in Fig. 4.5 b

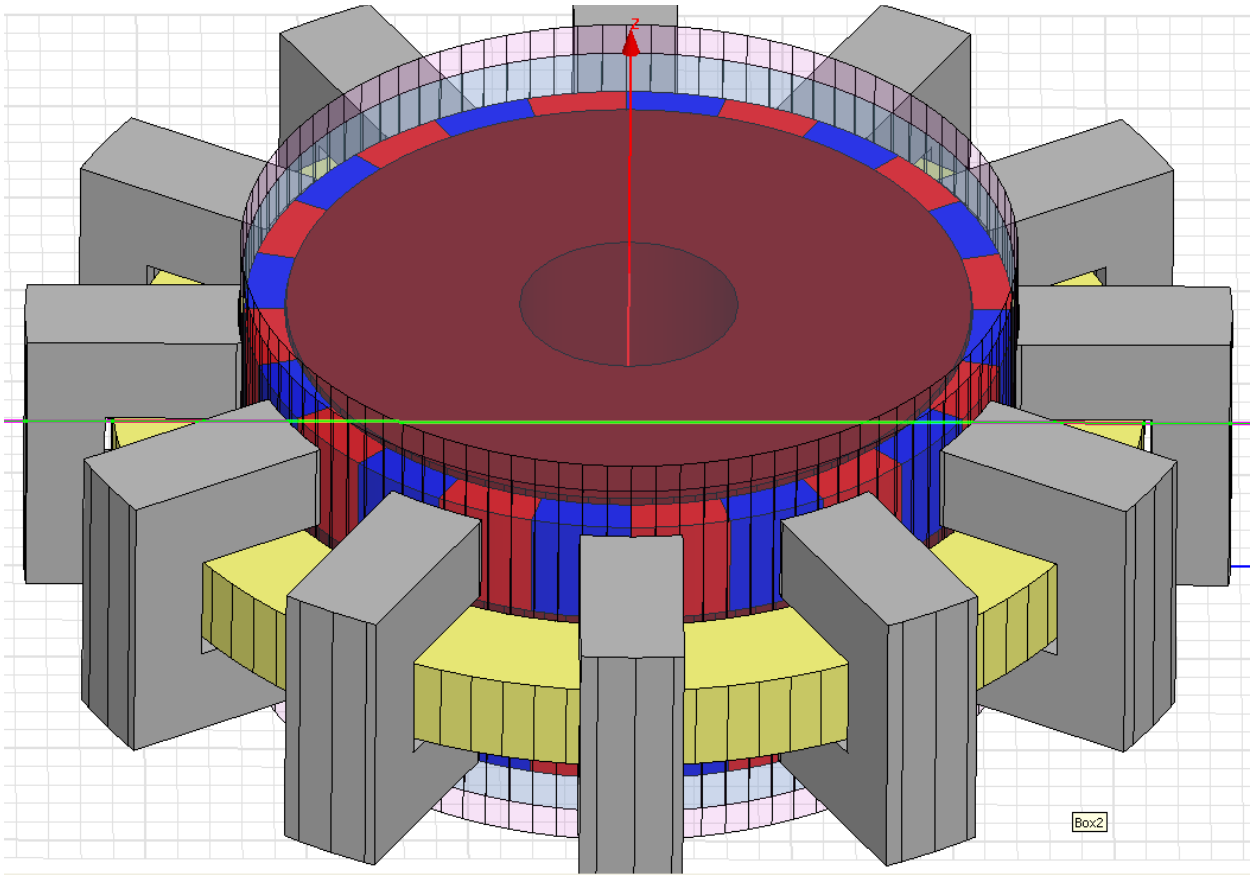

Figure 4.4 Generator with modified stator

a)

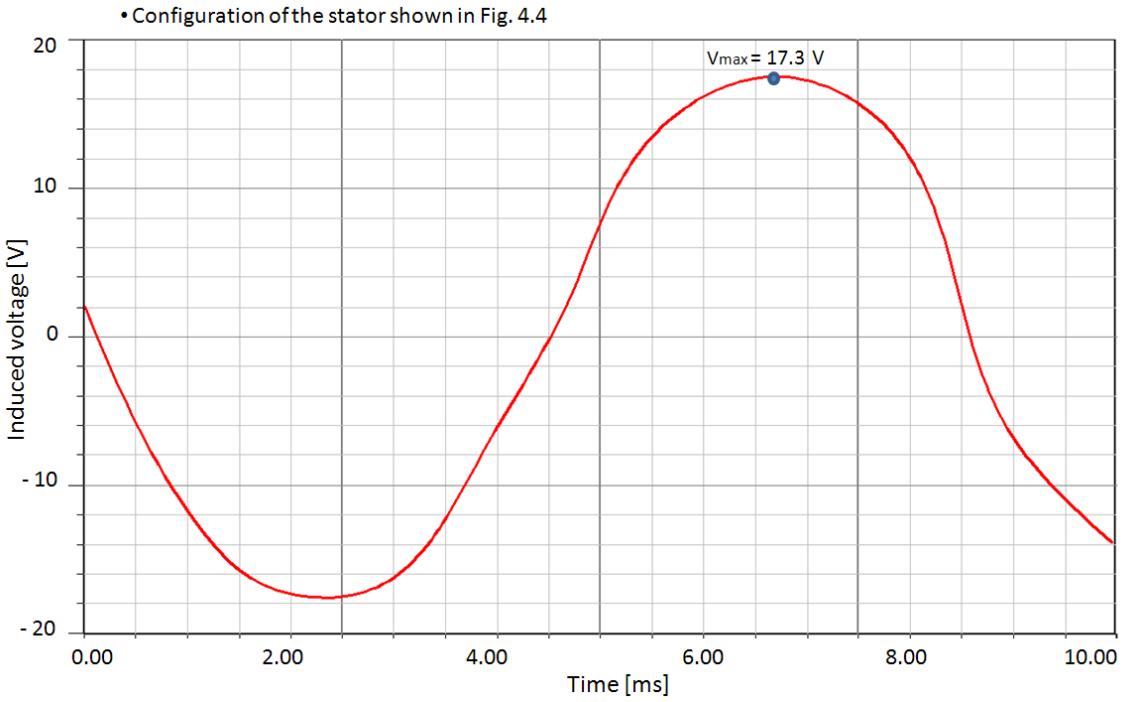

b)

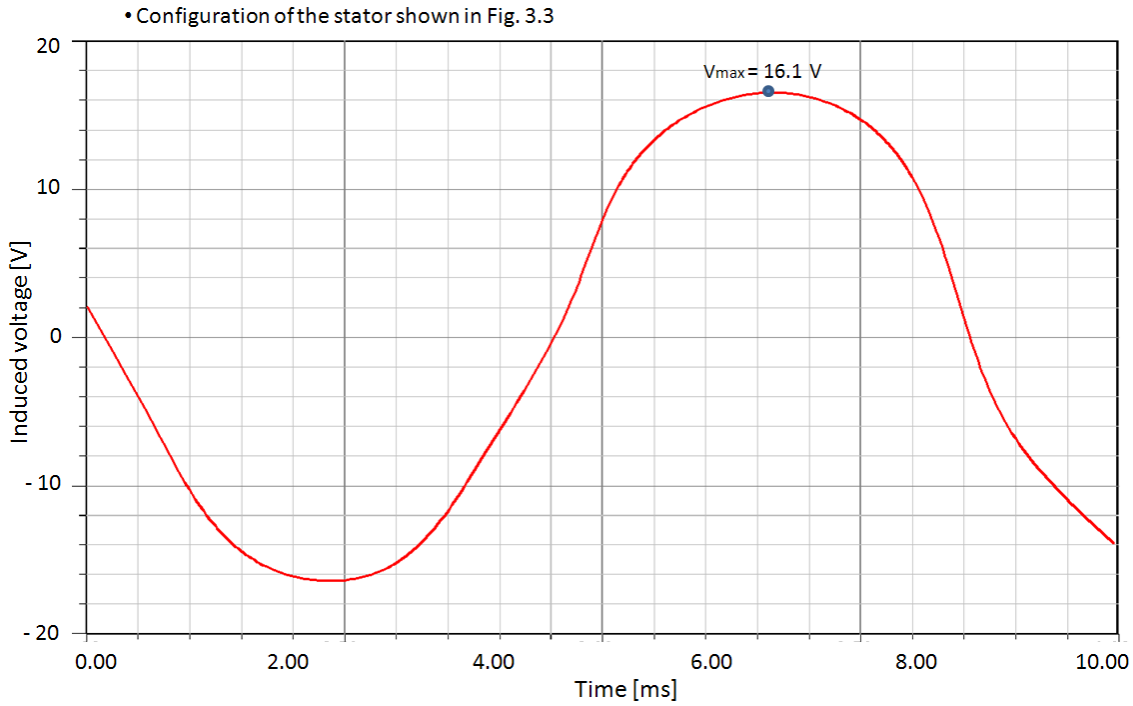

Figure 4.5 a) Induced voltage of the new version of the generator stator, b) induced phase voltage of the original version of the generator stator

The calculation results of the magnetic flux in the rotor area presented in Fig. 4. 6 shows that part of the flux is closed between adjacent magnets in circumferential direction.

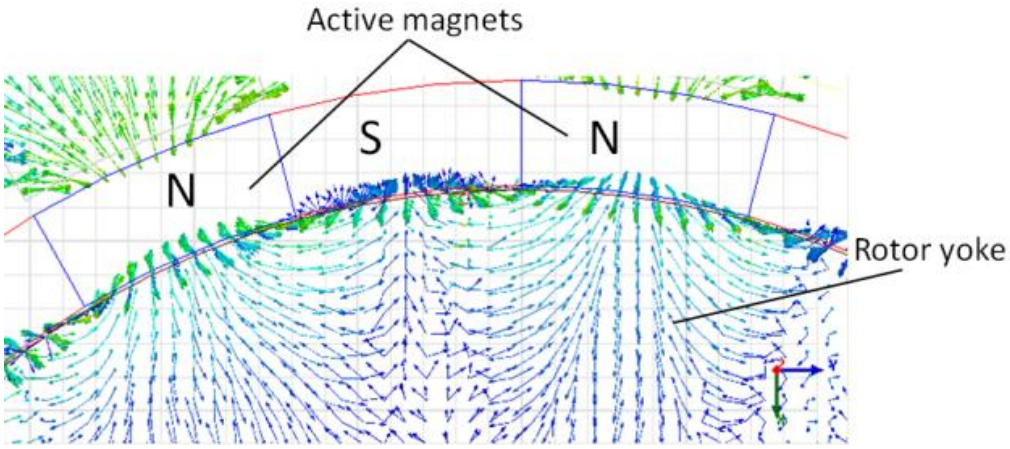

Figure 4.6 Magnetic flux in the rotor

This flux does not take part in energy conversion and can be cut off. Only the rotor axial component of the flux is vital for *emf* induction.

To minimize the circumferential flux components small gaps of 1.3 mm were introduced between the magnets as it shown in Fig. 4.7

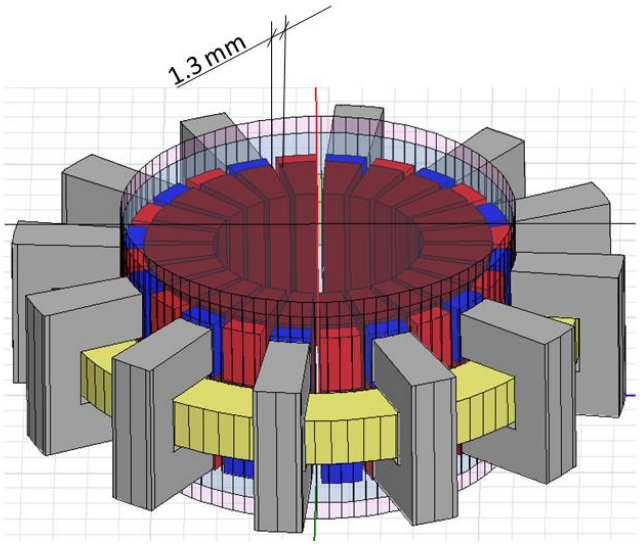

Figure 4.7 Generator with modified rotor

The voltage induced in the generator coil after this modification is equal to 18 V, which is 7% higher than that in the version without the gaps (Fig. 4.8). It means that this modification did not contribute significantly to the improvement in voltage induction.

The magnetic flux which contributes to the energy conversion at particular time instant is coming from the rotor magnets being actually under the stator poles. The flux of the rest of the magnets can be then "switched off". To find the percentage of the flux of the "active" magnets simulation was carried out for a generator structure without "inactive" rotor magnets as shown in Fig. 4.8.

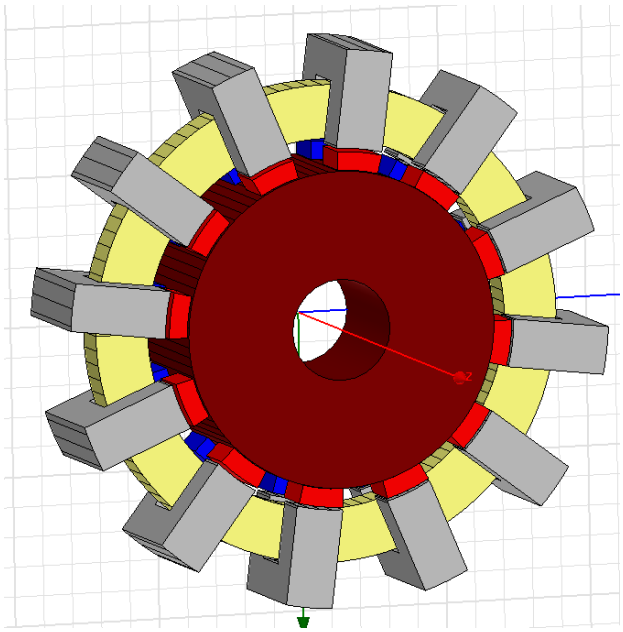

Figure 4.8 Generator without "inactive" magnets

The amplitude of the calculated flux linkage is shown in Fig. 4.9 and equal to 0.08 Wb. It is 70% higher than that of the flux linkage amplitude when both "active" and "inactive" magnets exist. It means that "inactive" magnets significantly diminish the flux linkage responsible for energy conversion.

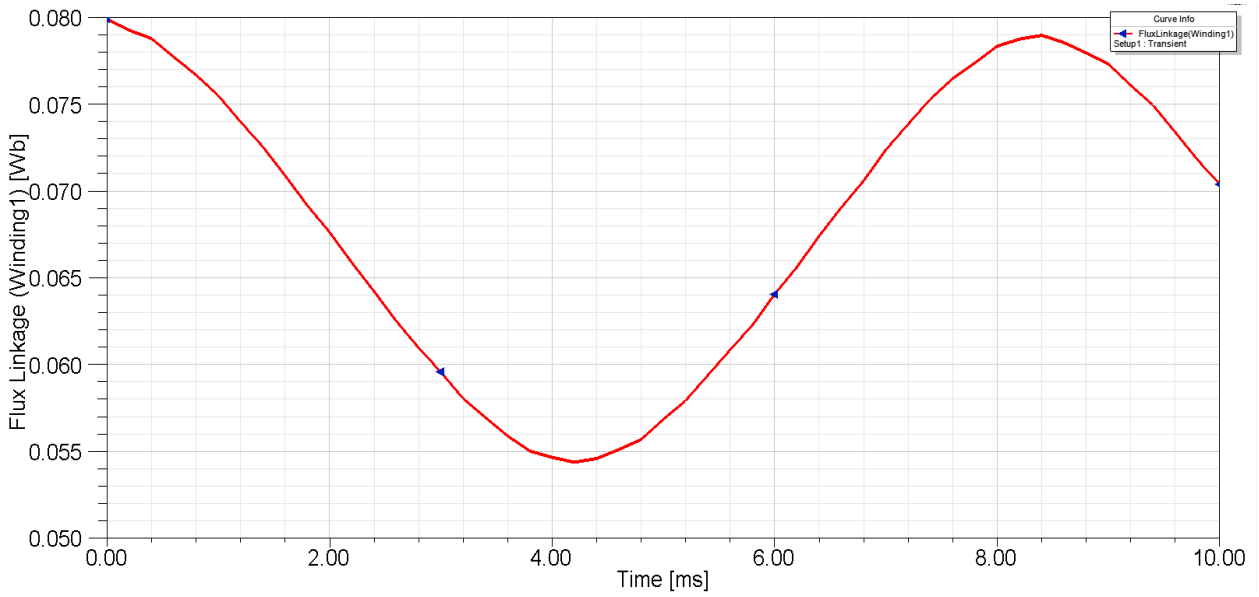

Figure 4.9 Flux linkage of the coil ("active" magnets only)

To find the percentage of the negative flux coming from the "inactive" magnets a calculation was done of the generator with a presence of only these magnets. The flux density distribution for this case is shown in Fig. 4.10.

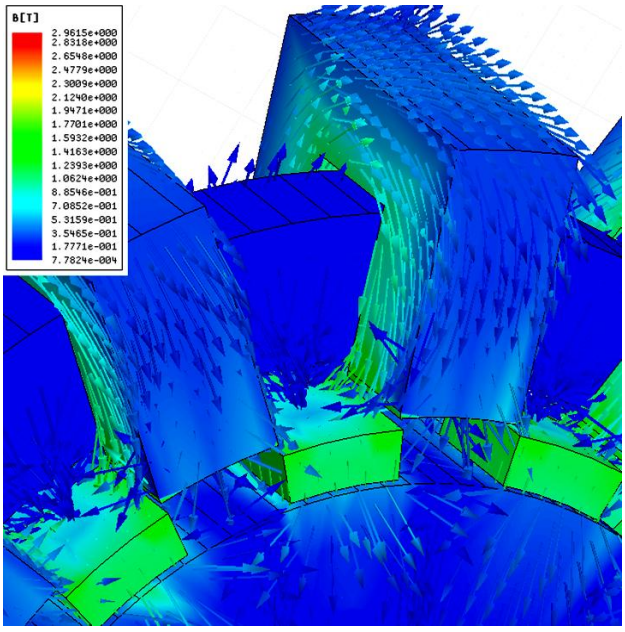

Figure 4.10 Generator with "inactive" magnets only

The flux density of this “negative” flux in the stator poles is around 70% of the “positive” flux coming from “active” magnets. Such “negative” flux significantly lowers the performance of the generator. It means it should be “switched off” during generator operation. This is a subject of the next subsection.

4.2 Implementation of the Magnetic Shunts in the Stator Structure

To eliminate the negative flux linkage magnetic shunts were applied between the stator poles as shown in Fig. 4.11. Similar type of shunts was also proposed in [5].

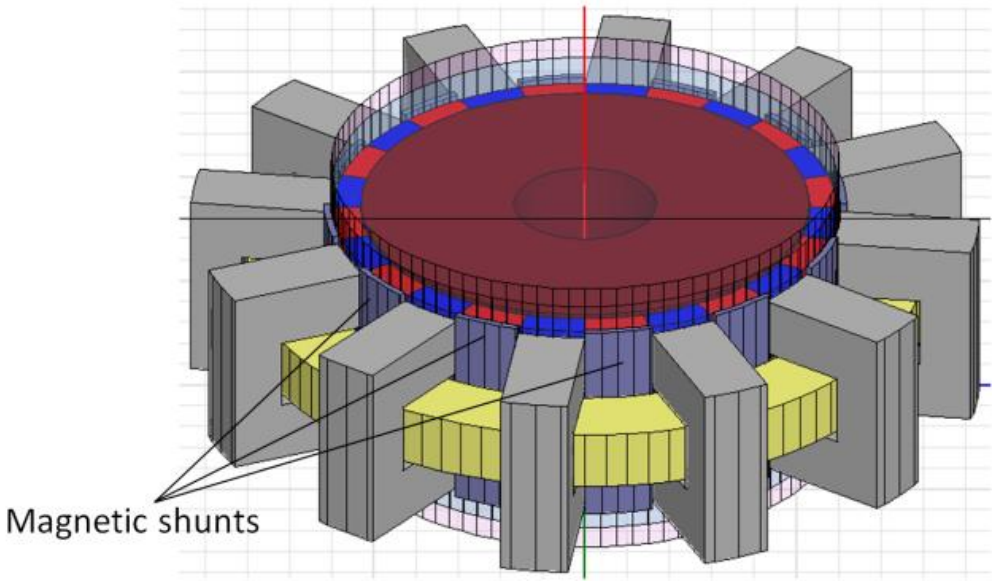

Figure 4.11 Single-phase generator ring with magnetic shunts

The calculation of *emf* in the coil were done for the shunts made of iron. The voltage waveform that was obtained is shown in Fig. 4.12. The voltage amplitude is nearly two times higher than that of

the model without magnetic shunts (see Fig. 4.5a). The effectiveness of blocking the negative flux coming from “inactive” magnets is almost 75%. This is proved by the amplitude of flux linkage in Fig. 4.13, which is now equal to: λ=0.06 Wb.

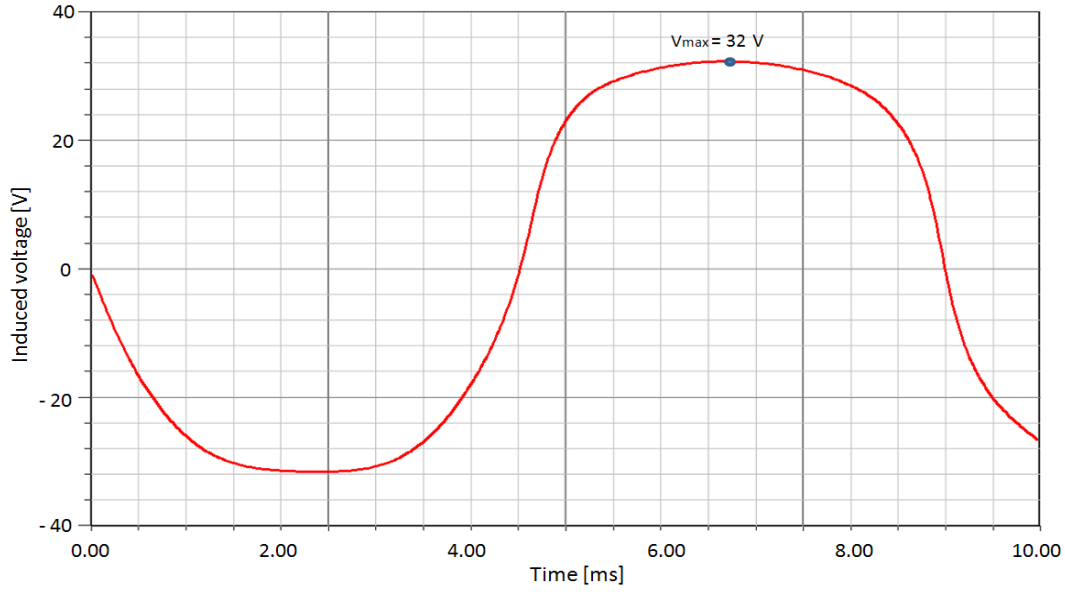

Figure 4.12 Induced voltage of the generator with magnetic shunts made of iron

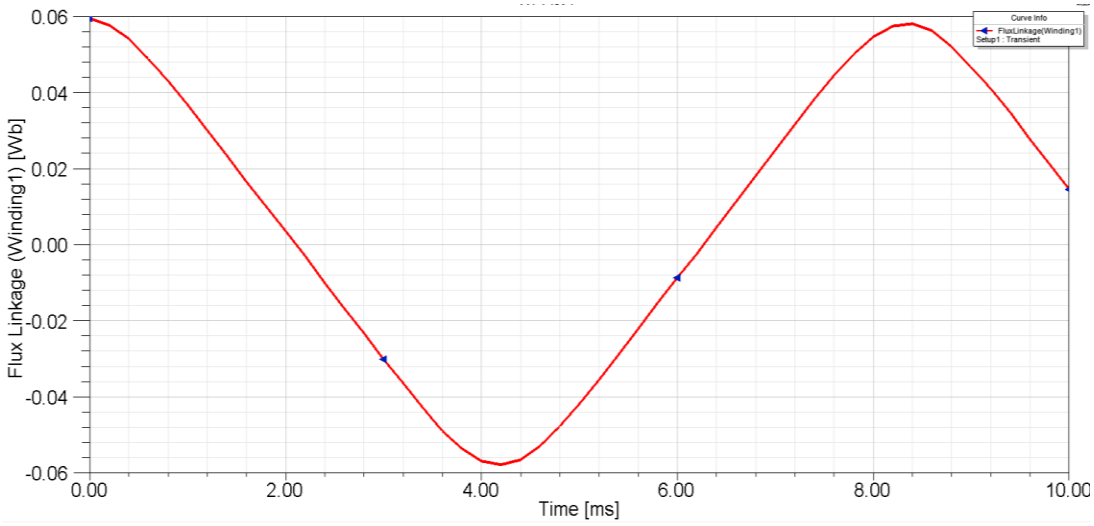

Figure 4.13 Flux linkage of the model with magnetic shunts made of iron

The amplitude of the flux linkage of generator with shunts is 30% lower than that of the generator without “inactive” magnets (see Fig. 4.9). It means that negative flux caused by “inactive” magnets is not totally blocked by the shunts. Part of this flux still links adjacent magnetic poles. This flux is shown in Fig. 4.14.

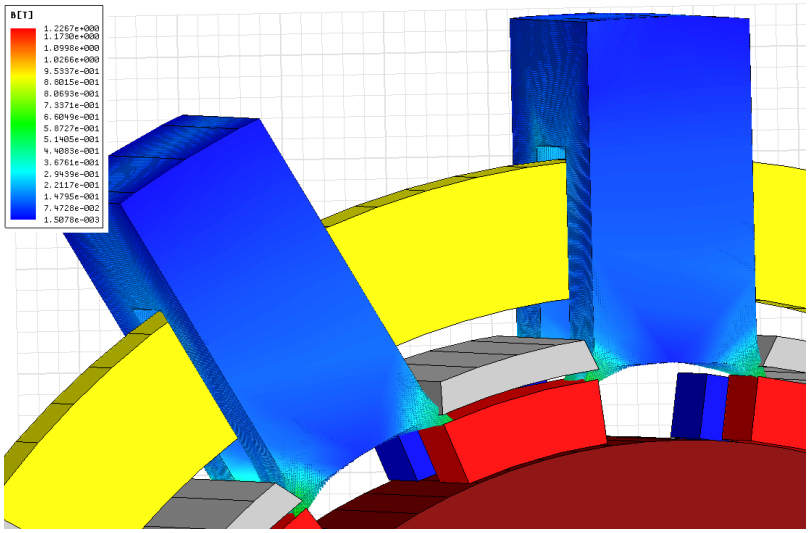

Figure 4.14 Negative flux of “inactive” magnets which links adjacent poles

How effective are the shunts in blocking the negative flux is also shown in Fig 4.15. In case of the model with shunts magnetic flux linking the coil is almost negligible (Fig. 4.15 a), whereas in case of the model without shunts, a much greater flux penetrates the coil (Fig. 4.15 b).

The magnetic shunts can be also made with laminated steel. In this case the eddy currents which are induced also repel the negative flux. They do not contribute to additional power losses like the shunts made of iron. Consequently, the efficiency of the generator is higher and the temperature of the winding and PMs will not be exceeded over the permissive value.

The simulation of the generator with cooper and aluminum shunts was also done, and the calculated induced voltages were as follows: $E_{max}=30V$ – for copper, and $E_{max}=28V$ – for aluminum. As results show, copper and aluminum shunts also reduce effectively the negative flux

linkage. But similarly to solid iron shunts they cause high power losses and an increase of winding temperature.

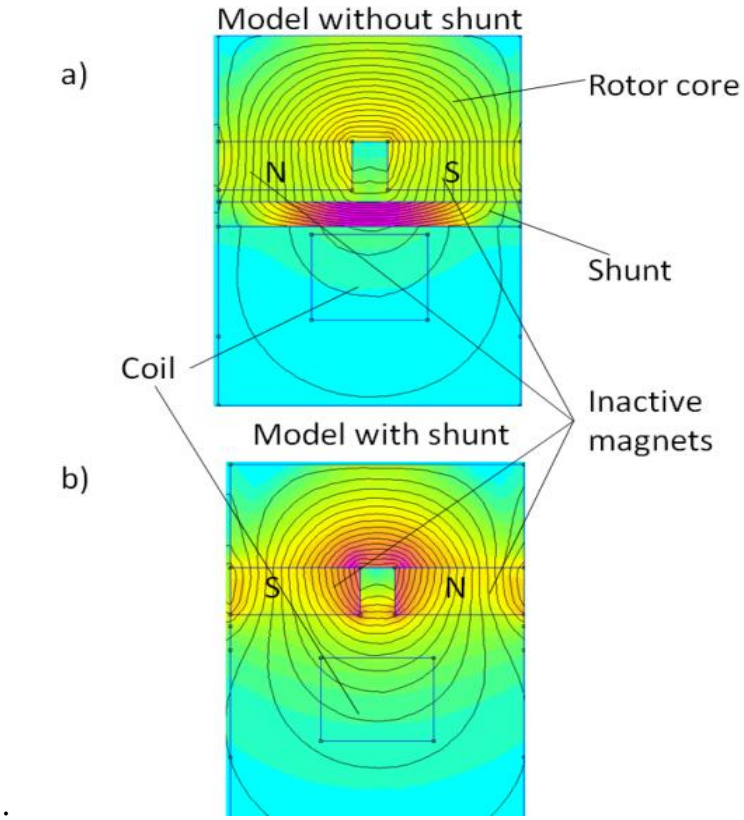

Figure 4.15 Distribution of magnetic flux in the generator: a) model with shunts, b) model without shunts

4.3 Torque Developed by the Generator

One of the most important parameters of electrical machine is the electromagnetic torque. It is important to know not only its average value but also how it changes in time. With help of FEM an electromagnetic torque was calculated at rated current separately for each phase and also as a resultant for the whole generator. The results are shown in Fig. 4.16 a, and 4.16 b. The waveform of torque for the single phase calculated for original design shows a significant torque ripple. Its value was calculated as follows [48]:

$$t_r = \frac{T_{max} - T_{min}}{T_{max} + T_{min}} \cdot 100\% \quad (4.1)$$

$$t_r = \frac{70-3}{70+3} \cdot 100\% = 92\%$$

This torque ripple is much smaller when all three phases are considered (Fig. 4.16 b). Its value is equal to:

$$t_r = \frac{101-76}{101+76} \cdot 100\% = 14\%$$

The main cause of the torque ripple is from the cogging torque. It is caused by interaction of the rotor magnets with stator poles. The cogging torque component is shown in Fig. 4.17 a and 4.17 b. Cogging torque amplitude of 23 Nm of a single phase is seven times higher than the one developed by all three phases (Fig. 17 b). The reduction of resultant cogging torque is caused by a 120 electrical degrees permanent magnets shift on the adjacent rotor discs that belong to the two other phases.

An implementation of magnetic shunts to the stator rings of all three phases influences the magnetic field distribution and this contributes to the further reduction of cogging torque. This is illustrated in Fig. 4.18 where the waveforms of the resultant torque (Fig. 4.18 a) and its cogging component (Fig. 4.18 b) are presented. The amplitude of the cogging torque is equal to 1 Nm. The torque ripple coefficient calculated for the generator with magnetic shunts is equal to 5%. The average torque developed by the generator equals to 105 Nm.

In general, the torque ripple causes noise and vibration of the rotor what can lead to the rotor deformation. Also, with a low cogging torque it is easier for a wind turbine to start rotating. These above mentioned reasons emphasize the importance of cogging torque reduction what has been achieved.

a)

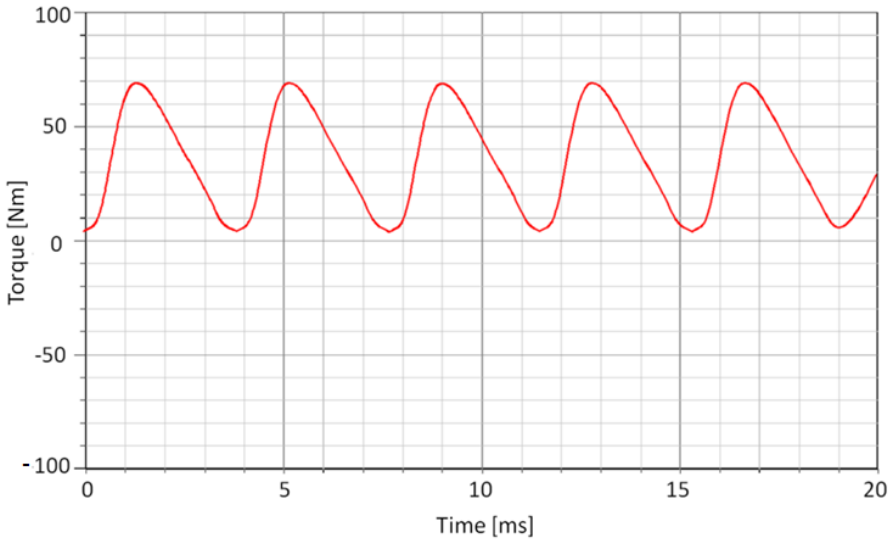

b)

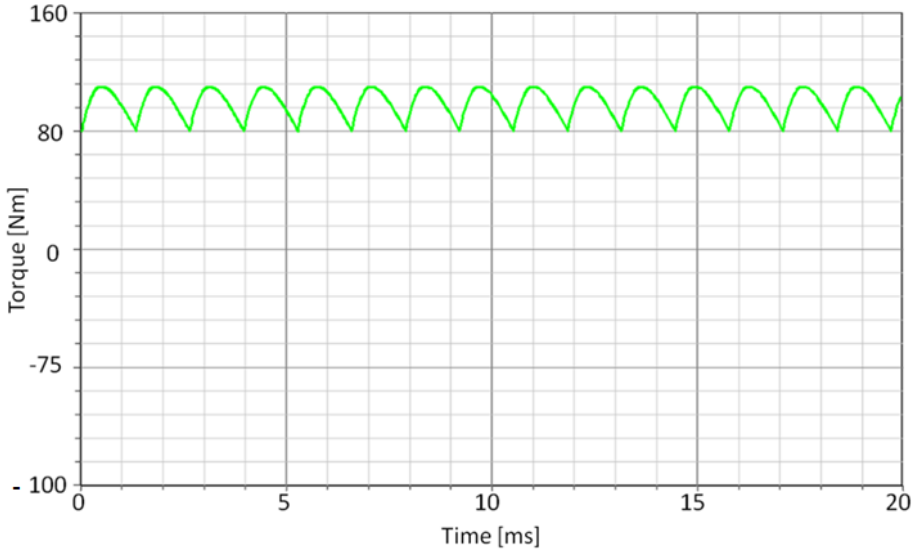

Figure 4.16 Torque developed by the generator: a) single-phase model, b) 3-phase model

a)

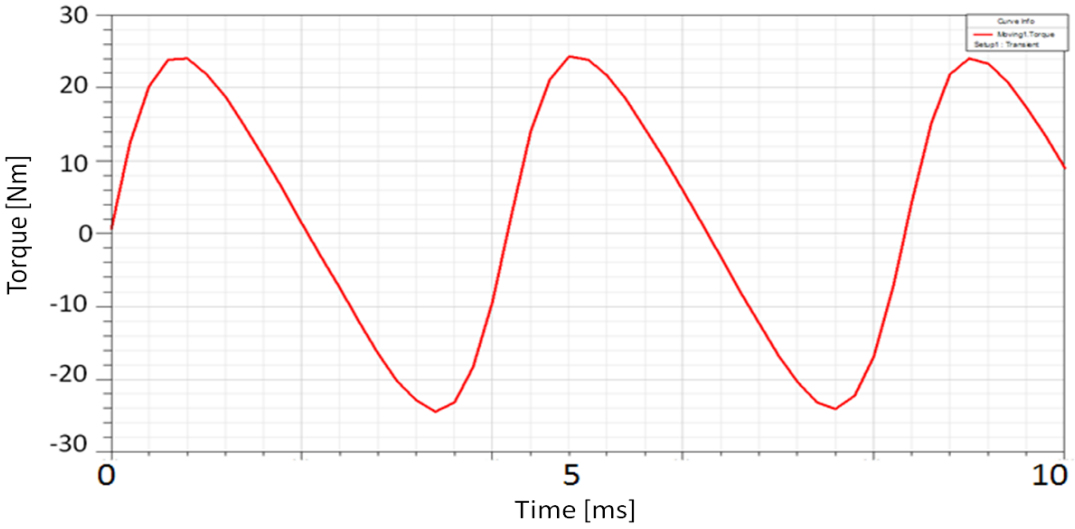

b)

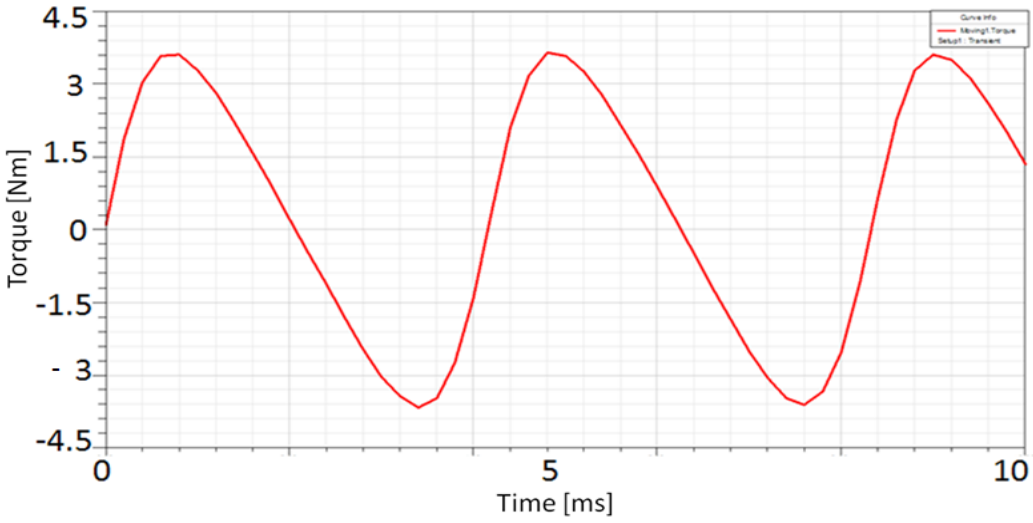

Figure 4.17 Cogging torque of the machine without the shunts: a) single-phase model, b) 3-phase model

For the 3-phase machine structure with shunts, cogging torque is almost negligible (Fig. 4.17 b)

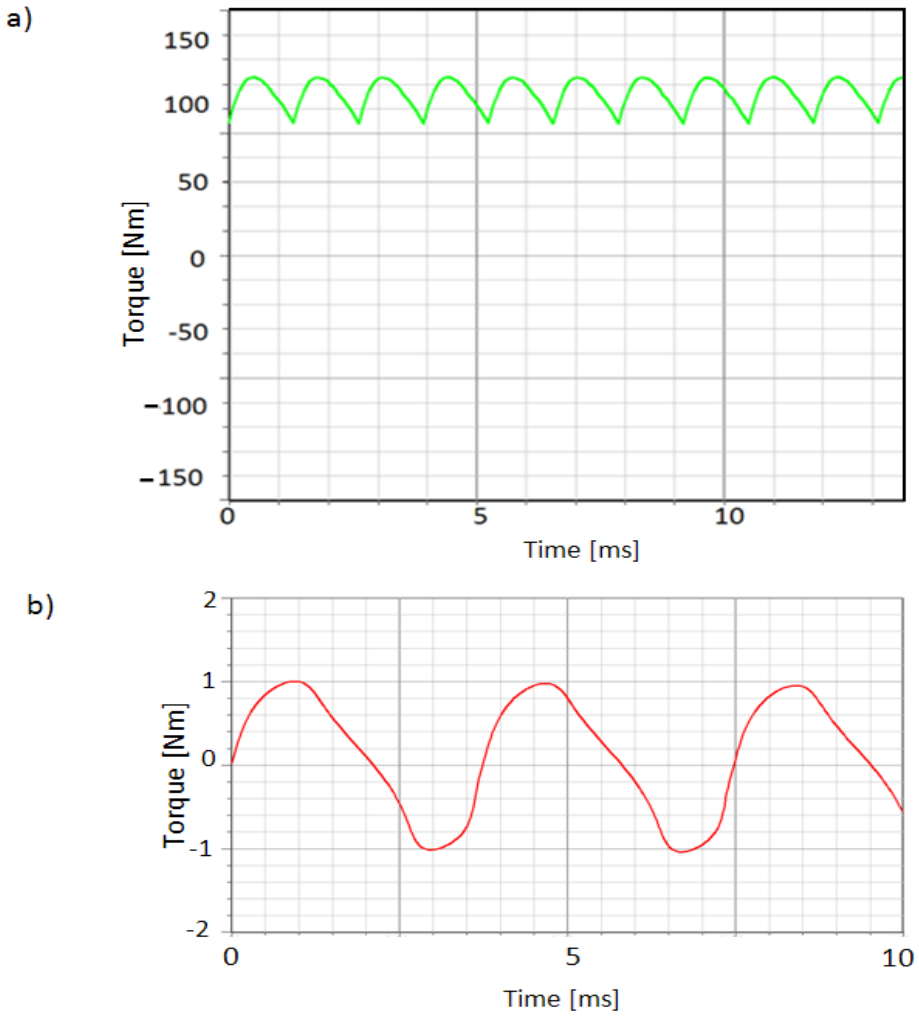

Figure 4.18 a) Torque of the machine with shunts for 3-phase model, b) cogging component of the torque

4.4 An increase of Flux Linkage with Stator Pole Shape Modification

Stator pole shape of the topology of 2010 (Fig. 1.1) is designed in such a way that the width of the pole shoe is the same as magnet width. In case of the presented machine, due to such a construction, magnetic flux density in the pole is 1.1 T and may be increased to 1.6 T (around saturation for laminated steel). To achieve this, stator poles were modified as it shown in Fig. 4.19.

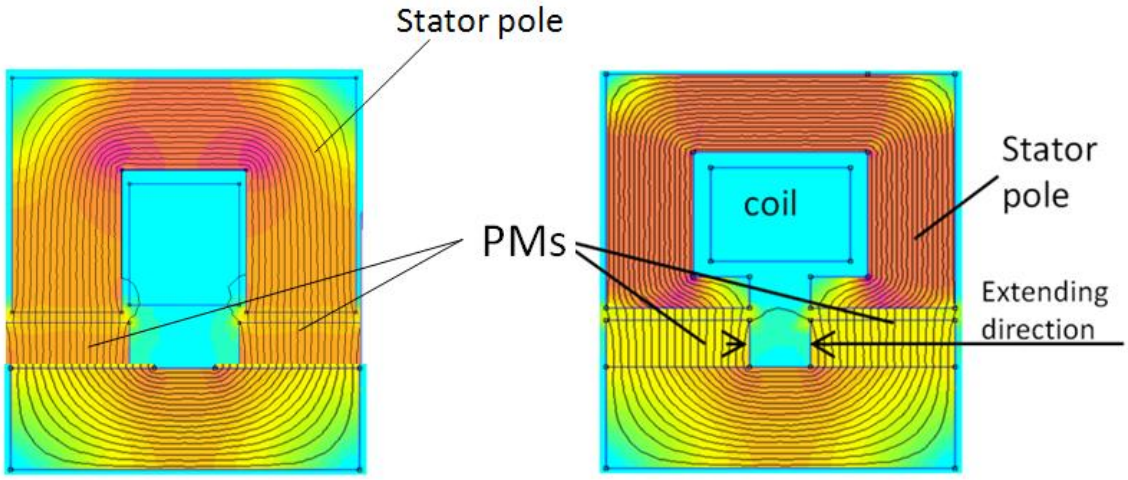

Figure 4.19 Stator pole configuration: a) original version, b) modified version with partially closed slots

Slots are partially closed around the coil and magnets are extended as it shown in Fig. 4.19. The dimensions of generator elements after modifications are shown in Fig. 4.20. They indicate that the diameter of the generator remains the same as well as the thickness of the stator pole core.

The number of turns of the same wire can be increased by 14 (50%) and magnetic field density in the pole core to 1.6 T. The induced voltage of the generator with the new stator pole configuration and with magnetic shunts is: $E_{max}=58\ V$, which is 80% higher than that of the generator with the original version of stator poles. It implies an increase of the generator power to 1.5 kW, it is by 35% with respect to construction with magnetic shunts shown in Fig. 4.11 and by 90% with respect to the original version shown in Fig. 3.3.

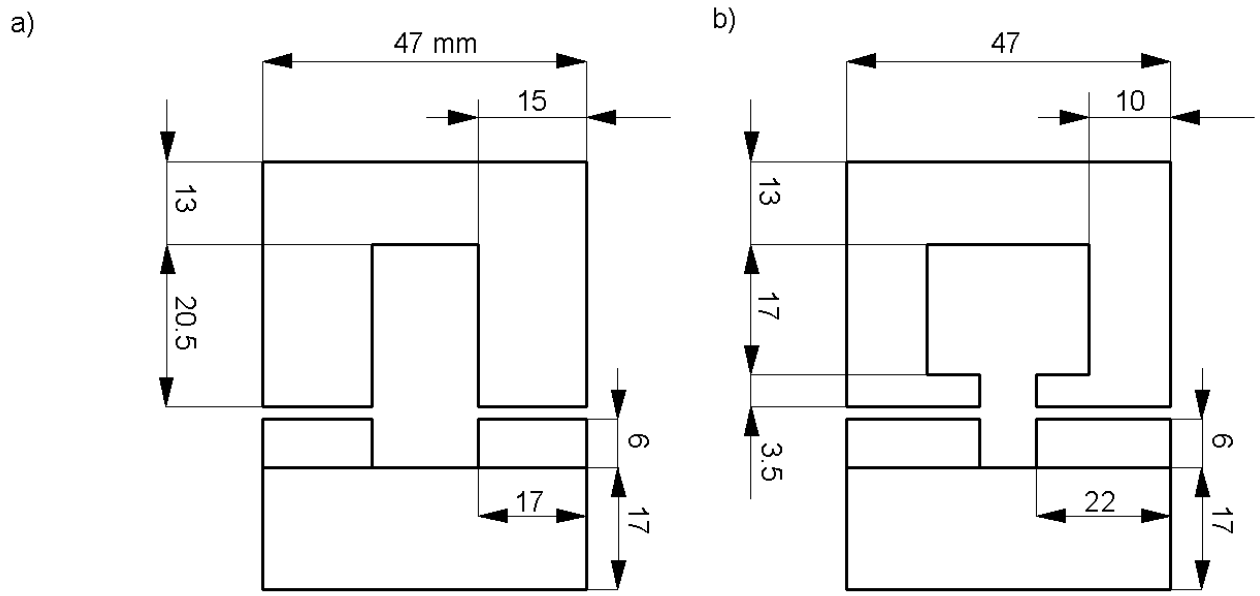

Figure 4.20 Dimensions of the generator elements: a) original version, b) modified version

Increasing number of turns might affect coil temperature. Coil Temperature analysis is done is the next section.

4.5 Coil Temperature Analysis

A simplified ePhysics 12v temperature model of the generator confined to one phase and one stator pole-pitch was created. It consists of the coil with certain number of conductors with rated current flowing through. The model is built based on the following assumptions:

1. There is no heat transfer between phase rings, so only one phase can be analyzed.

2. There is no heat transfer around the ring, so only one stator pole pitch is considered.

3. The heat is equally distributed in the ring, so a part of it can be analyzed.

4. Forced air cooling is ignored.

ePhysics 12v coil heat model is shown in Fig. 4.21.

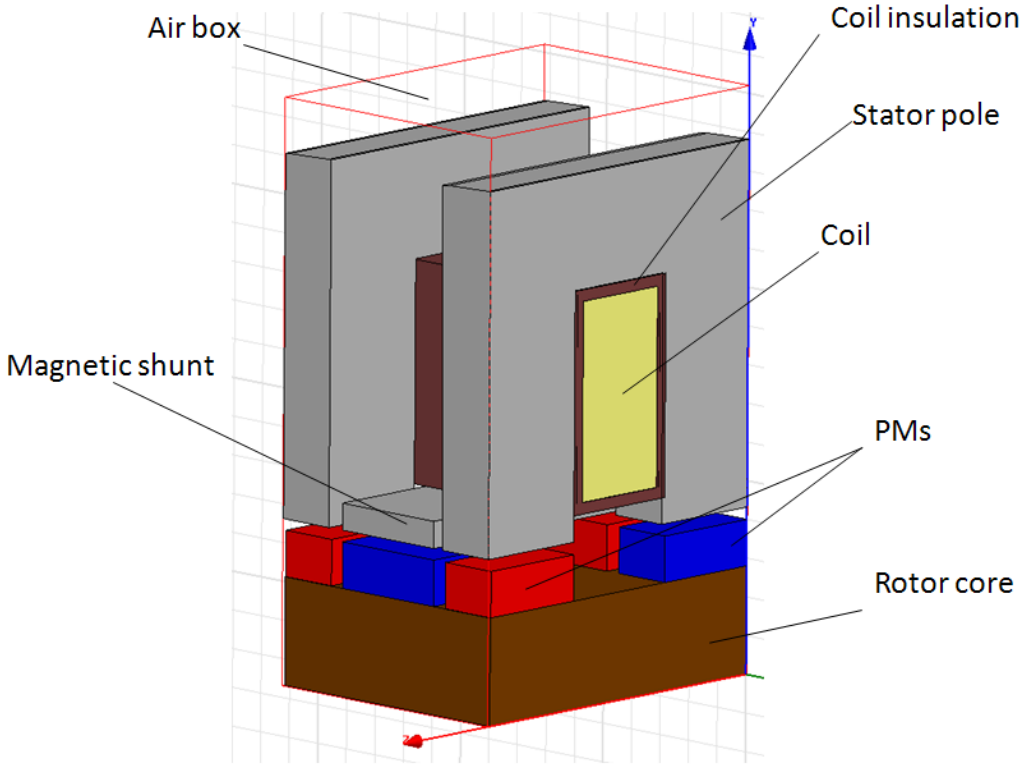

Figure 4.21 Heat computational model of the generator

To verify the correctness of the model, it was simulated with parameters of the prototype model (see Table 3.1). So, in this simulation the coil has 28 turns. The current applied to the winding is 17 A. Ambient temperature of the coil at initial time 0 is 21 C°. Results of simulation are shown in Table 4.1.

Table 4.1 Coil temperature results of the prototype and ePhysics 12v model

Model	Prototype	ePhysics model
Temperature of the phase winding, C°	24	25.1

The graph of winding temperature calculated in ePhysics is shown in Fig. 4.22.

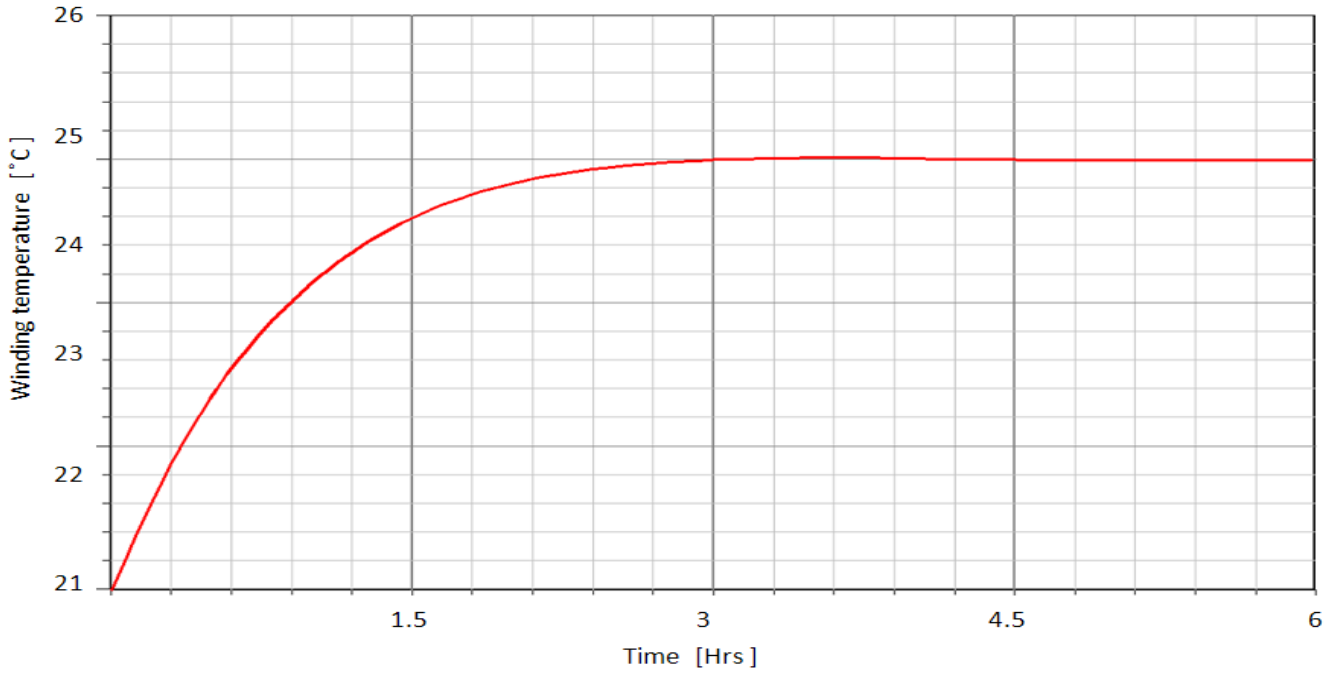

Figure 4.22 Temperature of the coil of the original version of the machine

The results obtained from the prototype test and FEM model slightly differ. This is because of the assumption 3. In normal operation condition the rotor is rotating and the generator is cooled more intensively

The temperature analysis of the improved model with modified slot (Fig. 4.20 b) that posses 44 turns was carried out too. The ambient temperature and the winding current remain the same as in previous simulation. The result of the simulation is plotted in Fig. 4.23.

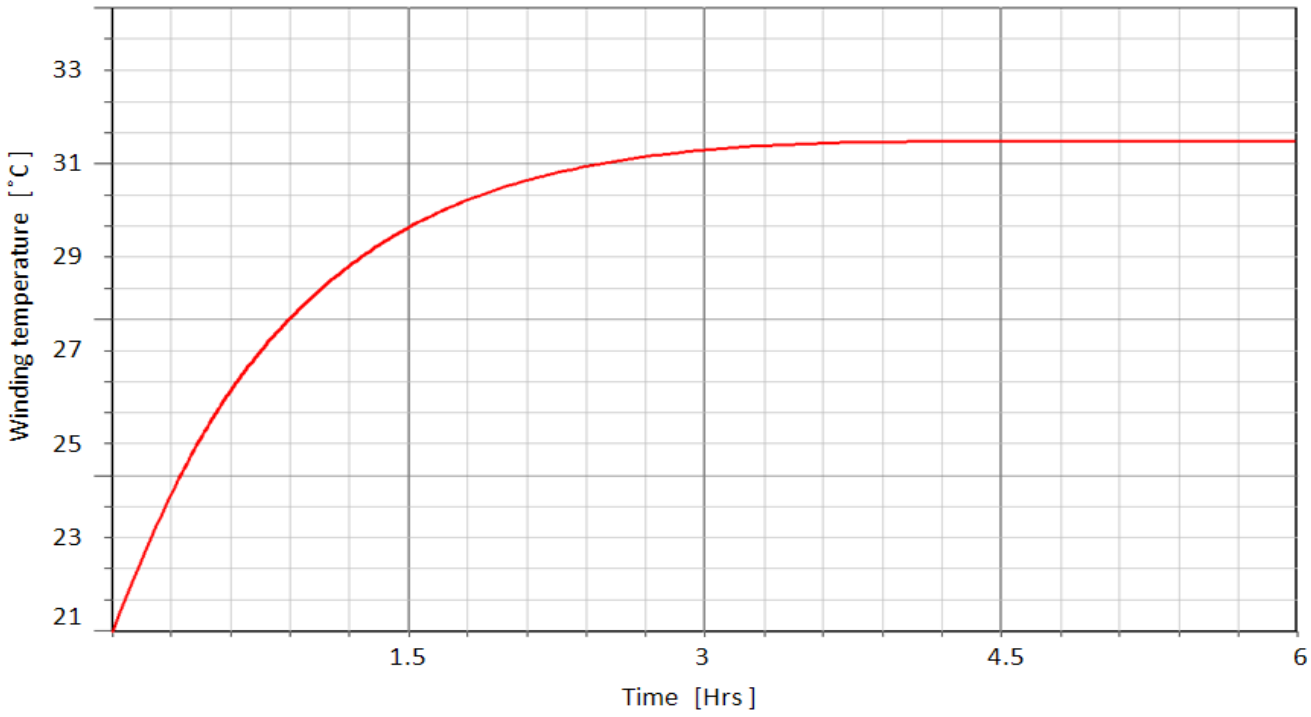

Figure 4.23 Coil temperature of the improved model with new number of turns

With the new number of turns and with the presence of the magnetic shunt (made with laminated steel), the coil gets heated to 31.5 C°.

The temperature analysis shows that new modifications introduced in this chapter will not contribute to overheating of the winding. However, temperature of the winding can be affected by the temperature of magnetic shunts. The simulation shown above was done in case of the machine with laminated steel shunts. If another material is selected (iron), temperature of the shunt might be higher due to high eddy current induced in the shunts. The temperature with different metals for shunts is studied in the next chapter.

The results presented in this chapter and conclusions lead out to designing the new generator of 1 kW power on the request of the Nevada University, Reno, which sponsored the project.

CHAPTER 5: 1 KW PMTF GENERATOR WITH INTERNAL STATOR

5.1 General Description of Generator Construction

In PMTF generators only half of the PMs are “active” at particular time instant. The other half of PMs contribute to the negative flux linkage what causes the smaller voltage to be induced in the generator winding. Thus, lower output power is generated. To diminish this negative influence iron bridges are proposed in [16] which are placed between stator poles. This, however, increases generator dimensions what causes lower power to mass ratio. Moreover, eddy currents are induced in these bridges what increases the power losses and temperature of the winding and PMs.

In the previous chapter laminated magnetic shunts were proposed. And a thorough analysis of flux distribution in the generator was done in order to maximize the power of the generator at a given volume. In this chapter a 1 kW PMTF generator with internal stator and magnetic shunts is proposed and its performance is analyzed.

A scheme of the generator is shown in Fig. 5.1. The inner stator attached firmly to the shaft consists of three rings of magnetic poles, each for different phase. The magnetic poles are U-shaped cores distributed evenly around the stator with the coil placed inside of the stator slots (see Fig. 5.2). The outer rotor also has three rings that match the stator rings. Each ring has two rows of PMs. To increase the flux linkage of the coils, magnetic shunts are placed axially between the stator poles (see Fig. 5.1). The effectiveness of the magnetic shunts was discussed in Chapter 4.

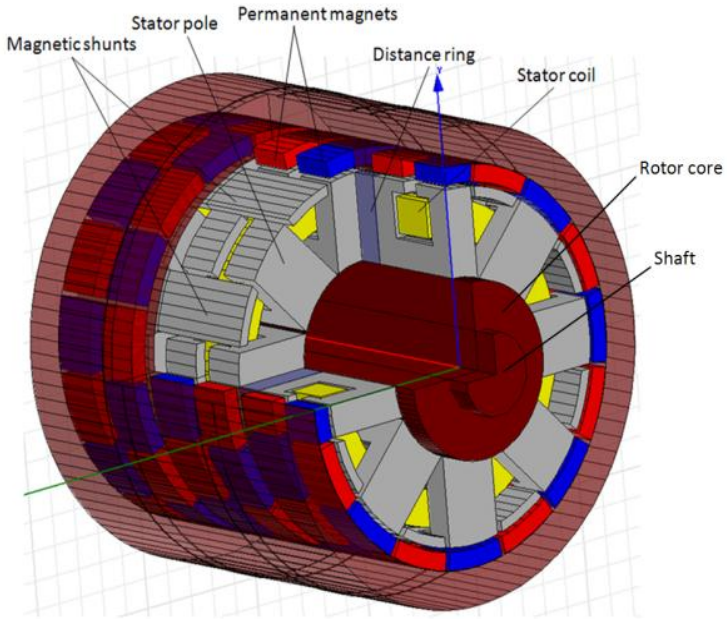

Figure 5.1 PMTF generator with inner stator

In order to obtain 3-phase voltages displaced in time by 120 degrees, magnet pairs of each phase ring have a shift as it shown in Fig. 5.3. In the generator discussed here with eight pole pairs this shift is equal to 15 degrees.

a) **b)**

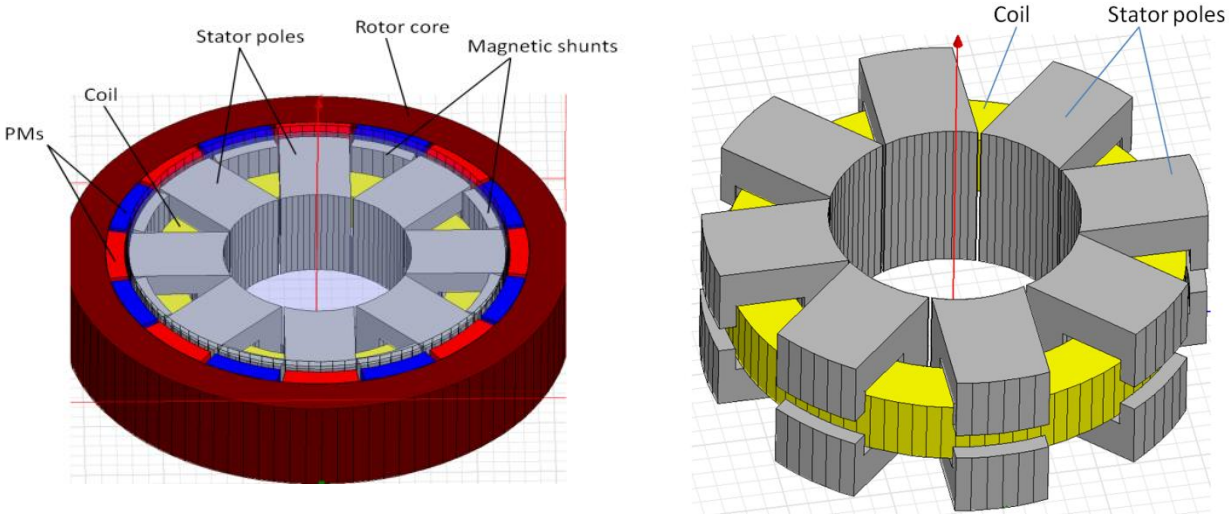

Figure 5.2 a) A single-phase ring of PMTF generator, b) stator poles with the coil

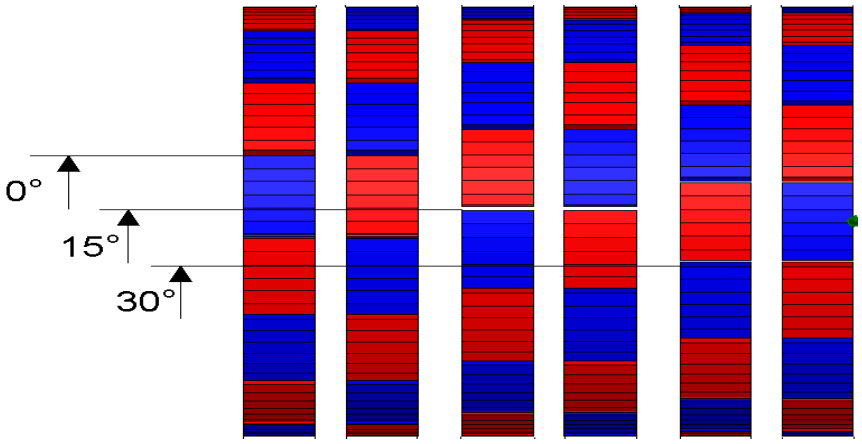

Figure 5.3 Magnets axial layout

5.2 Determination of Design Parameters of PMTF Generator

To determine the provisional dimensions of the generator the magnetic circuit model is applied in which the real machine is simplified. This simplification is described by the assumptions that are declared. Once the dimensions are determined and the winding parameters are calculated the generator is modeled in FEM software and its designed parameters are optimized.

5.2.1 Magnetic Circuit Model of the Generator and Design Calculations

The generator model is defined by following assumptions:

- The magnetic permeability of the stator and rotor cores is infinitely high ($\mu_c \approx \infty$).
- The magnetic flux that links the stator winding changes in time sinusoidally (magnetic flux linkage: $\lambda = \lambda_m \sin \omega t$).
- The flux linkage comes entirely from “active” magnets (magnetic shunts eliminate the negative flux linkage coming from “inactive” magnets).

- There is no magnetic link between phase windings.
- The coil current does not influence the magnetic flux in the air-gap which is set by the permanent magnets.

The initial data of the generator to be designed are as follows:

- $S_{in} = E_f I_a = 1200\ VA$ - input apparent power;
- $V_{ph} = \frac{V}{\sqrt{3}} = \frac{60}{\sqrt{3}} = 35.3V$ - phase voltage;
- $n = 600\ rpm$ – rated angular speed of the rotor;
- $f = 60\ Hz$ – supply frequency;
- $B_{av} = 0.9\ T$ - average magnetic flux density in the air-gap;
- $C_m = 0.9$ – coefficient: $C_m = B_{av}/B_{max}$, where B_{max} – air-gap flux density under the magnets;
- $g = 0.0015\ m$ - air-gap;
- $B_{s,Fe} = 1.6\ T$ - flux density in the stator core;
- $B_{r,Fe} = 1.2\ T$ - flux density in the rotor core;
- $J = 19000\ A/m$ - current loading (linear current density of the stator in axial direction);
- $J_w = 4$ A/mm^2– wire current density;
- $K_E = \frac{V_{ph}}{E_f} = 0.85$ – ratio of phase voltage to stator emf;
- $K_n = 1$ – decreasing flux linkage coefficient;
- $K_M = 0.8$ - ratio of axial stator pole width to total magnet width: $K_M = W/W_m$ (Fig. 5.4);
- $K_W = 0.7$ - winding filling coefficient;

- $b_{Fe} = 0.004$ - width of the stator slot closing.
- $B_r = 1.2\ T$ - Remnant magnetic flux density for magnets NdFeB 35;
- $Hc = 90000\ \mathrm{A/m}$ – Coercive field strength of the magnets ;

Dimensions of the machine which are to be determined are shown in Fig. 5.4.

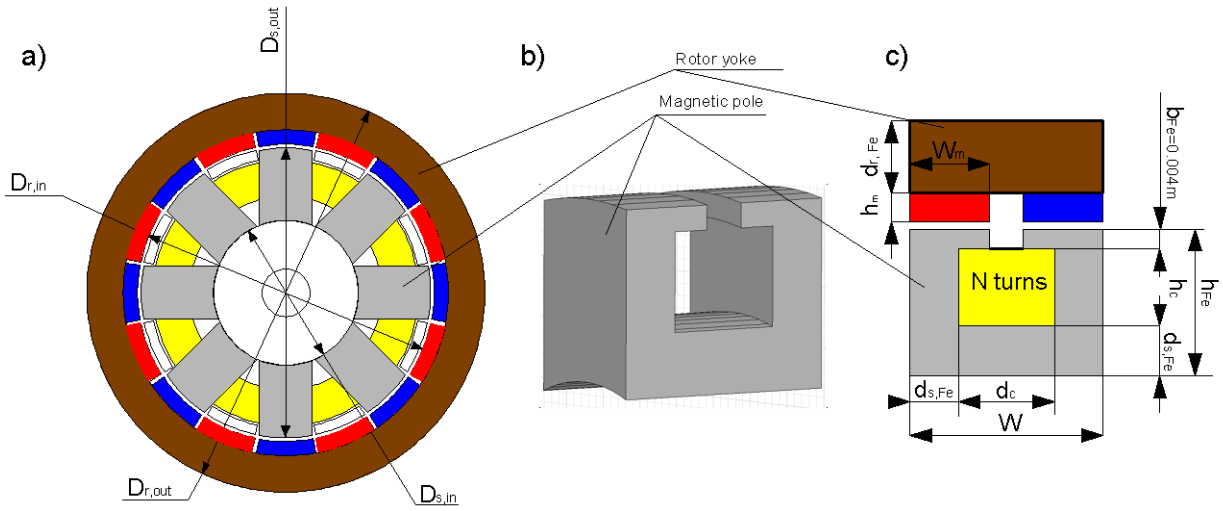

Figure 5.4 Dimensioning details of PMTF machine: a) radial cross-section, b) stator pole view, c) axial cross-section view

❖ Determination of generator dimensions.

➢ Magnet height l_m. Referring to Fig. 5.5, equations for calculating the magnet height can be derived.

The magnet height depends on the type of magnet material (its B-H characteristic) and the air-gap. To derive the equation for the magnet height let the half of stator pole rotor magnet be considered as in Fig. 5.6.

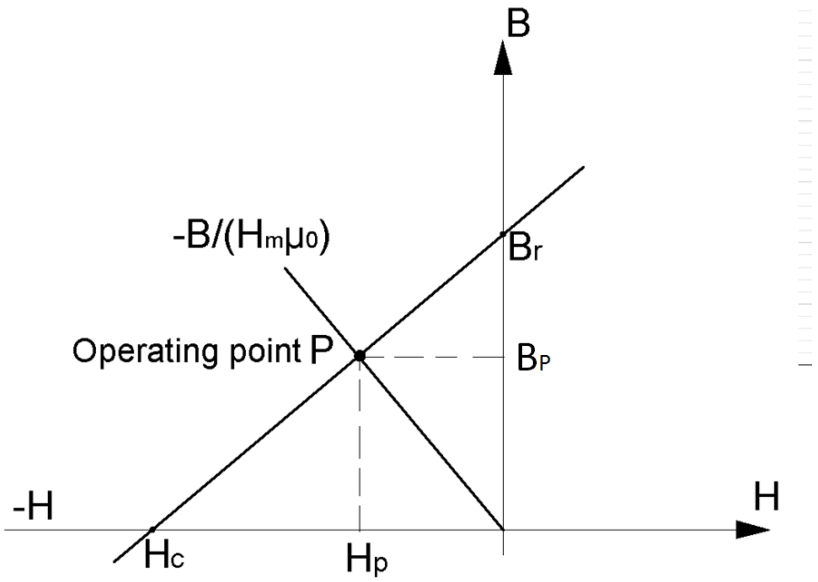

Figure 5.5 Demagnetization part of B-H characteristic for air-gap [65]

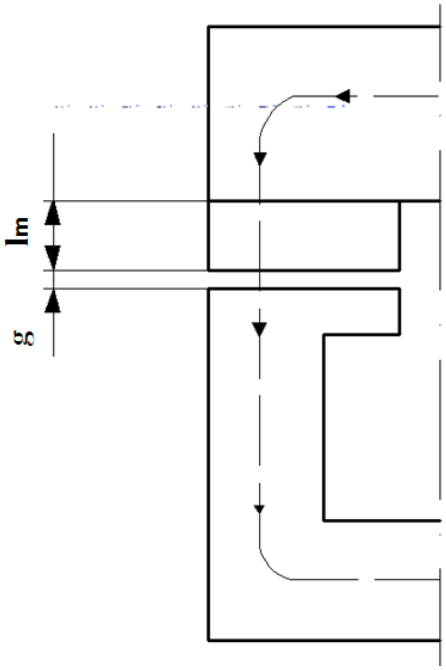

Figure 5.6 Half of the stator pole with PM

Assuming stator and rotor core permeability $\mu_c = \infty$, according to Amper's Law:

$$H_m l_m + H_g g = 0 \tag{5.1}$$

where:

H_m - magnetic field intensity of the PM

H_g - magnetic field intensity in the air-gap

l_m - magnet height

g - air gap width.

From Eqn. 5.1 the field intensity in the air-gap is:

$$H_g = -\frac{l_m}{g} H_m \tag{5.2}$$

After multiplication by μ_0:

$$B_g = -\frac{l_m}{g} H_m \mu_0 \tag{5.3}$$

Since for NdFeB magnets the demagnetization curve shown in Fig. 5.5 is straight line it can be described as:

$$B_m = \frac{B_r H_m}{|H_c|} + B_r \ \rightarrow H_m = \frac{(B_m - B_r)|H_c|}{B_r} \tag{5.4}$$

For air-gap from Eqn. 5.2:

$$B_g = -\frac{l_m}{g} \mu_0 H_m \ \rightarrow H_m = -\frac{B_g g}{\mu_0 l_m} \tag{5.5}$$

Equaling equations (5.4) and (5.5) for H_m gives:

$$\frac{(B_m - B_r)|H_c|}{B_r} = -\frac{B_g g}{\mu_0 l_m} \tag{5.6}$$

At the operation point P $B_m = B_g$ (see Fig. 5.5), thus solving (5.6) for l_m:

$$l_m = \frac{g B_r B_g}{\mu_0 |H_c| (B_r - B_g)} \tag{5.7}$$

- Number of pole pairs p is found from:

$$p = \frac{120f}{n} \tag{5.8}$$

- Stator outer diameter $D_{s,out}$ calculation.

The stator outer diameter can be found from the equation for the input power S. Considering one phase:

$$S_{ph} = E_{ph} I_{ph} \tag{5.9}$$

where:

I_{ph} - is rms current

E_{ph} - is rms electromotive force which for sinusoidal changing flux $\Phi = \Phi_{max} sin\omega t$ equals:

$$E_{ph} = \overline{2}\pi f \phi_{max} N_{ph} K_n \tag{5.10}$$

where:

N_{ph} - number of turns per phase

ϕ_{max} – maximum in time flux.

The magnetic flux ϕ_{max} is found as:

$$\phi_{max} = B_{av} A_{st} \tag{5.11}$$

where: A_{st} – is the resultant area under the stator pole in the air-gap.

$$A_{st} = \frac{W}{2} \pi D_{s,in} \tag{5.12}$$

Hence,

$$\phi_{max} = \pi D_{s,in} \frac{W}{2} B_{av} \tag{5.13}$$

Substituting (5.13) into (5.10) the induced phase voltage is:

$$E_{ph} = \overline{2}\pi f \pi D_{s,in} \frac{W}{2} B_{av} N_{ph} K_n \quad (5.14)$$

Expressing the voltage frequency as:

$$f = pn/120 \quad (5.15)$$

and substituting (5.14) into (5.9) the equation for input power S_{ph} looks like:

$$S_{ph} = \overline{2}\pi \frac{pn}{120} \pi D_{s,in} \frac{W}{2} B_{av} N_{ph} I_{ph} K_E K_n \quad (5.16)$$

Since the current loading,

$$J = \frac{N_{ph} I_{ph}}{W} \quad (5.17)$$

substituting it into (5.9) results:

$$S_{ph} = \overline{2}\pi^2 \frac{pn}{120} D_{s,in} \frac{W^2}{2} J B_{av} K_E K_n \quad (5.18)$$

From this equation active surface of the generator $\pi D_{s,in} W$ multiplied by the stator width W is found:

$$\pi D_{s,in} W^2 = S_{ph} * 60/(1.06 \pi pn J B_{av} K_E K_n) \quad (5.19)$$

$D_{s,in}$ - can be assumed on this stage of calculation. The assumption is based on the choice of the designer who can decide about generator proportion as length to the diameter ratio.

- Pole pitch of the stator poles τ at outer diameter is determined by:

$$\tau = \frac{D_{s,in} \pi}{p/2} \quad (5.20)$$

Since, according to design configuration (Fig. 5.4 a)

- Stator inner periphery:

$$D_{s,in} \pi = \frac{p}{2} \tau \quad (5.21)$$

- Stator outer periphery:

$$D_{s,out}\pi = p\tau \tag{5.22}$$

The equation (5.22) takes the form:

$$\tau = \frac{D_{s,out}\pi}{p} \tag{5.23}$$

- Stator pole height:

$$h_{Fe} = (D_{s,out} - D_{s,in})/2 \tag{5.24}$$

- Stator ring width :

$$W = \frac{\overline{D_{s,in}W^2}}{D_{s,in}} \tag{5.25}$$

- Now, after obtaining actual stator dimensions input power S of the generator for all three phases can be verified as:

$$S = 3 \cdot 1.06 \frac{pn}{2 \cdot 60} \pi^2 B_{av} J K_n K_E D_{s,in} W^2 \tag{5.26}$$

- Magnet axial width:

$$W_m = K_M W/2 \tag{5.27}$$

- Width of the stator core: (see Fig. 5.4):

$$d_{s,Fe} = \frac{B_{av}W}{2B_{s,Fe}} \tag{5.28}$$

- Width of the rotor core:

$$d_{r,Fe} = \frac{B_{av}W}{2B_{r,Fe}} \tag{5.29}$$

- Width of the coil:

$$d_c = W - 2d_{s,Fe} \tag{5.30}$$

- Rotor inner diameter:

$$D_{r,in} = D_{s,out} + 2g \tag{5.31}$$

- Rotor outer diameter:

$$D_{r,out} = D_{s,out} + 2g + 2h_m + 2d_{r,Fe} \tag{5.32}$$

❖ Determination of generator winding parameters.

- Due to the voltage drop across generator phase impedance, the output voltage V_{ph} is smaller than emf E_{ph} and this can be expressed by coefficient K_E. Thus, electromotive force:

$$E = \frac{V_{ph}}{K_E} \tag{5.33}$$

- Number of turns N can be found rearranging the equation (5.16) for electromotive force:

$$E_{ph} = \frac{\overline{2}N_{ph}\pi^2 fWD_{sin}B_{av}K_n}{2} = \frac{\overline{2}N_{ph}\pi^2 p/2nWD_{sin}B_{av}K_n}{240}$$

$$\rightarrow N_{ph} = \frac{E_{ph}}{0.058p/2nWD_{s,in}B_{av}K_n} \tag{5.34}$$

- Calculated number of turns N_{ph} can be rounded by a designer. After this new number of turns N is verified to satisfy phase *emf*:

$$E_{ph} = N_{ph} \cdot 0.058p/2nWD_{s,in}B_{av}K_n \tag{5.35}$$

- For a three-phase Y-connected supply, depending on load power factor $\cos(\varphi)$ the current rating is obtained :

$$I = S/3V_{ph} \tag{5.36}$$

- Wire diameter:

$$D_w = 2\ \overline{I/(J_w\pi)} \tag{5.37}$$

Based on the calculated wire diameter, the wire type can be selected from AWG gauge table (Table 5.1) which is shown below.

Table 5.1 American Wire Gauge

AWG	Diam mm	Sect. mm²	Resist. ohm/m	AWG	Diam mm	Sect. mm²	Resist. ohm/m
0000	11.7	107,0	0.000161	19	0,91	0,6530	0.0264
000	10.4	85.0	0.000203	20	0,81	0,5190	0.0333
00	9.26	67.4	0.000256	21	0,72	0,4120	0.0420
0	8.25	53.5	0.000323	22	0,64	0,3250	0.0530
1	7,35	42,4	0.000407	23	0,57	0,2590	0.0668
2	6,54	33,6	0.000513	24	0,51	0,2050	0.0842
3	5,83	26,7	0.000647	25	0,45	0,1630	0.106
4	5,19	21,2	0.000815	26	0,40	0,1280	0.134
5	4,62	16,8	0.00103	27	0,36	0,1020	0.169
6	4,11	13,3	0.00130	28	0,32	0,0804	0.213
7	3,67	10,6	0.00163	29	0,29	0,0646	0.268
8	3,26	8,35	0.00206	30	0,25	0,0503	0.339
9	2,91	6,62	0.00260	31	0,23	0,0415	0.427
10	2,59	5,27	0.00328	32	0,20	0,0314	0.538
11	2,30	4,15	0.00413	33	0,18	0,0254	0.679
12	2,05	3,31	0.00521	34	0,16	0,0201	0.856
13	1,83	2,63	0.00657	35	0,14	0,0154	1.08
14	1,63	2,08	0.00829	36	0,13	0,0133	1.36
15	1,45	1,65	0.0104	37	0,11	0,0095	1.72
16	1,29	1,31	0.0132	38	0,10	0,0078	2.16
17	1,15	1,04	0.0166	39	0,09	0,0064	2.73
18	1,02	0,82	0.0210	40	0,08	0,0050	3.44

- Coil cross-section area is found (packing coefficient is ignored due to selection of rectangular type of wire):

$$A_c = \frac{\pi {D_w}^2}{4} N_{ph} \tag{5.38}$$

- Total area of the slot is calculated taking into account winding insulation:

$$A_{(slot)total} = A_c / K_w \tag{5.39}$$

- Height of the coil:

$$h_c = A_{(slot)total} / d_C \tag{5.40}$$

- Actual height of the stator pole :

$$h_{Fe} = b_{Fe} + h_C + d_{s,Fe} \tag{5.41}$$

- Average length of the coil:

$$L_C = \pi (D_{s,out} - 2b_{Fe} - d_{s,Fe}) \tag{5.42}$$

- Coil resistance:

$$R_C = R_{Cw} L_C N \tag{5.43}$$

where R_{Cw} - resistance of the selected wire in Ω/m (see Table 5.3).

- **Example of calculations:**

  Magnet height (Eqn. 5.7):

$$l_m = \frac{1.5 \cdot 1.2 \cdot 0.9}{1.0099 \cdot 905000(1.2-0.9)} = 5.96 \text{ mm}$$

  The chosen magnet height:

$$l_m = 6 \text{ mm}$$

  Number of rotor poles (Eqn. 5.8):

$$p = 120f/n = 16$$

  Pole pitch of the stator poles τ at outer diameter (Eqn. 5.23). $D_{s,out}$ is chosen to be equal 120 mm:

$$\tau = \frac{120\pi}{16} = 23.55 \text{ mm}$$

  Stator inner periphery (Eqn. 5.21):

  Stator inner periphery:

$$D_{s,in}\pi = \frac{16}{2} 23.55 = 188.4 \text{ mm}$$

  Inner diameter of the stator (from Eqn. 5.21):

$$D_{s,in} = \frac{188.4}{\pi} = 60 \text{ mm}$$

  Stator pole height (Eqn. 5.24):

$$h_{Fe} = (120 - 60)/2 = 30 \text{ mm}$$

After selecting a value for stator ring width $W = 40\ mm$ power S of the generator is verified (Eqn. 5.26):

$$S = 1.06 \cdot \pi^2 \cdot \frac{16}{2} \cdot \frac{600}{60} \cdot 19000 \cdot 1 \cdot 0.9 \cdot 0.87 \cdot 60 \cdot 40^2 = 1195\ W$$

Magnet axial width (Eqn. 5.27):

$$W_m = 0.8 \cdot 40/2 = 16 \text{ mm}$$

Width of the stator core (Eqn. 5.28):

$$d_{s,Fe} = \frac{0.9 \cdot 40}{1.6 \cdot 2} = 11.25 \text{ mm}$$

Width of the rotor core (Eqn. 5.29):

$$d_{r,Fe} = \frac{0.9 \cdot 40}{1.2 \cdot 2} = 15 \text{ mm}$$

Width of the coil (Eqn. 5.30):

$$d_c = 40 - 2 \cdot 11.25 = 17.5 \text{ mm}$$

Rotor inner diameter (Eqn. 5.31):

$$D_{r,in} = 120 + 3 = 123 \text{ mm}$$

Rotor outer diameter (Eqn. 5.32):

$$D_{r,out} = 120 + 2 \cdot 1.5 + 2 \cdot 6 + 2 \cdot 15 = 165 \text{ mm}$$

❖ Determination of generator winding parameters.

Electromotive force (Eqn. 5.33):

$$E = \frac{60}{0.87\ \overline{3}} = 39.82\ V$$

Number of turns (Eqn. 5.34):

$$N_{ph} = 39.82/(0.058 \cdot 600 \cdot 16/2 \cdot 60 \cdot 40 \cdot 0.9 \cdot 1) = 66.22$$

The chosen number of turns is 66.

Number of turns is verified (Eqn. 5.35):

$$E_{ph} = 66 \cdot 0.058 \cdot 16/2 \cdot 600 \cdot 40 \cdot 60 \cdot 0.9 \cdot 1 = 39.8 \text{ V}$$

Current rating (Eqn. 5.36):

$$I = 1200/(3 \cdot 39.82 \cdot 0.87) \text{ = } 11.546 \text{ A}$$

The current is chosen to be 11.55 A.

Wire diameter (Eqn. 5.37):

$$D_w = 2 \sqrt{11.55/(4\pi)} = 1.9174 \text{ mm}$$

From the Table 5.3 AWG 12 wire is selected. Its diameter is 2.05.

Coil cross-section area (Eqn. 5.38):

$$A_c = \frac{\pi 2.05^2}{4} 66 = 217.842 \text{ mm}^2$$

Total area of the slot is calculated taking into account winding insulation Eqn. (5.39):

$$A_{(slot)total} = \frac{217.842}{0.7} = 311.203 \text{ mm}^2$$

Height of the coil (Eqn. 5.40):

$$h_C = 311.203/18 \text{ = } 17.78 \text{ mm}$$

The chosen value for coil height is 18 mm.

Actual height of the stator pole (Eqn. 5.41):

$$h_{Fe} = 4 + 18 + 11.25 \text{ = } 33.25 \text{ mm}$$

Average length of the coil (Eqn. 5.42):

$$L_C = \pi(120 - 2 \cdot 4 - 18) \text{ = } 295.3 \text{ mm}$$

Coil resistance (Eqn. 5.43):

$$R_C = 0.0052 \cdot 0.2953 \cdot 66 = 0.101 \ \Omega$$

Calculated parameters are enclosed in Table 5.2 and shown in Fig. 5.7. Detailed drawings of the generator parts with all dimensions are enclosed in Apendix A.

Note, that some of the dimensions which are shown on the fig 5.7 do not match those which are in table 5.2. This is because some of the dimensions were optimized to satisfy the requirements of the manufacturer (see Apendix B for more details).

Table 5.2 Dimensions of the machine

Parameters	Calculated
Rotor outer diameter $D_{r,out}$, mm	165
Rotor inner diameter $D_{r,in}$, mm	123
Magnet height h_m, mm	6
Magnet axial width W_m, mm	16
Stator pole height h_{Fe}, mm	33.25
Stator outer diameter $D_{s,out}$, mm	120
Stator inner diameter, $D_{s,in}$, mm	30
Stator ring width W, mm	40
Width of the stator core $d_{s,Fe}$, mm	11.25
Width of the rotor core $d_{r,Fe}$, mm	15

The calculated dimensions were optimized using 3D FEM modeling. The optimization of dimensions, which is discussed later, was done in order to satisfy magnetic flux distribution in the machine. This flux is shown in Fig. 5.8. The dimensions of the magnetic shunts were determined too and Fig. 5.9 shows how the shunts are assembled.

The flux distribution in axial cross-section of the single phase ring is shown in Fig. 5.10. Summarized parameters of the machine used for further analysis are enclosed in Table 5.3.

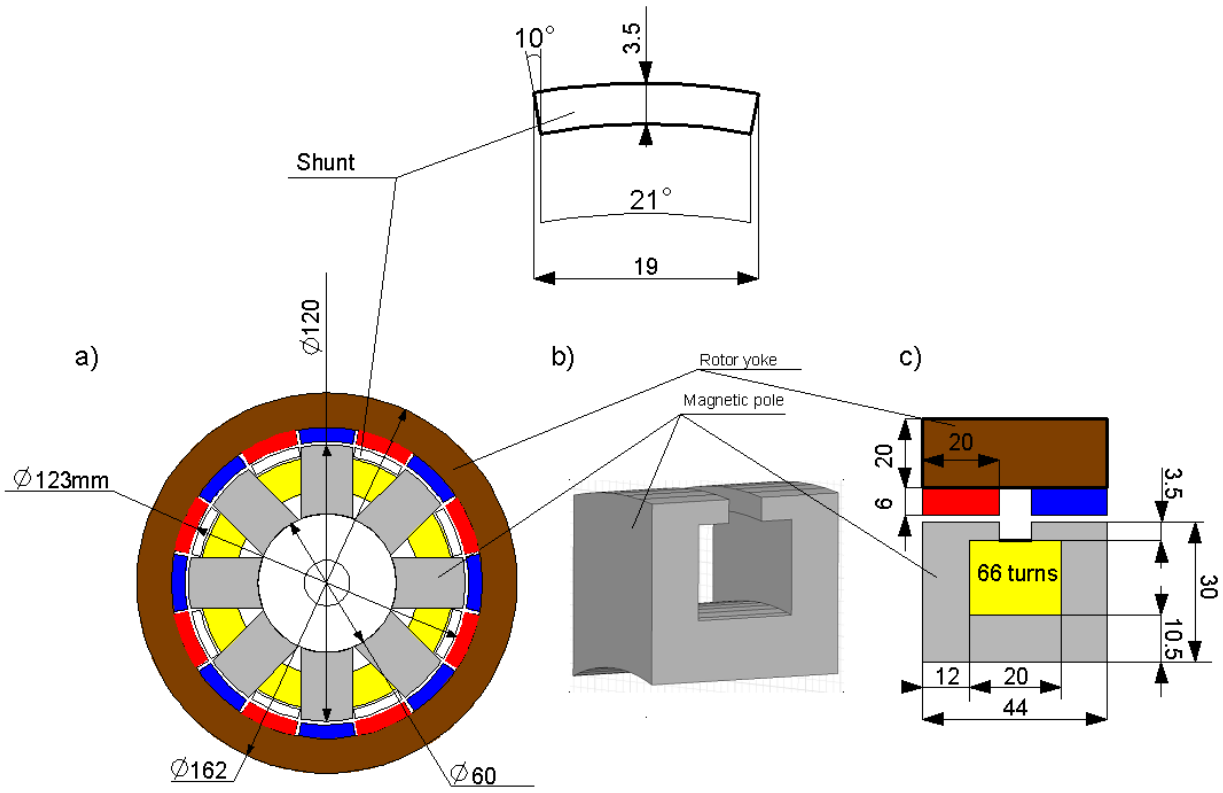

Figure 5.7 Optimized dimensions of the generator: a) radial cross-section, b) stator pole view, c) axial cross-section view

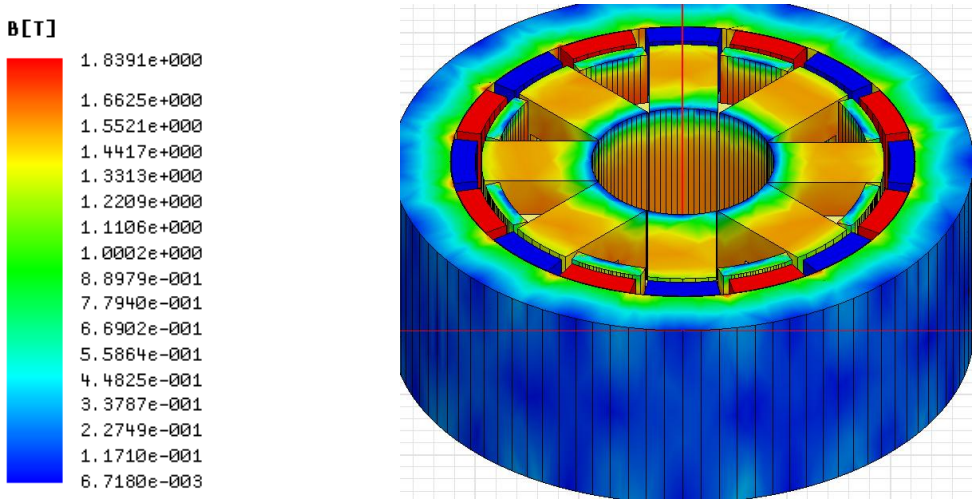

Figure 5.8 Magnetic flux distribution in the rotor and stator cores

Table 5.3 Stator winding and PMs data

Stator winding:	
- Number of phases	3
- Number of turns per phase	66
- Wire	AWG 12
- Load current I_a	11.55 A
- Winding filling factor, k_{fill}	0.7
Magnetic Circuit:	
- Number of rotor poles	p = 16
- Number of stator poles	N = 8
PM's:	
- Type	NdFeB 35
- Relative permeability, μ	1.09967
- Bulk conductivity, γ	625000 S/m
- Residual flux density, B_r	1.2T
- Thickness (radial lengths)	6 mm

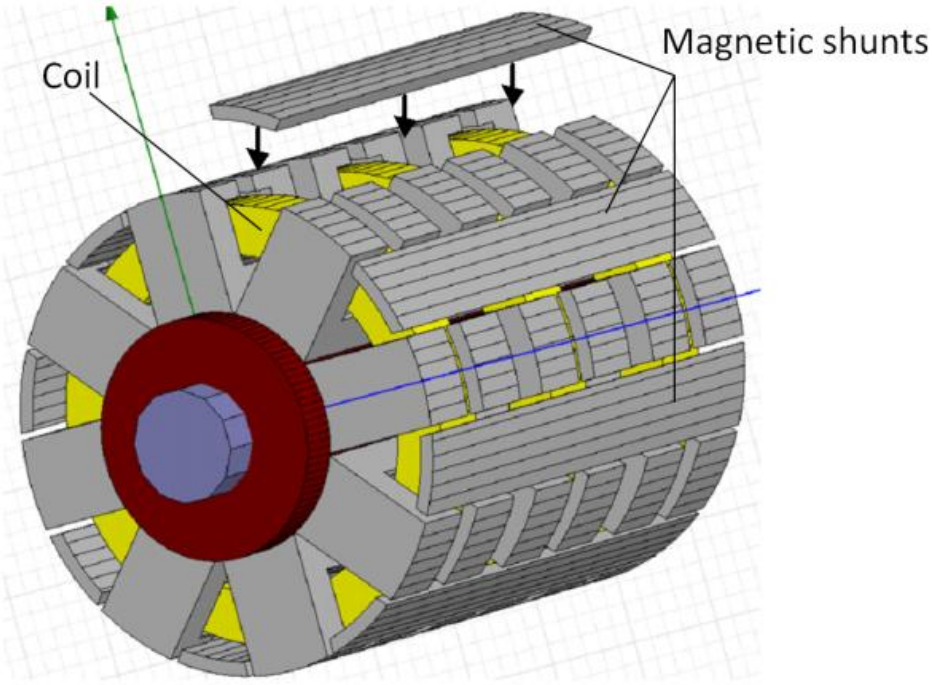

Figure 5.9 Shunt assembly

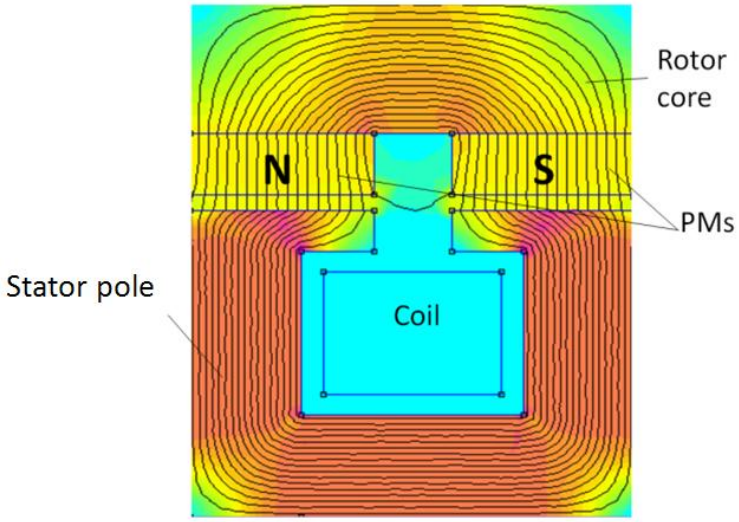

Figure 5.10 View of magnetic flux distribution in axial cross-section of the single phase ring

5.3 Performance of the Generator in Steady-State Conditions

The performance of wind power generator depends primarily on speed of the wind turbine, which is dependent on wind speed. Wind speed may change within a broad range.

5.3.1 Analysis of Induced Voltage

The 3D FEM software allows determining the induced voltage at different speeds. The current directly depends on the voltage at constant load impedance, thus the induced *emf* influences the output power of the generator.

The amplitude of the induced voltage *vs* speed characteristic is shown in Fig. 5.11. The waveforms of induced voltage calculated at speed 600 rpm (rated speed) for models with shunts made of iron and laminated steel are shown in Fig. 5.12 a, b. The voltage is distorted with respect to sinusoidal shape. This distortion can be measured by the contents of higher harmonics. Applying the Fourier's series analysis for the waveform of *emf* the spectrum of higher harmonics can be found using FFT (Fast

Fourier Transform) function in Matlab 2010 software. The diagram of higher harmonic contents is shown in Fig. 5. 14 a, b).

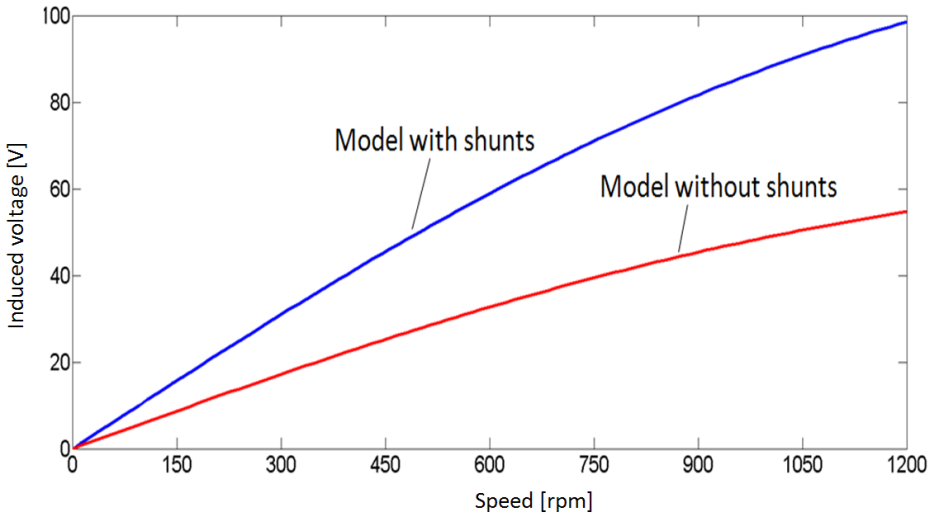

Figure 5.11 Induced phase voltage vs. speed characteristic at no load

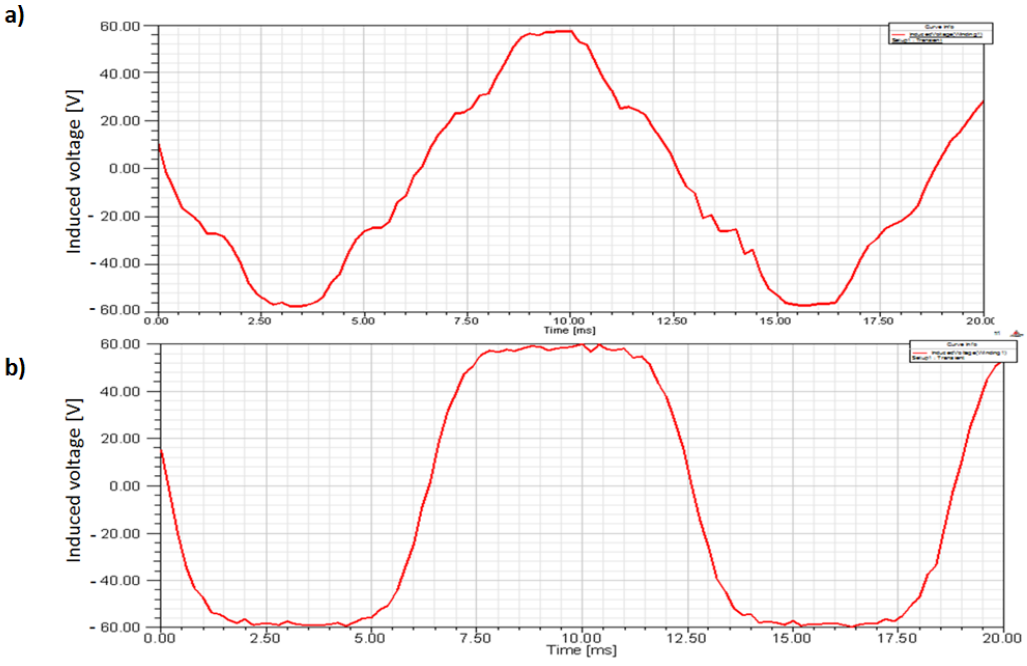

Figure 5.12 Amplitudes of induced phase voltages for the generators with: a) iron shunts, b) laminated steel shunts

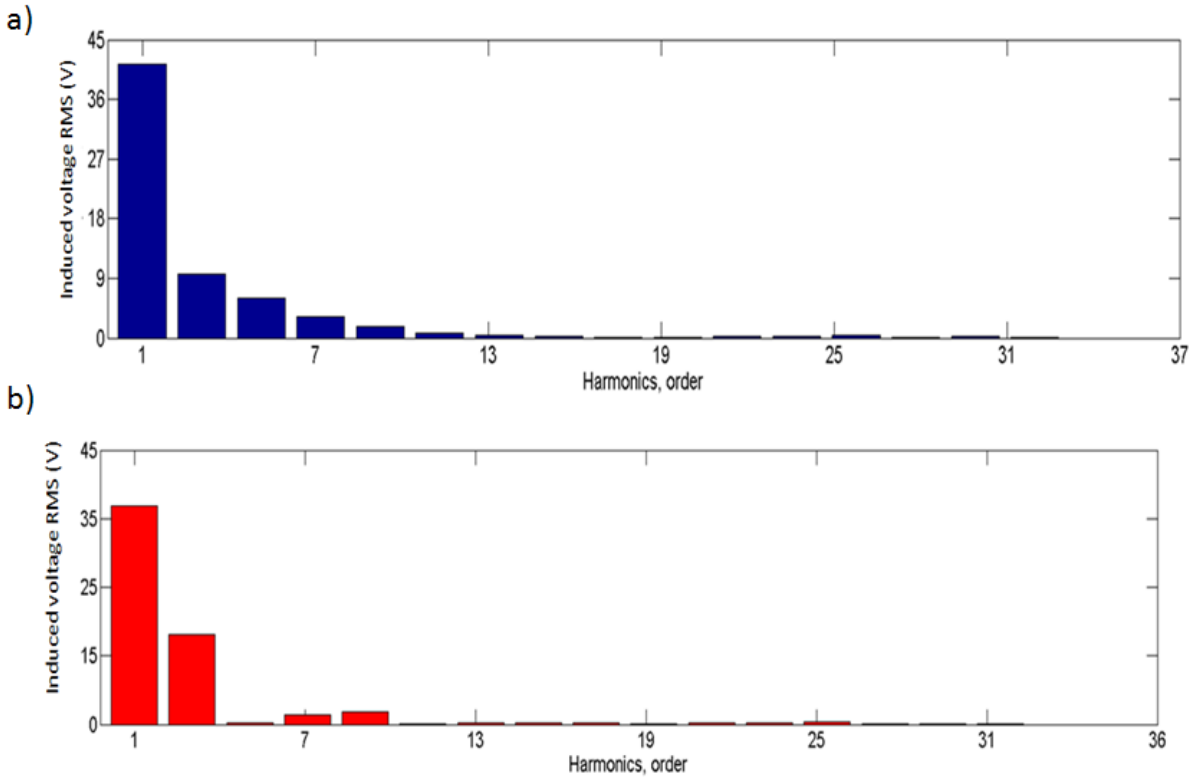

Figure 5.13 Higher harmonic content of induced voltages of the generators with: a) iron shunts, b) laminated steel shunts

For the generator with shunts made of laminated steel the 1-st harmonic is nearly 89% of the voltage peak value. The 3-rd harmonic is very high too (42%) and has a significant impact of the waveform (Fig. 5.12 b). Also some minor distortions of the waveform are caused by the 7^{th} (3%) and 9^{th} (4%) order harmonics.

In case of shunts made of solid iron, voltage waveform of the machine is more of sinusoidal shape (Fig. 5.12 a). This is because in this case the 3^{rd} harmonic is lower in its amplitude (21%). The 1-st harmonic is 88% of the voltage peak value (Fig. 5.12 a).

5.3.2 Analysis of Torque Developed by the Machine

As it was written in previous chapter torque developed by the generator is a key parameter in the machine performance. Its magnitude decides about effectiveness of energy conversion, and its waveform shows how it changes in time and influences the operation of the wind turbine at a generator set.

The analysis of the generator torque is done on the basis of the results obtained form 3D FEM modeling. The waveform of the torque developed by the generator with single phase without magnetic shunts is shown in Fig. 5.14 a. This waveform exhibits significant oscillations, which are generated by two torque components: electromagnetic torque and cogging torque. The nature of these components has been discussed in the previous chapter. The cogging torque component is shown in Fig. 5.14 b. As it is seen the percentage of this component in the total single-phase torque is very high.

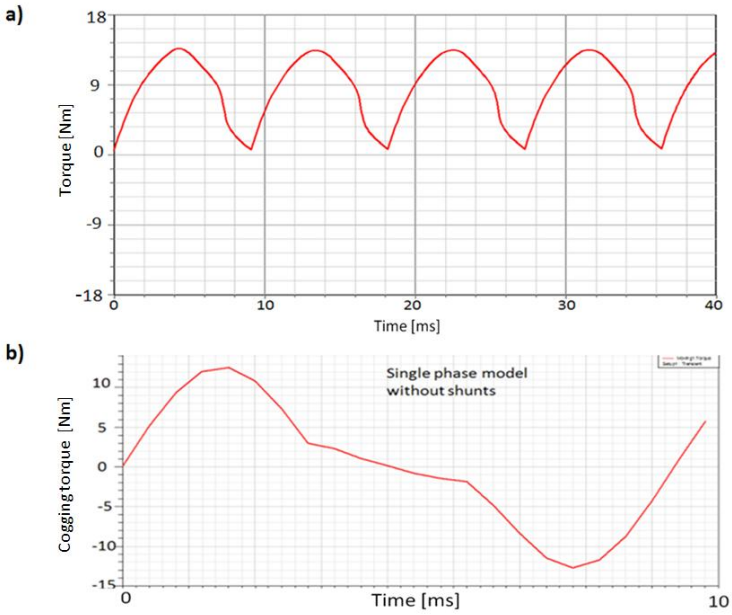

Figure 5.14 Torque developed by the generator with single phase without magnetic shunts: a) total single-phase torque, b) single-phase cogging component

In the generator without magnetic shunts the torque developed by 3 phases is greater and its waveform is shown in Fig. 5.15 a. This torque is smoother but still has some ripple. It is measured by ripple coefficient defined as follows [66]:

$$t_r = \frac{T_{max} - T_{min}}{T_{max} + T_{min}} \cdot 100\% \tag{5.44}$$

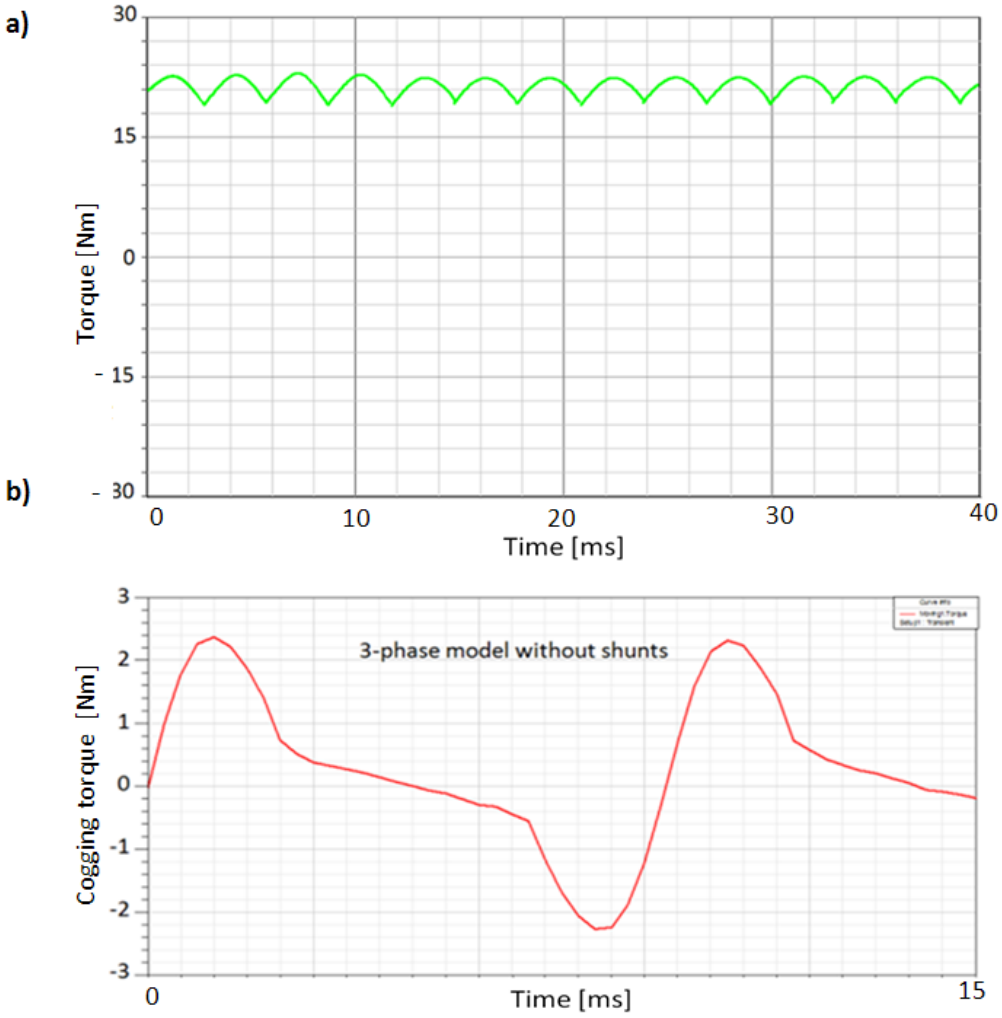

Figure 5.15 Torque developed by the generator with 3-phases without magnetic shunts: a) total torque, b) cogging component of the total torque

The torque ripple is of 14%. The main contribution for this ripple comes from cogging torque, which is shown in Fig. 5.15 b. Its amplitude is much smaller than that of the single phase, but still high enough to disturb the wind turbine operation.

All presented torque waveforms are obtained from 3D FEM simulations for the generator without shunts at rated current of 11.55 A. The torque developed by the generator with magnetic shunts at the same current is shown in Fig. 5.16 a. Comparing with torque of machine without shunts its average value of 21 N·m is greater and the torque ripple is significantly reduced. Its value is equal to:

$$t_r = \frac{25-21}{25+21} \cdot 100\% = 5\%$$

One of the reasons of smaller torque ripple is a significant reduction of cogging torque (≈50% reduction) which waveform is shown in Fig. 5.16 b. This shows that that the implementation of the magnetic shunts does not only increase the induced voltage but also reduces the torque ripple. This is very important since the torque ripple is a source of noise and vibration. And in case of mounting the generator on the roof of a house as it is proposed in section 5.7, these negative effects will not bother the habitants.

The total torque developed by the generator can be verified by formula:

$$T = \frac{P_{em}}{2\pi n} \tag{5.45}$$

where P_{em}- electromagnetic power inside of the machine, n - speed of rotation (rev/sec). P_{em} can be found as:

$$P_{em} = 3 \cdot I \cdot E_m = 3 \cdot 11.55 \cdot \frac{60}{\overline{2}} = 1485\ W$$

$$T = \frac{1485}{2 \cdot 10 \cdot 3.14} = 23.64 \text{ N·m}$$

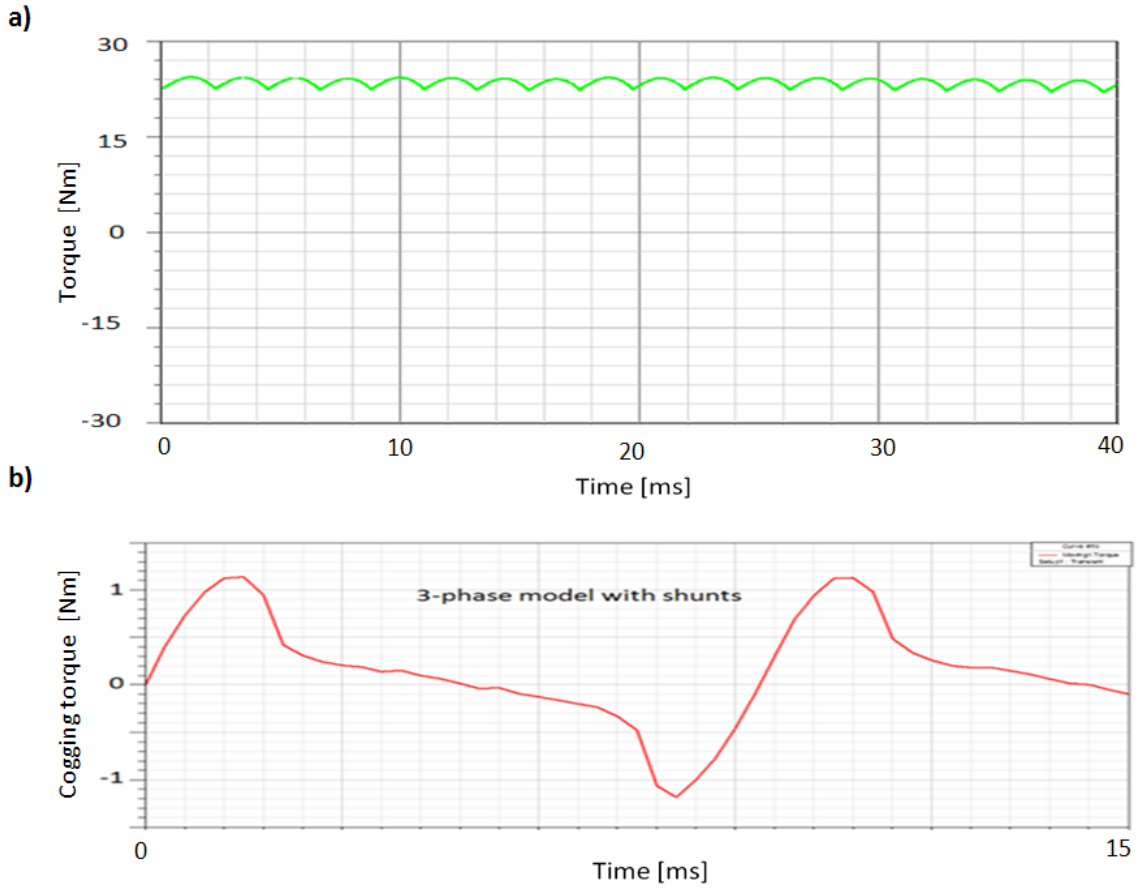

Figure 5.16 Torque developed by the generator with 3-phases with magnetic shunts: a) total torque, b) cogging component of the total torque

5.3.3 Analysis of Output power of the Generator

The output power depends not only on the induced voltage but also on the circuit parameters. The per-phase equivalent circuit of the generator is shown in Fig. 5.17

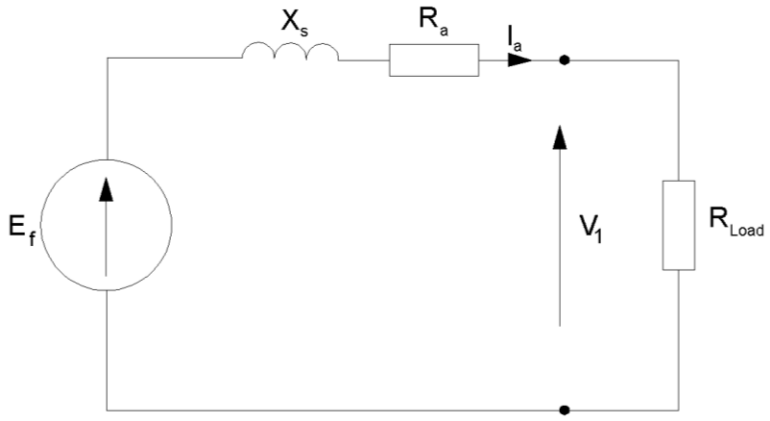

Figure 5.17 Equivalent circuit of the generator

Flux linkage of the coil and coil inductance L, using 3D FEM model of the generator for one phase. From the equivalent circuit of the generator (Fig. 5.17) the current I_a:

$$I_a = \frac{E_f}{(R_{Load}+R_a+j2\pi f L_s)} \tag{5.46}$$

where E_f is emf of the generator at rated speed of 600 rpm. Varying load resistance R_{Load} in the range from 0 to 12 Ohms the dependency of current I_a from load resistance is obtained. This dependency is shown in Fig. 5.18.

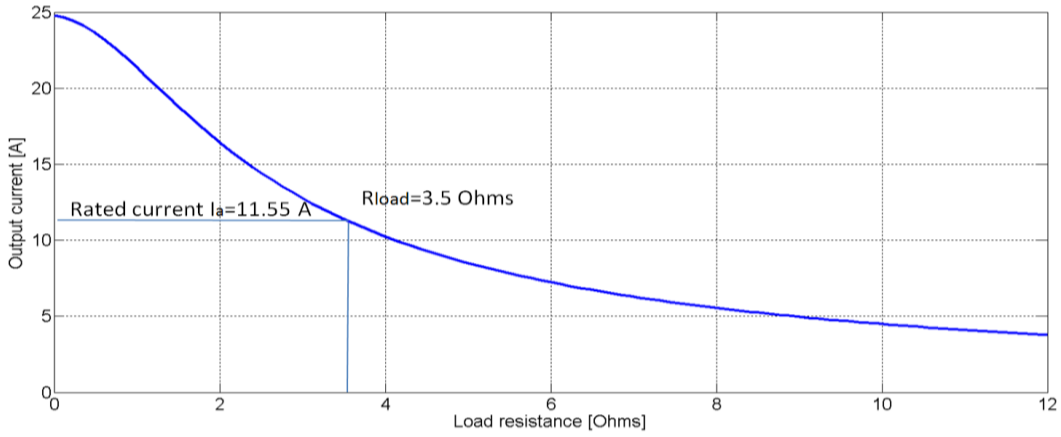

Figure 5.18 Output current as a function of load resistance of the generator

The load resistance which is relevant to rated current of the generator (11.55 A) is equal to 3.5 Ohms.

The electromotive force E_f :

$$E_f = 4.44f\lambda \tag{5.47}$$

The voltage V_1 at the generator terminals:

$$V_1 = E_f - I_a R_a - j2\pi f L_a I_a \tag{5.48}$$

Expressing the voltage V_1 as:

$$V_1 = R_L I_a \tag{5.49}$$

and substituting it in (5.48) the equation looks like:

$$R_{Load} I_a = E_f - I_a R_a - j2\pi f L_a I_a \tag{5.50}$$

From (5.48) phase current:

$$I_a = \frac{4.44f\lambda}{R_{Load} + R_a + j2\pi f L_a} \tag{5.51}$$

The output power for 3-phases is expressed as follows:

$$P = 3\, R_L\, |I_a|^2 \tag{5.52}$$

Expressing frequency f through rotary speed n:

$$f = \frac{np}{120} \tag{5.53}$$

The formula for the output power P is as follows:

$$P = 3\,R_L\left(\frac{4.44np/120\lambda}{R_{load}+R_a+j2\pi nL_a/120}\right)^2 \quad (5.54)$$

where n is rotary speed in rpm.

Table 5.4 Equivalent circuit parameters

PARAMETER	VALUE
Number of rotor poles, p	16
Flux linkage in the coil at rated speed at no load, λ	0.135 Wb·turns
Coil inductance, L	0.0037 H
Coil resistance, R_a	0.101Ω
Frequency of the rotor, f	80 Hz
Load resistance R_{Load}	3.5 Ω

The characteristics of output power vs. rotor speed calculated using formula 5.54 is shown in Fig. 5.19. The rated output power for the 3-phase generator with magnetic shunts at rated speed ($n = 600\,rpm$) is equal: $P_{rat} = 1380\,W$. The difference between output powers of the generators with magnetic shunts and without them is significant as it can be seen on the figure. This is because the induced voltage of the generator without shunts is much smaller due to the negative effect of "unused magnets" what was discussed in Chapter 4.

The terminal voltage V_1 can be found using equation 5.48. The terminal voltage versus speed characteristic is shown in Fig. 5.20.

Calculation parameters of the equivalent circuit are enclosed in Table 5.4.

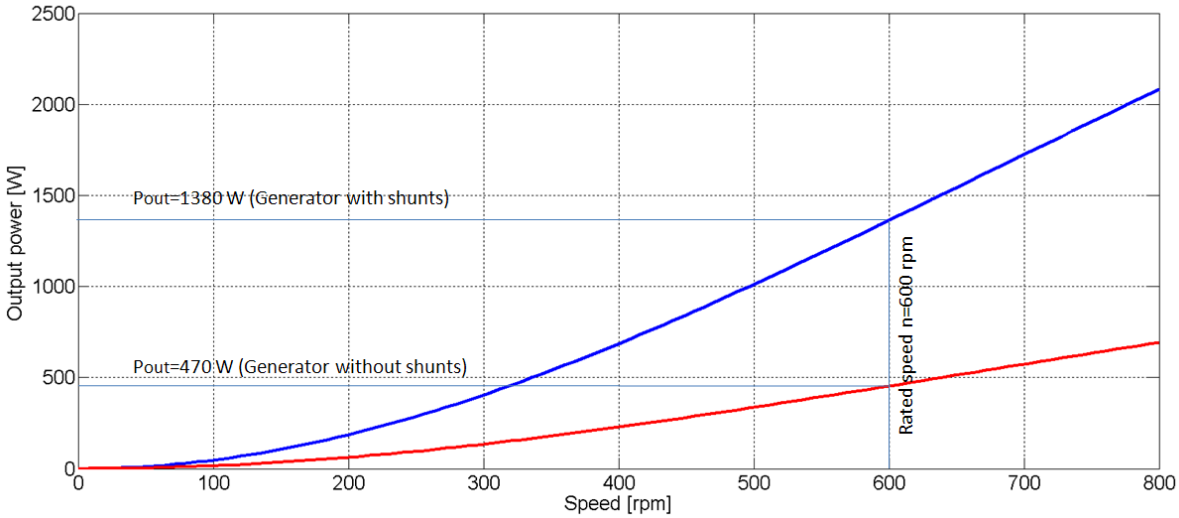

Figure 5.19 Output power vs speed characteristic at rated load resistance R_{Load}=3.5 Ω

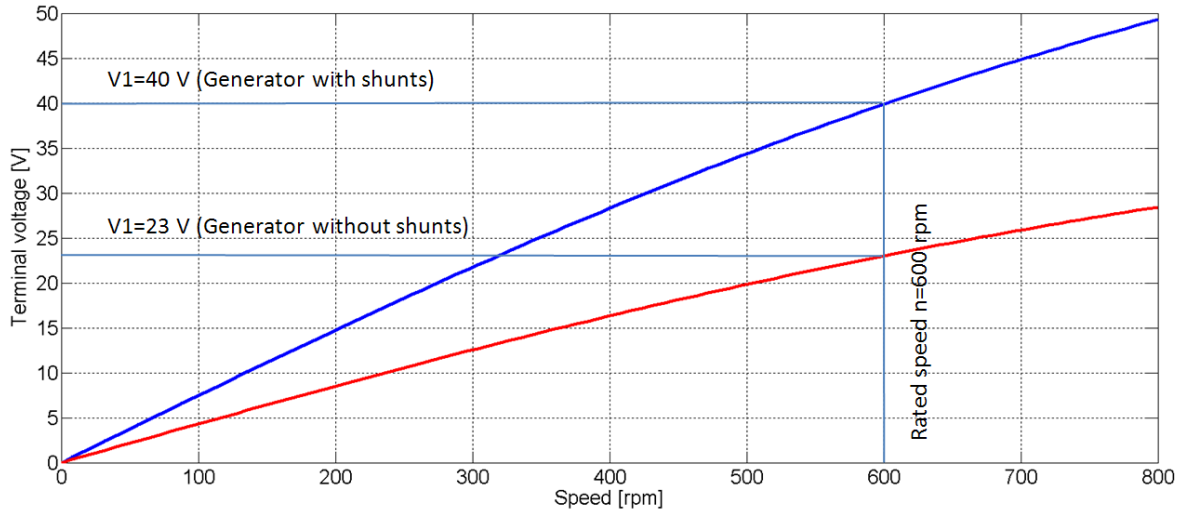

Figure 5.20 Terminal phase voltage vs speed characteristic at rated load resistance R_{Load}=3.5 Ω

The amplitude of induced voltage of the generator with magnetic shunts is 60 V (see Fig. 5.12 a, b). In case of the generator without magnetic shunts the induced voltage is 47% lower. The amplitude of this voltage is shown in Fig. 5.21.

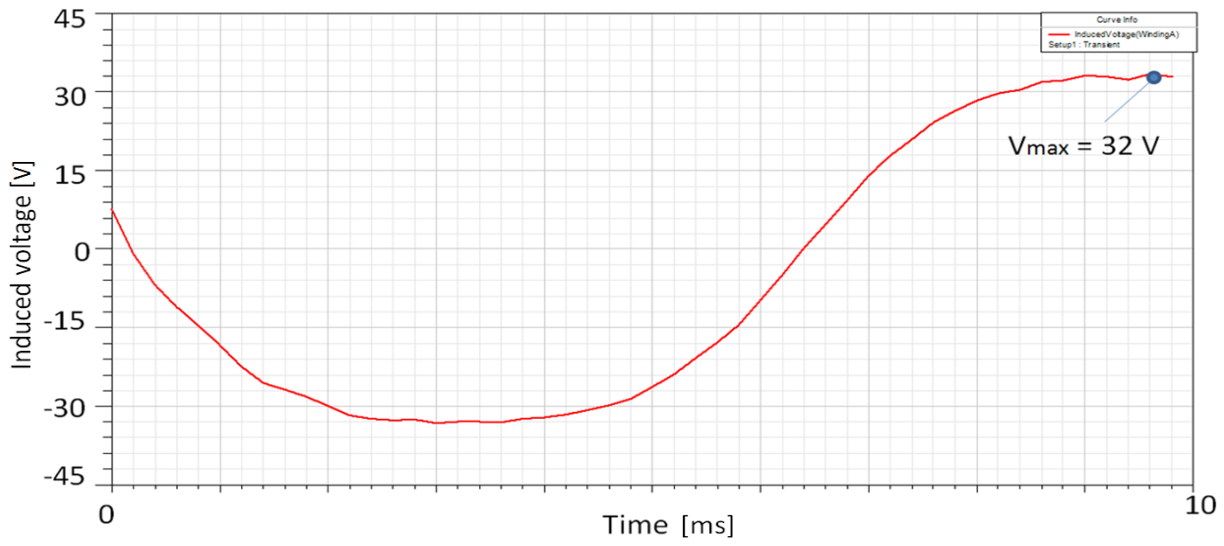

Figure 5.21 Induced voltage of the machine without shunts

This indicates the important role of magnetic shunts.

The rated parameters of the generator are enclosed in Table 5.5.

Table 5.5 Rated parameters of the generator

PARAMETER	VALUE
1. Rated current 2. Rated speed 3. Rated phase voltage (amplitude) 3. Rated power 4. Number of rotor poles	11.55 A 600 rpm 60 V 1,380 kW 16

In order to conclude what have been gained by applying the generator with the internal stator instead of the version with external stator the volumes of both design versions should be compared assuming the same power. The power of both versions is equal if the air-gap diameters are the same. Since the stator poles have the same height and assuming the same rotor yoke thickness the outer diameter of the generator with internal stator is: $D_{int} = 162\ mm$, and with outer stator is: $D_{out} =$

$190\ mm$. Thus, the power P to volume Q ratio of the generators with inner and outer stators consequently is:

$$k_{p.int} = \frac{P}{Q} = 368\ kW/m^3$$

$$k_{p.out} = \frac{P}{Q} = 290\ kW/m^3$$

It means that the internal stator generator power density is 21% higher than that of the outer stator generator.

5.4 Thermal Analysis of the Generator

In the PM synchronous machines there are following sources of heat:

- Stator core
- Stator winding
- Stator magnetic shunts
- Permanent magnets
- Rotor core.

In general, the amount of heat generated in permanent magnets and in the rotor core is ignored due to its negligible amount. This heat is generated by the AC components of magnetic flux, which is produced when the flux density distribution in the air-gap is not sinusoidal one.

Heat that is produced in a stator core and stator magnetic shunts is caused by eddy currents induced in the core and hysteresis losses. Since the stator core and magnetic shunts are laminated these loses are relatively small and also can be omitted. However, if they are made of solid material

like steel, copper or aluminum, it is reasonable to consider them separately since the heat generated by the eddy currents is much greater than the heat produced in laminated shunts.

The main source of heat is the losses in the stator winding. Thermal analysis of the machine was done applying ePhysics 12v software which is based on Finite Element Method. For description of the software and basic equations used for temperature flow calculation see Chapter 2, subsection 2.2 Finite Element Method.

Due to a complexity of the generator structure, temperature analysis is based on the simplified model outlined by the following assumptions:

1. There is no heat transfer in axial direction. It means that no heat end effects at both ends of the generator are considered.
2. The temperatures of each of the machine segments are equal ($T_1 = T_2 = T_3 = T_4$) and don't influence each other (Fig. 5.22). The overall temperature of the segment is not affected when the segment is transformed into rectangular shape (Fig. 5.23) when keeping the element volumes the same. The necessity of transforming the machine segment into rectangular shape is explained by the fact that in rectangular shapes boundary conditions can be assigned more precisely.

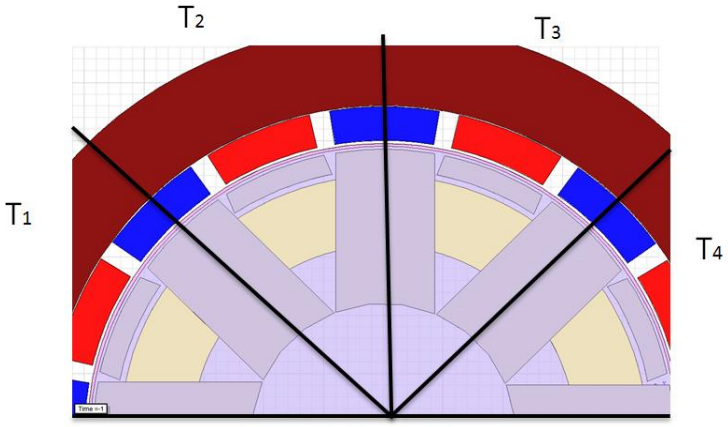

Figure 5.22 PMTF generator segment selected for temperature analysis

3. Ambient temperature of generator elements on the beginning of the simulation is 40 ˚C.
4. The surfaces of the elements have perfect smoothness.
5. Air is moving synchroniously with the generator elements, and doesn't not contribute to cooling.

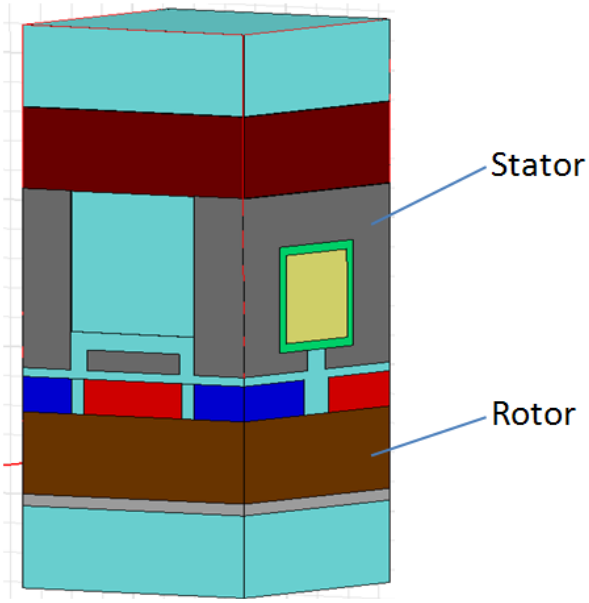

Figure 5.23 Generator segment in rectangular form

The computational simplified model of the generator created in ePhysics 12v is shown in Fig. 5.24.

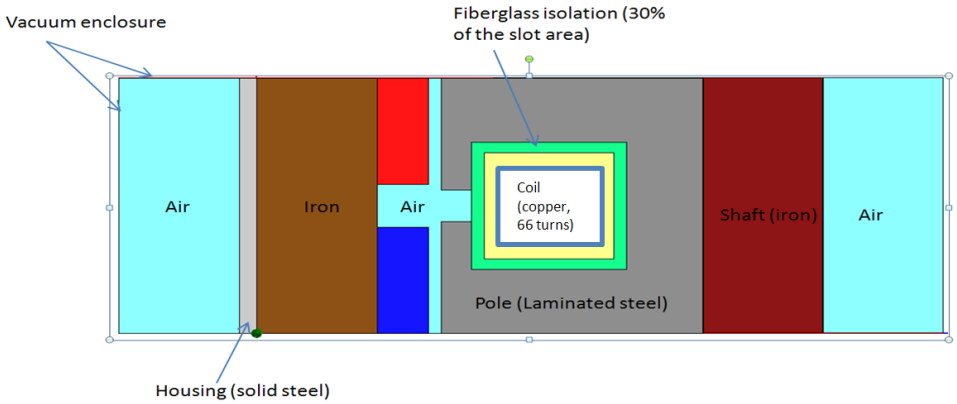

Figure 5.24 ePhysics 12v temperature computational model

Blocking ability of the negative flux for shunts made of different metals is almost the same and varies between 3-5%. However, the temperature distribution in the generator segment might be dependent on the shunt material. Shunts made of: laminated steel, solid iron, aluminum, and cooper were selected for the simulation model. The results of simulations carried out at rated current and rated frequency are enclosed in Table 5.6.

Table 5.6 Temperatures of the generator elements

Temperature of	Model with laminated steel shunt	Model with iron shunt	Model with copper shunt	Model with aluminum shunt	Time when temperature reaches steady state, Hr
Coil	164 ˚C	177 ˚C	178 ˚C	194 ˚C	2.7
Shunt	78 ˚C	182 ˚C	182 ˚C	201 ˚C	3.8
PM	67 ˚C	121 ˚C	119 ˚C	170 ˚C	4.3
Outer core	55 ˚C	92 ˚C	89 ˚C	112 ˚C	5.2
Housing	48 ˚C	74 ˚C	80 ˚C	97 ˚C	6.4

Temperatures of the generators' elements obtained from simulation are expected to be higher as in reality due to the assumptions.

As the results show, to use solid iron, aluminum, or cooper shunts cause an increase of machine temperature. The maximum temperature which the "*H*" class of coil insulation can withstand is 180 ˚C. In case of iron shunts the coil temperature is very close to the permissible value. In case of aluminum shunts the coil will be overheated. Laminated steel magnetic shunts are better in terms of

temperature. It can be explained by the fact that eddy currents in laminated steel material are very small and do not contribute to high power losses.

The temperature graph of the laminated steel magnetic shunt along with coil temperature is shown in Fig. 5.25.

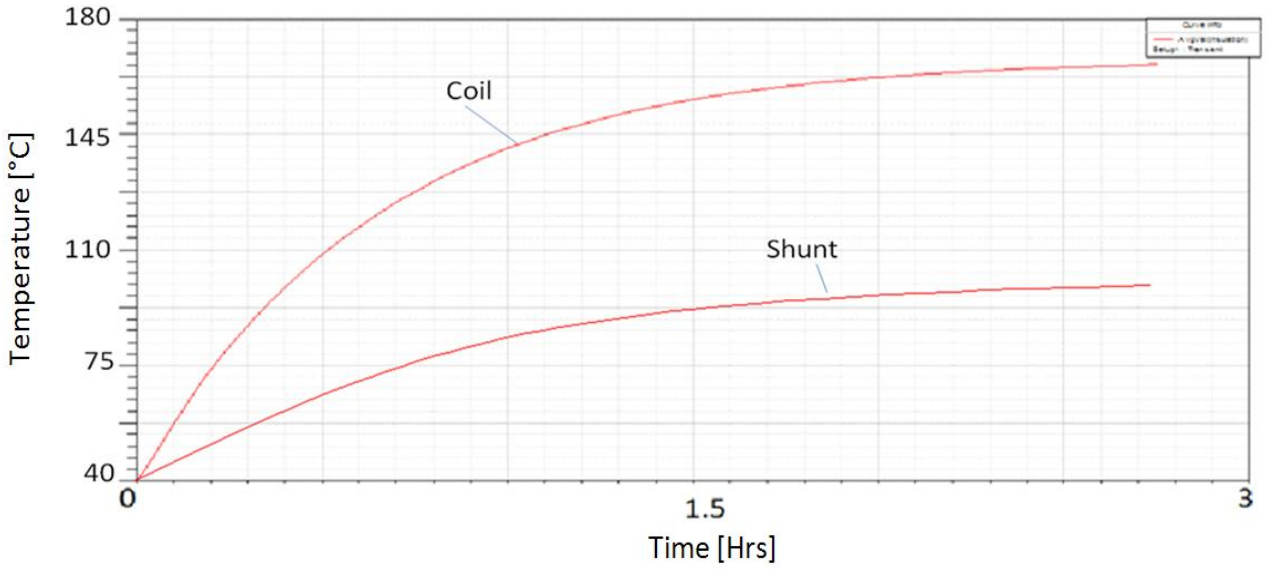

Figure 5.25 Temperature of the laminated steel shunt and coil

After 3 hours of generator operation at rated 600 rpm speed the temperatures of the shunt and coil reach steady-state.

5.5 Optimization of Magnetic Shunt Structure

The role that magnetic shunts play in PMTF generator has been discussed in Chapter 4. These shunts do not only allow increasing the output power at the given generator volume, but also contribute to diminishing of torque ripple. To play this role in most efficient way the shunts must be adjusted to the particular generator construction.

If shunts are made of laminated steel and the distance to adjacent stator poles is small, the magnetic field concentrated on the shunt is partially transferred to these poles. Due to this, the magnetic field density in the poles is significantly reduced. In Fig. 5.26 two trapezoidal shunt shapes with corresponding to them negative flux linkages in the coil, detected in steady-state simulation, are shown. In Fig. 5.26 a) where the distance between shunts to adjacent poles is less than 1 mm, the negative flux linkage is higher than that where the distance from shunts to poles is more than 2 mm (Fig. 5.26 b). Optimized shunt dimension for the represented generator with smallest negative flux linkage value are shown in Fig. 5.27.

Shunts can be attached to the generator in both ways: either to the stator poles, or to the shaft. If the shunts are attached directly to the stator poles as it is shown in Fig. 5.28, then the flux from "inactive" magnets will diminish the total flux linkage of the coil making the induced voltage small. The calculations show that in this case the voltage induced in the coil is reduced by 45%. The voltage waveform is shown in Fig. 5.29. To solve this problem another structure is proposed (Fig. 5.30) where shunts are attached to the iron rings on both sides of the generator which in turn are supported by the bars that are radially oriented and attached to the stator shaft.

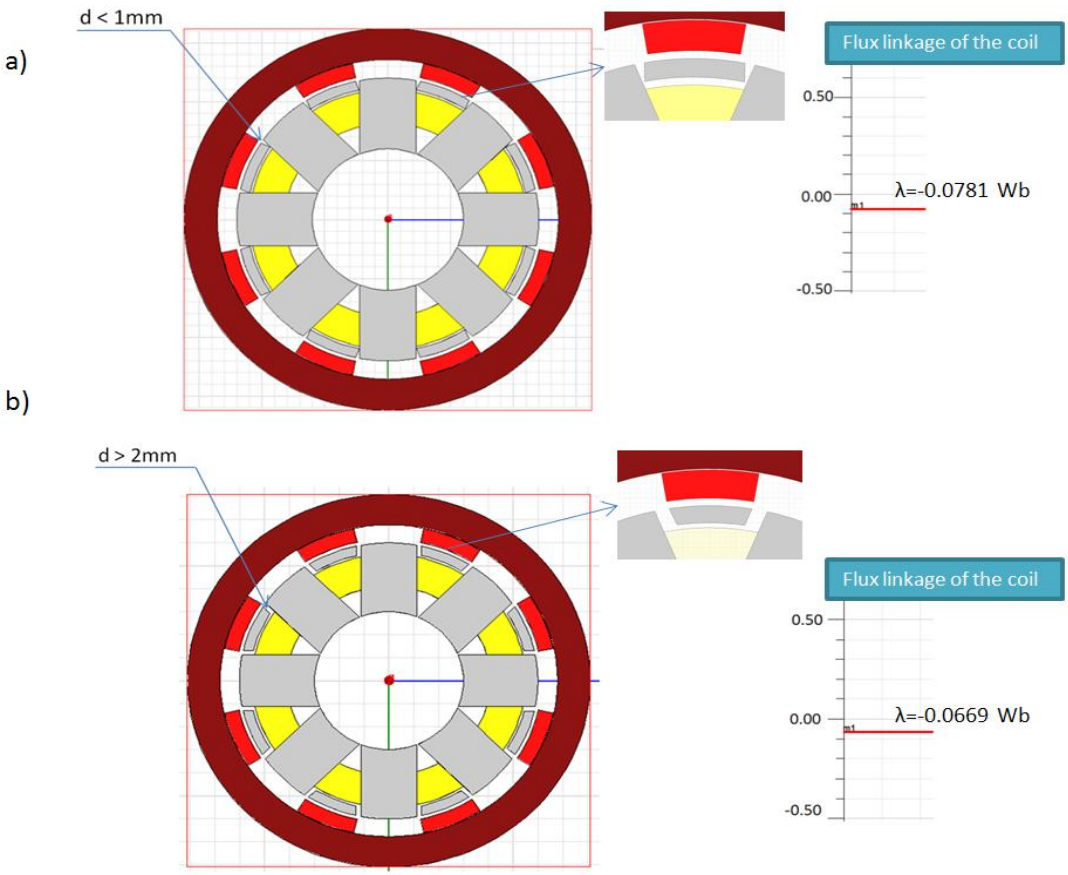

Figure 5.26 Negative flux linkage from "inactive" PMs at the gap between shunts and stator pole: a) less than 1 mm, b) more than 2 mm

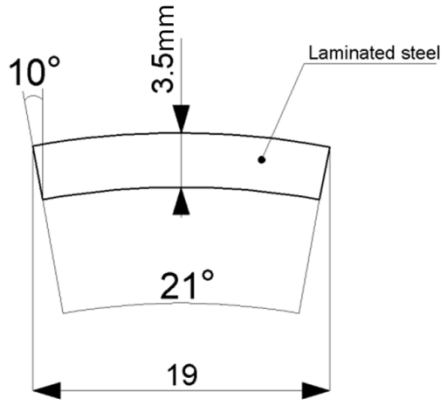

Figure 5.27 Optimum shunt dimensions

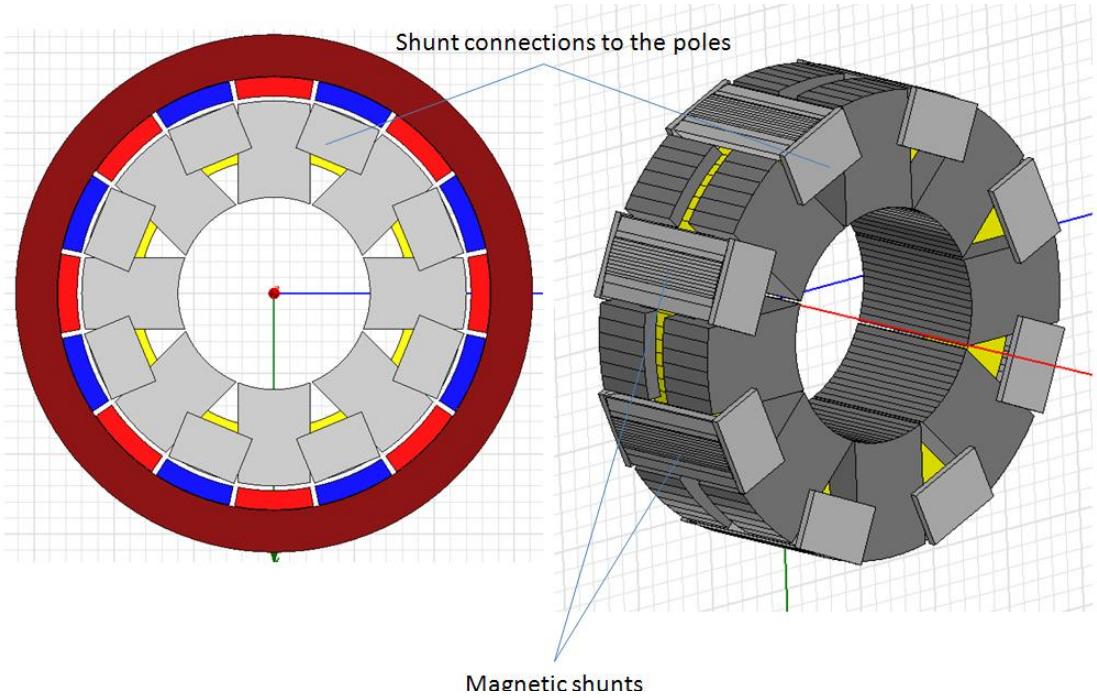

Figure 5.28 Shunt connected to the stator poles

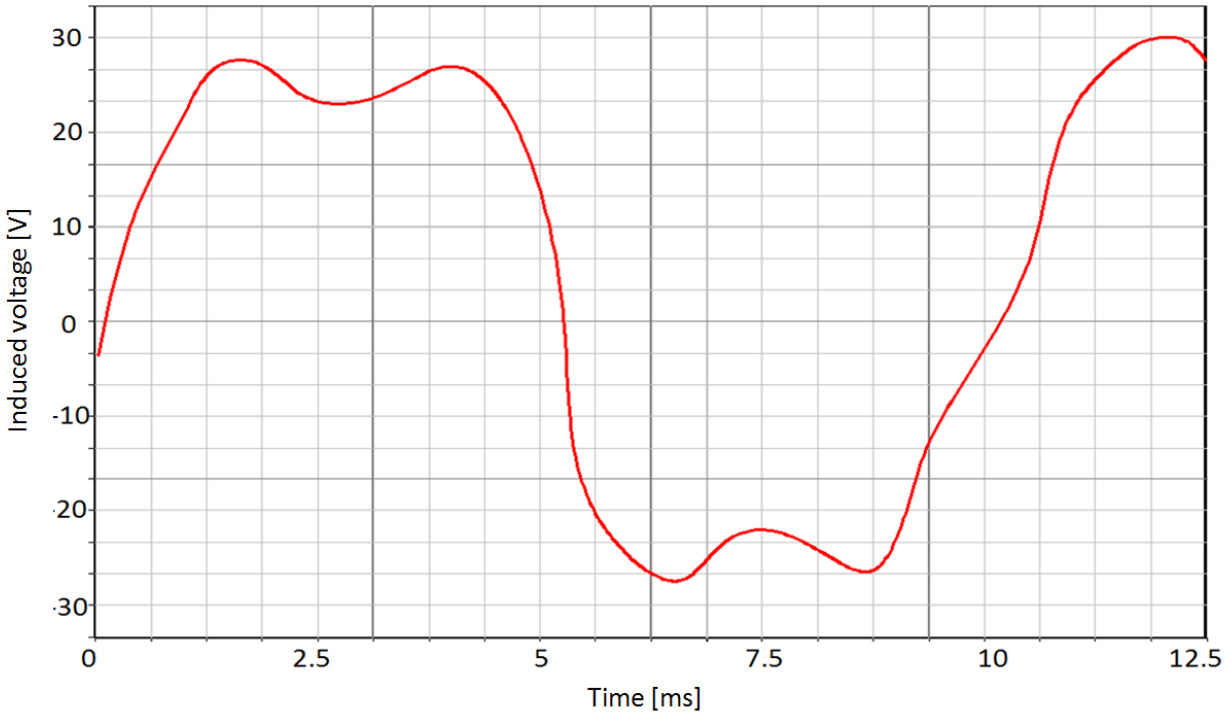

Figure 5.29 Induced voltage of the generator with shunts attached to stator poles

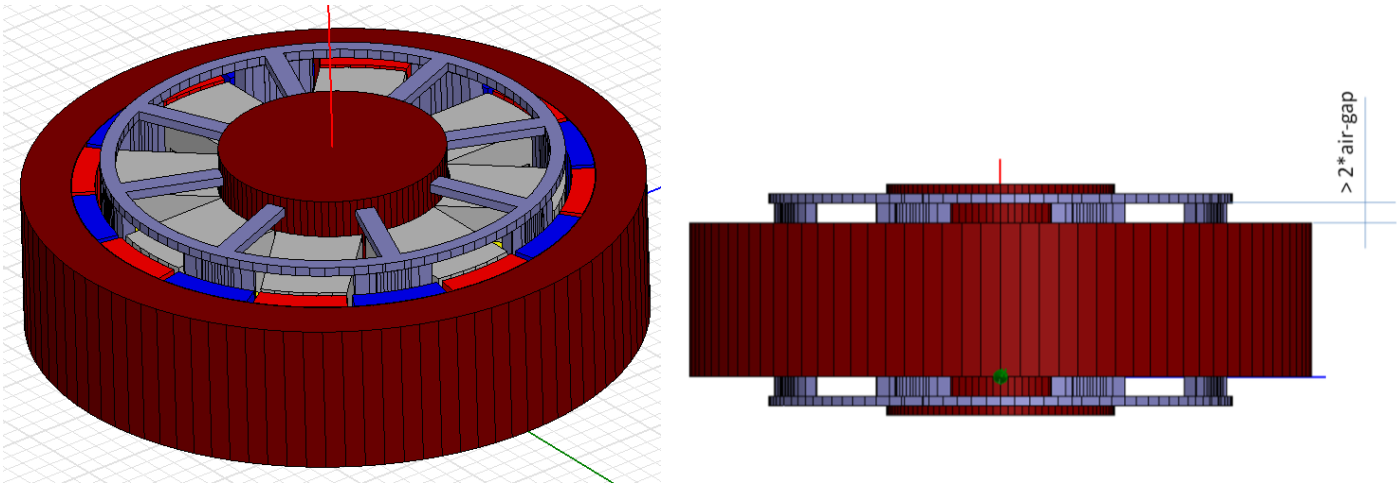

Figure 5.30 Shunt assembly fixed to the stator shaft

With the new design of shunts' attachments induced voltage of the generator is as it was determined in section 5.3.1. Its waveform is shown in Fig. 5.31.

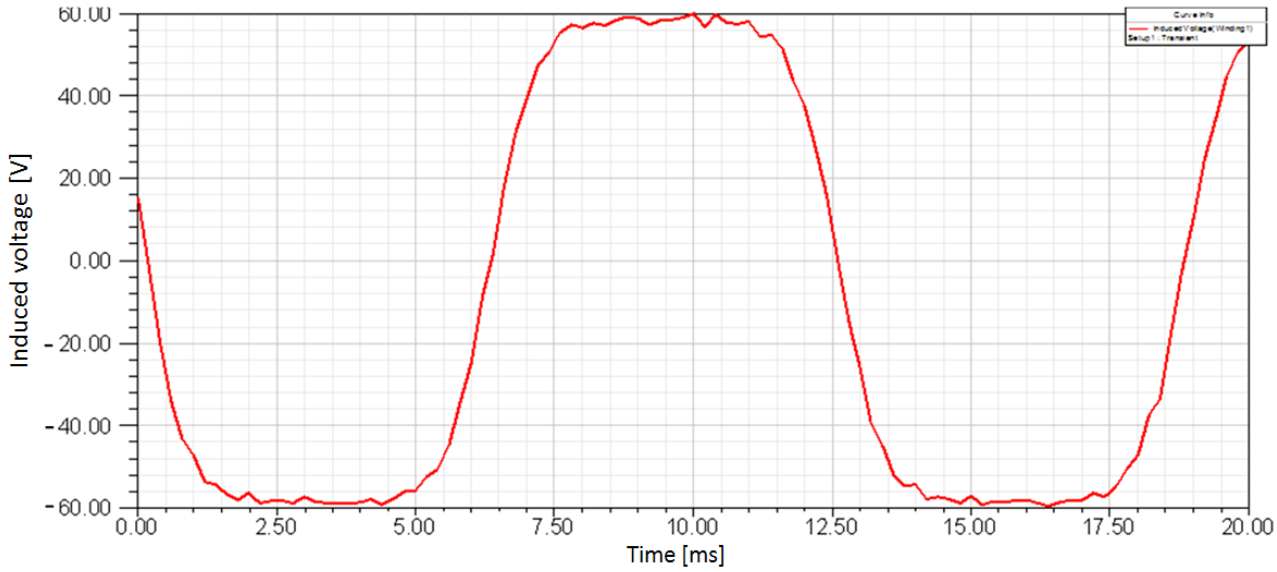

Figure 5.31 Induced voltage of the generator with shunts connected to the iron rings

5.6 Generator Performance in Dynamic Condition

To evaluate generator performance in dynamic condition a circuit model of the generator is applied. This model represents the generator under the following assumptions:

- all elements of the generator are linear and no core losses are considered;
- electromotive force e_a changes sinusoidaly with the rotational electric angle θ;
- generator terminals are connected to the 3-phase resistive load;
- due to the surface mounted permanent magnets winding inductance is constant (does not change with the θ_e angle).
- cogging torque is neglected.

The generator model is graphically represented by the circuit diagram of 3-phase winding shown in Fig. 5.32, and its mechanical model is shown in Fig. 5.33.

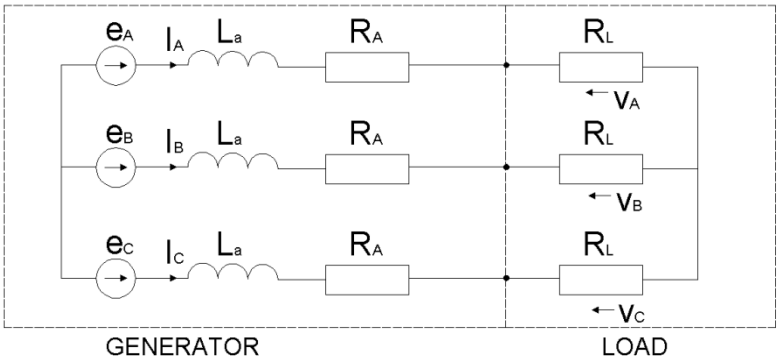

Figure 5.32 Circuit diagram of 3-phase winding of the generator

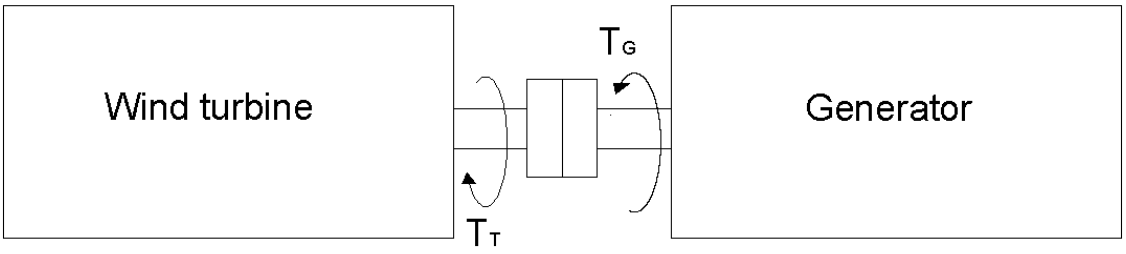

Figure 5.33 Mechanical model of the generator

They are described by the following equilibrium equations:

- **v**oltage equations:

$$e_A = R_a\, i_A + L_a \frac{di_a}{dt} + v_A \tag{5.55}$$

$$e_B = R_a\, i_B + L_a \frac{di_a}{dt} + v_B \tag{5.56}$$

$$e_C = R_a\, i_C + L_a \frac{di_a}{dt} + v_C \tag{5.57}$$

where:

R_a - phase resistance

L_a - phase self-inductance equal to synchronous inductance L_s

R_L - load phase resistance

$i_{A,B,C}$ - phase currents

$e_{A,B,C}$ - phase voltages induced in 3-phase generator winding

$v_{A,B,C}$ - generator terminal phase voltages.

The voltages $e_{A,}\, e_{B,}\, e_C$ depend on rotational electrical angle θ_e and on rotor speed ω_r according to equations:

$$e_A = K_e \omega_m \sin(\theta_e) \tag{5.58}$$

$$e_b = K_e \omega_m \sin(\theta_e - \tfrac{2}{3}\pi) \tag{5.59}$$

$$e_C = K_e \omega_m \sin(\theta_e - \tfrac{4}{3}\pi) \tag{5.60}$$

The electrical angle θ_e is related to mechanical angle θ_m by equation:

$$\theta_e = \frac{p}{2}\theta_m \tag{5.61}$$

where mechanical angle θ_m is reffered to the position of the rotor magnets as shown in Fig. 5.34

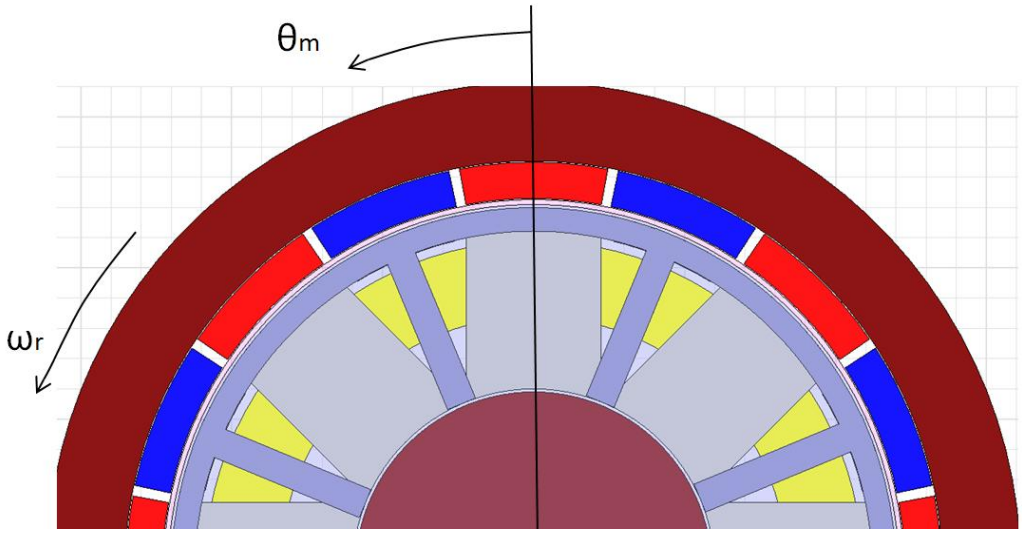

Figure 5.34 Mechanical angle $\boldsymbol{\theta_m}$ with rotor speed $\boldsymbol{\omega_r}$

The equations 5.55-5.57 written in matrix form are as follows:

$$\begin{matrix} e_A \\ e_B \\ e_C \end{matrix} \begin{matrix} R_a & 0 & 0 \\ 0 & R_a & 0 \\ 0 & 0 & R_a \end{matrix} \begin{matrix} i_A \\ i_B \\ i_C \end{matrix} = \begin{matrix} i_A \\ i_B \\ i_C \end{matrix} + \frac{d}{dt} \begin{matrix} L_s & 0 & 0 \\ 0 & L_s & 0 \\ 0 & 0 & L_s \end{matrix} \begin{matrix} i_A \\ i_B \\ i_C \end{matrix} + \begin{matrix} v_A \\ v_B \\ v_C \end{matrix} \tag{5.62}$$

Equations 5.52-5.54 written in a form of matrix:

$$e_A = \frac{K_E}{p/2} \begin{matrix} sin\theta_e \\ \sin(\theta_e - \frac{2}{3}\pi) \\ \sin(\theta_e - \frac{4}{3}\pi) \end{matrix} d\theta_e/(dt) \tag{5.63}$$

Torque equation:

$$T_D = T_T + T_J + T_{em} \tag{5.64}$$

where T_{em} – is the torque developed by the generator:

$$T_{em} = \frac{e_A i_A}{\omega_m} + \frac{e_B i_B}{\omega_m} + \frac{e_C i_C}{\omega_m} = K_E(f_a(\theta_a) i_A + f_{\ b}\ \theta_e\ i_B + f_c(\theta_e)\ i_C) \tag{5.65}$$

$$f_a(\theta_e) = \sin(\theta_e) \tag{5.66}$$

$$f_b(\theta_e) = \sin(\theta_e - \frac{2}{3}\pi) \tag{5.67}$$

$$f_c(\theta_e) = \sin(\theta_e - \frac{4}{3}\pi) \tag{5.68}$$

T_J - Inertia torque:

$$T_J = J \frac{d\omega_r}{dt} \tag{5.69}$$

T_D - Viscous friction torque:

$$T_D = D\omega_r \tag{5.70}$$

$T_T -$ Torque of the turbine driving the generator

Combining all the above equations, the system in state-space form is:

$$x = Ax + Bu \tag{5.71}$$

Where coefficients A and B:

$$A = \begin{bmatrix} -\frac{R_a}{L_s} & 0 & 0 & K_E(f_a(\theta_e)/L_s & 0 \\ 0 & -\frac{R_a}{L_s} & 0 & K_E(f_a(\theta_e)/L_s & 0 \\ 0 & 0 & -\frac{R_a}{L_s} & K_E(f_a(\theta_e)/L_s & 0 \\ -K_E\frac{f_a(\theta_e)}{J} & -K_E\frac{f_b(\theta_e)}{J} & -K_E\frac{f_c(\theta_e)}{J} & -\frac{D}{J} & 0 \\ 0 & 0 & 0 & p/2 & 0 \end{bmatrix} \tag{5.71}$$

$$B = \begin{bmatrix} -\frac{1}{L_s} & 0 & 0 & 0 \\ 0 & -\frac{1}{L_s} & 0 & 0 \\ 0 & 0 & -\frac{1}{L_s} & 0 \\ 0 & 0 & 0 & \frac{1}{J} \\ 0 & 0 & 0 & 0 \end{bmatrix} \tag{5.72}$$

$$x = [i_A \;\; i_B \;\; i_C \;\; \omega_m \;\; \theta_e]^T \tag{5.74}$$

$$u = [v_A \; v_B \; v_C \; T_T]^T \tag{5.75}$$

The generator described by the above equations was modeled in Matlab/Simulink and its block diagram is shown in Fig. 5. 35.

A moment of inertia of the rotor was determined from the following equation:

$$J = \frac{M_r}{2}((D_{r,in}/2)^2 - (D_{r,out}/2)^2) + J_{turbine} \tag{5.71}$$

where:

$J_{turbine}$ - moment of inertia of the turbine (assumed value is 0.003 $kg \cdot m^2$)

$M_r -$ is the rotor mass

$D_{r,in}$ - internal diameter of the rotor

$D_{r,out}$ – external diameter of the rotor.

Assuming that rotor magnets and rotor core have the same mass density ρ , which is for iron 7850 kg/ m^3, the mass is found:

$$M_r = 3Q\rho \tag{5.72}$$

where Q – rotor volume:

$$Q = \frac{2\pi W(D_{r,out} - D_{r,in})^2}{4} = 2 \cdot 3.14 \cdot 44 \cdot \frac{(162-123)^2}{4} = 0.0001\ m^3 \tag{5.73}$$

$$M_r = 3 \cdot 0.0001 \cdot 7850 = 2.36 \text{ kg.}$$

$$J = \frac{2.36}{2}\left(\left(\frac{162}{2}\right)^2 - \left(\frac{123}{2}\right)^2\right) \quad + 0.003 = 0.0063\ kg \cdot m^2$$

Block diagram parameters are enclosed in Table 5.7

Table 5.7 Block diagram parameters of the generator

PARAMETER	VALUE
1. Inductance of the coil	$L = 0.0037\ H$
2. Coil resistance	$R = 0.101\ \Omega$
3. Moment of inertia of the rotor	$J = 0.0063\ kg \cdot m^2$
4. Damping coefficient	$D = 0.002$
5. Number of rotor pole pairs	$p = 8$
6. EMF constant	$k_E = 0.96$
7. Load resistance	$R_L = 3.5\ \Omega$
8. Turbine torque	$T_T = 18.5\ N \cdot m$

In the simulation the rotor is driven by the rated torque (depending in reality on wind speed) and starts from zero rotor speed, being loaded by rated resistance R_L=3.5 Ohms. After the steady-state speed operation is reached, the load resistance changes in step.

The simulation results are shown in Figs. 5.36 and 5.37. When load resistance suddenly increases from 3.5 to 3.5·1.5 Ohms, rotor initially rotates with the same speed because of inertia. That is why electromotive force E_f is constant. The phase current is found using equivalent circuit of the machine: $I_a = \frac{E_f}{R_L + R_a + j2\pi f L_a}$. Since, E_f, R_a, and L_a are constants, the current is dependent on load resistance only; and if the load resistance increase, the current decrease (Fig. 5.36 a). Output power of the generator is decreased too according to the equation: $P_{out} = R_L\,|I_a|^2$. Electromagnetic torque of the generator decreases if current decreases. Since the driving torque remains constant, the speed of the machine increases. (Fig. 5.36 b). This causes higher *emf* to be induced in the winding (Fig. 5.36 a). Higher *emf* brings current value up close to the initial level (Fig. 5.36 a). Electromagnetic torque

T_{em} is approximately equal to driving torque. Output power of the machine is increasing due to increase of the speed, according to the equation: $P = T_{em}\omega_m$ (Fig. 5.36 b).

In Figs. 5.37 a) and b) electromechanical parameters of the generator are shown when the load resistance changes from 3.5 to 3.5/1.5 Ohms. In this case electromechanical characteristic behavior is opposite to what was discussed above.

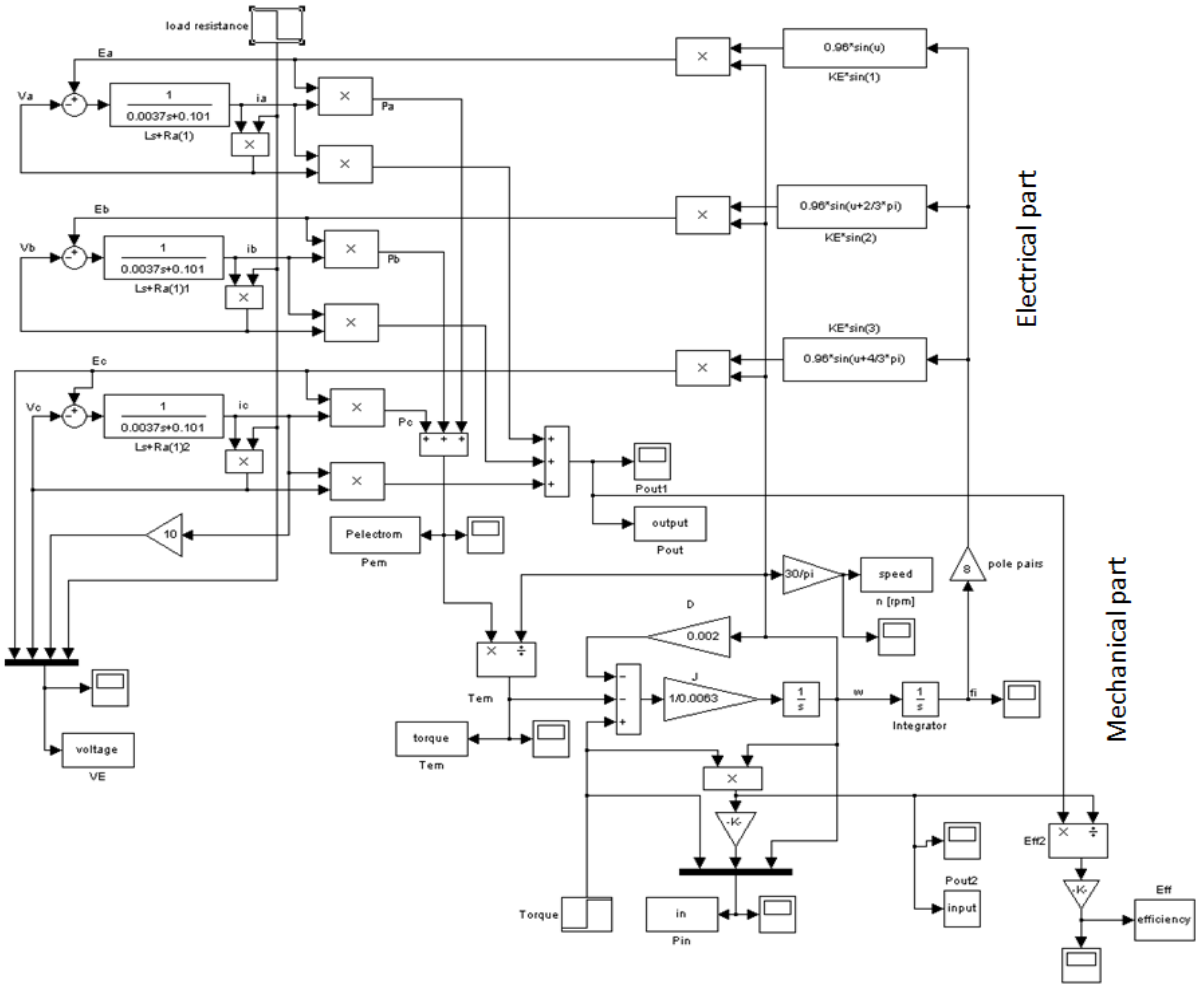

Figure 5.35 SIMULIMK model of the PMTF generator

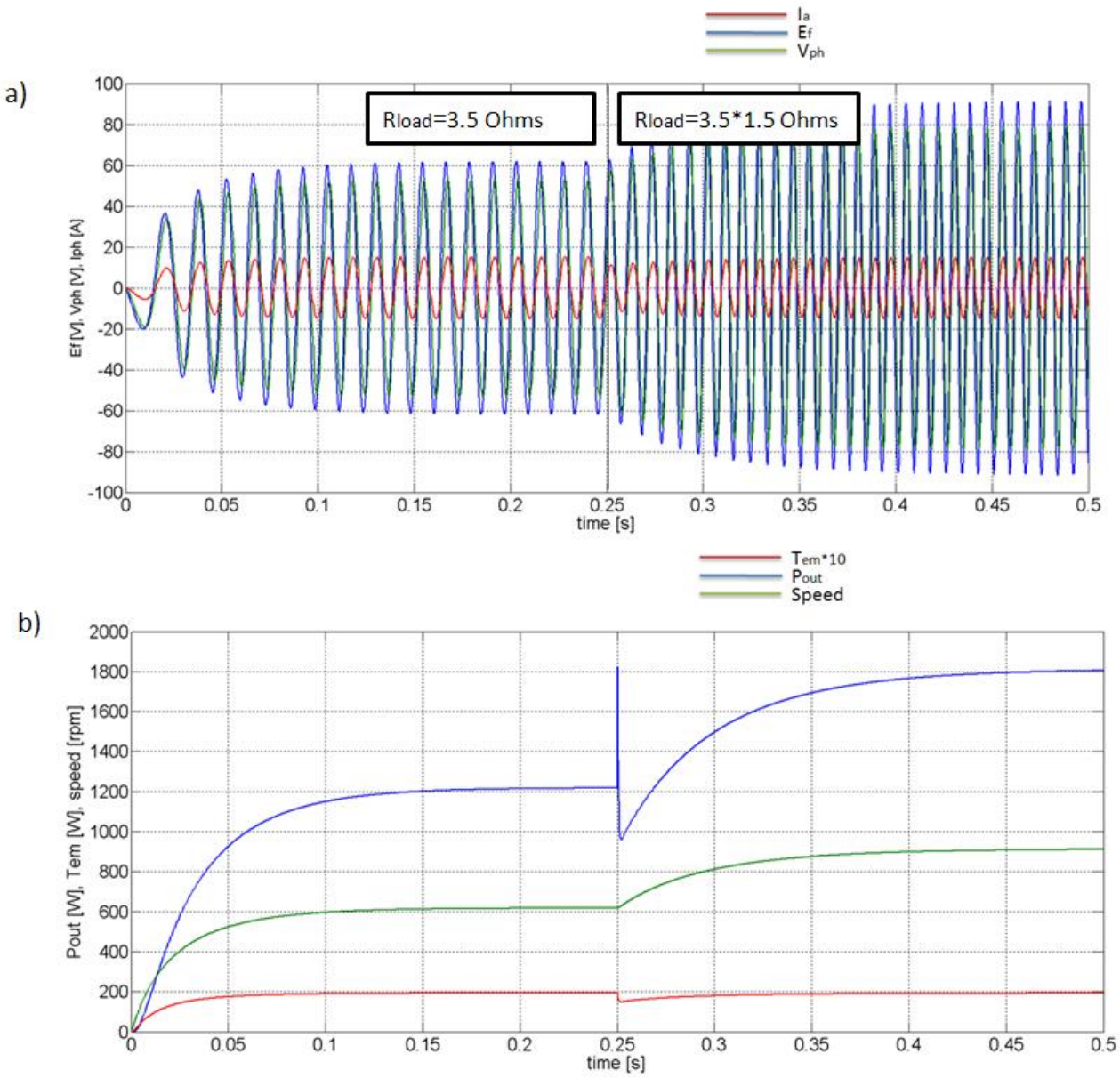

Figure 5.36 Electromechanical parameters of the generator in dynamic condition at load resistance changing from 3.5 Ω to 3.5*1.5 Ω. a) Induced and phase voltages with phase current, b) output power, speed and electromagnetic torque

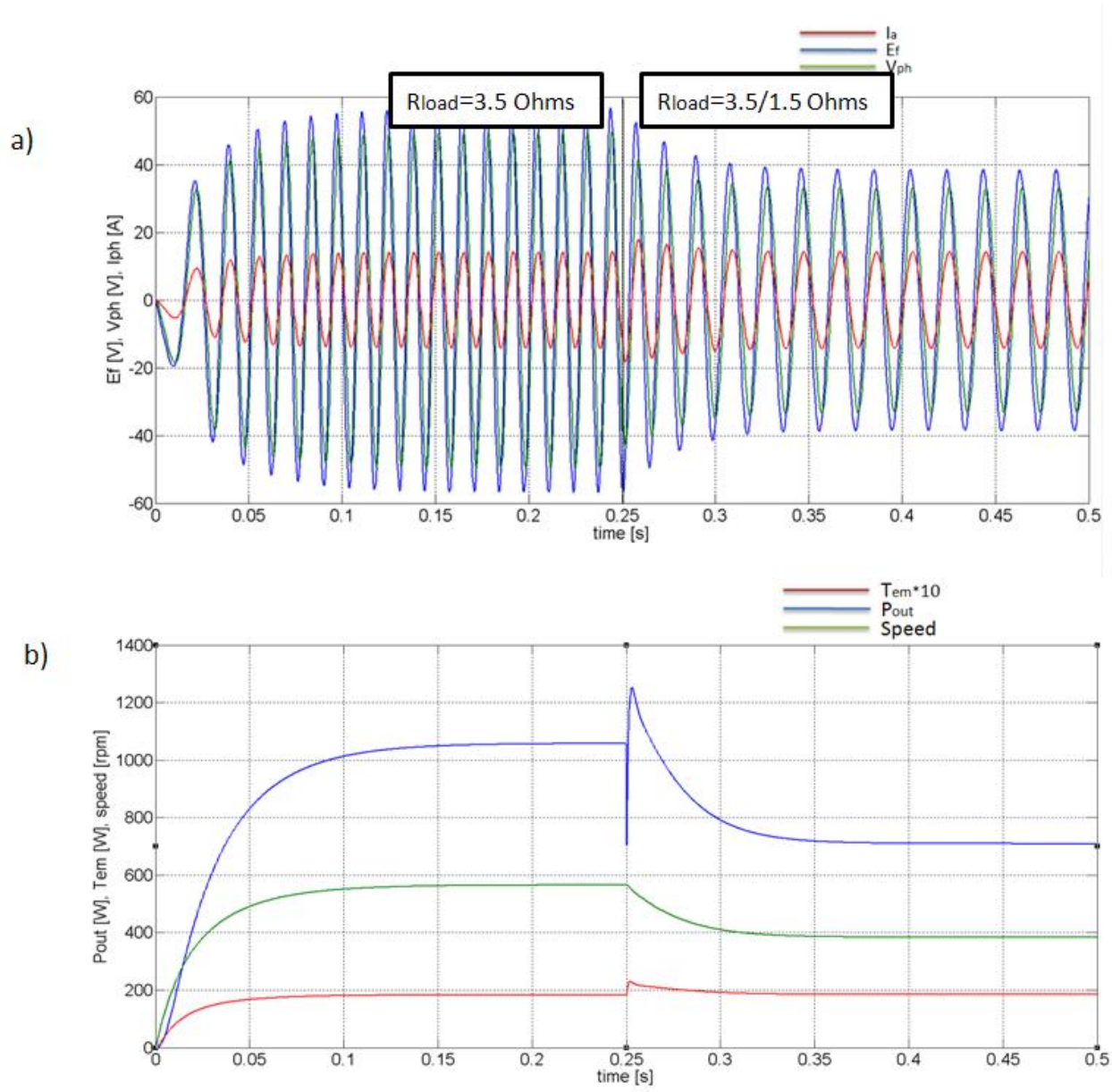

Figure 5.37 Electromechanical parameters of the generator in dynamic condition at load resistance changing from 3.5 Ω to 3.5/1.5 Ω. a) Induced and phase voltages with phase current, b) output power, speed and electromagnetic torque

5.7 Generator Prototype Test

The generator prototype was built according to the drawings discussed in Chapter 5 and presented in Appendix A. Machine was manufactured and tested by "Komel" the Polish company for the University of Nevada – Reno. The pictures of the machine prototype are shown in Fig. 5.38 a-d.

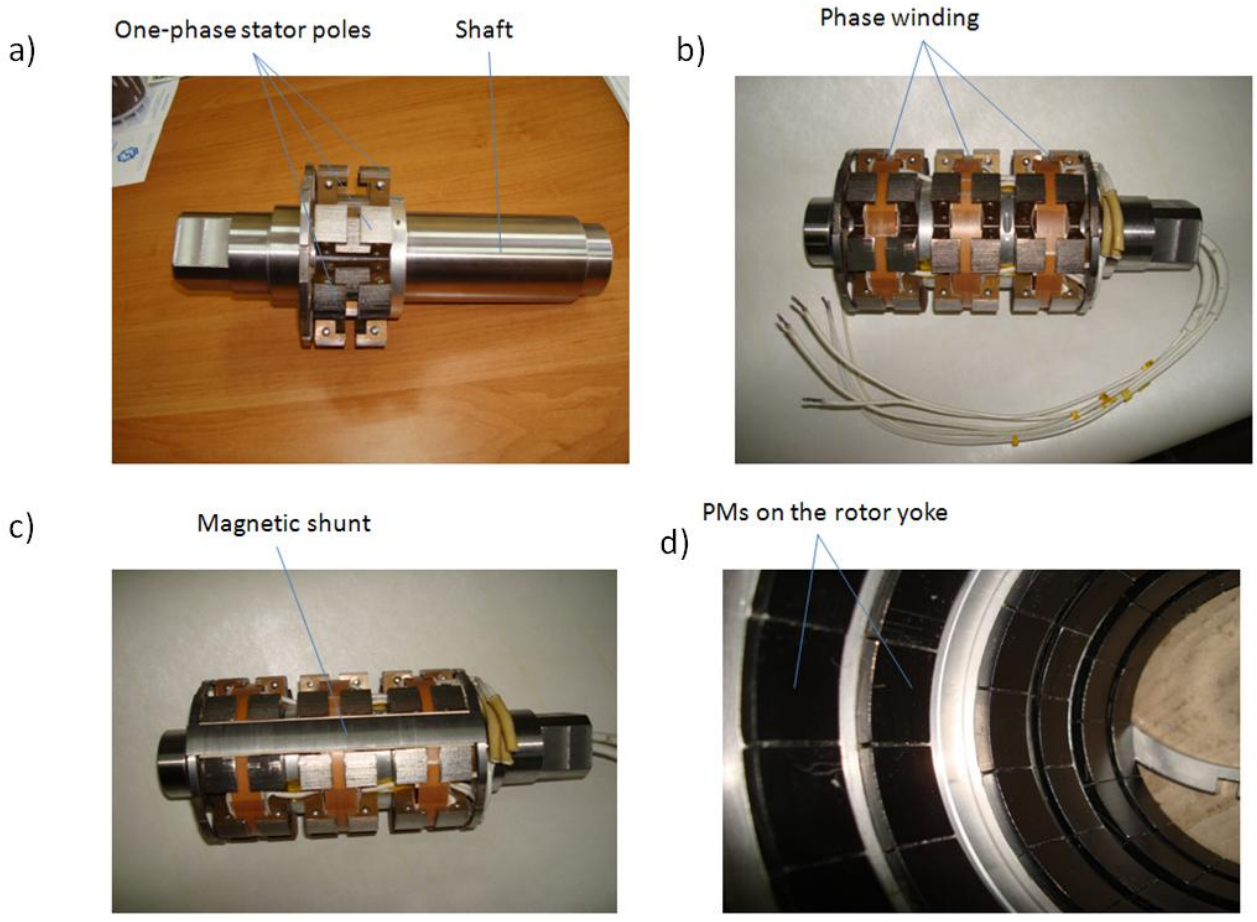

Figure 5.38 PMTF machine prototype: a) one phase stator poles on the shaft, b) shaft with 3 rings of stator poles, c) stator with magnetic shunts, d) rotor with permanent magnets

The magnetic shunts were made of solid iron due to the problem with assembling of laminated shunts.

No load test at rated speed 600 rpm was done in order to record induced voltages in the generator's windings. Phase voltages of the machine obtained experimentally and calculated using 3D model are show in Fig. 5.39.

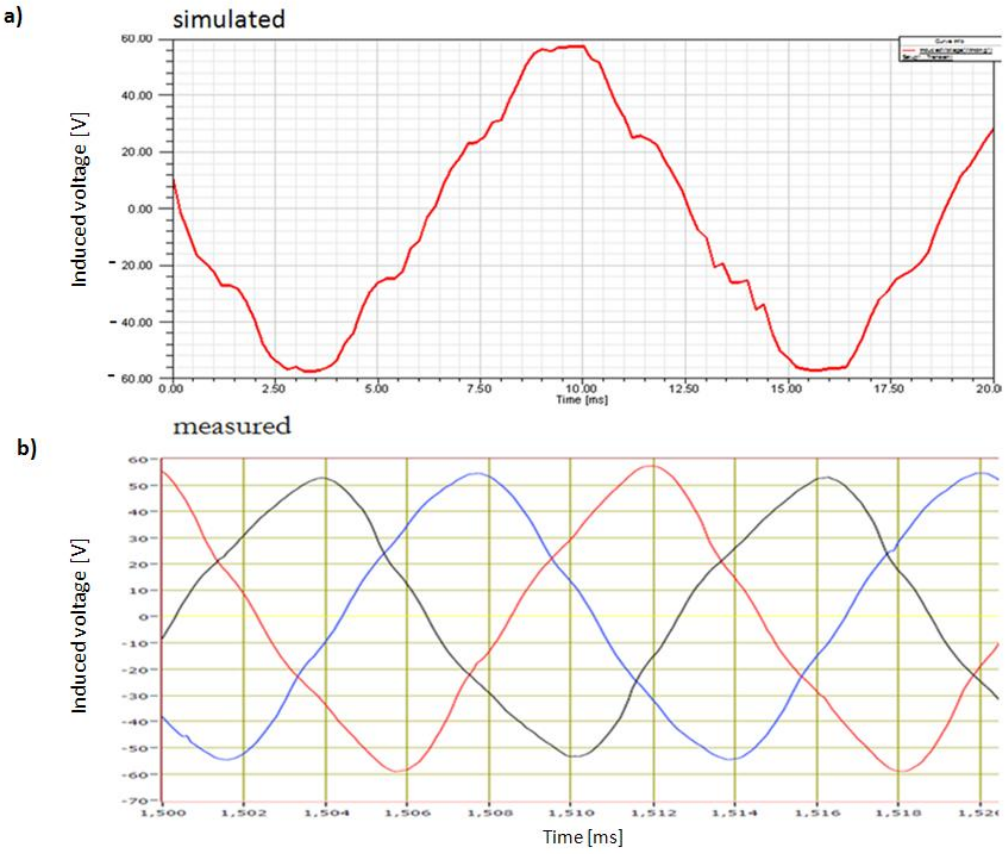

Figure 5.39 Calculated and measured induced voltages of the generator's windings

The amplitudes of phase voltages calculated and measured during the laboratory test are almost the same which proves the the magnetic circuit of the generator was designed properly. The small differences in amplitudes of 3-phase voltages may result from inaccuracy of manufacturing of generator magnetic circuit or stator coils.

The power losses of the generator measured during no load laboratory test at rated speed 600 rpm are equal to 415 W. Such high power losses are caused mainly by eddy currents induced in the magnetic shunts. According to computer simulation these power losses are of 316 W. The distribution of eddy currents on the magnetic shunts is shown in Fig. 5.40 confirms this result. Some small power losses of 16 W generated in aluminum distance rings placed between stator phases. The rest of the power losses are generated in the stator core and mechanical friction. Some negligible losses losses of power are expected to be in permanent magnets.

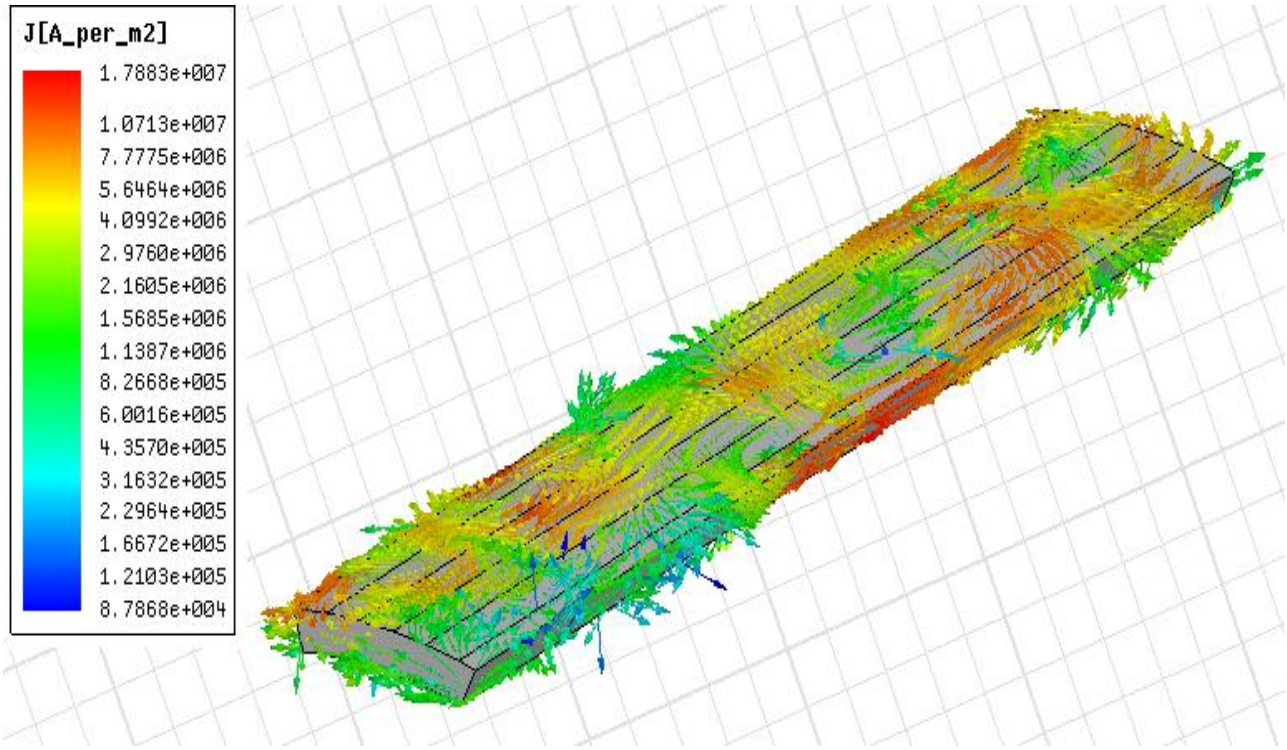

Figure 5.40 Eddy current density on the shunt's surface

When magnetic shunts are made of laminated steel, the total power losses at no load test according to 3D FEM simulation are of 20 W.

Conclusion: the solid iron magnetic shunts should be replaced by laminated shunts. It is too difficult to do if these shunts are made of magnetic powder.

5.8 Gearless Wind Power Generator Aggregate

Gearless wind power generators are the object of many papers [14, 15]. Their advantage over the generators driven by the wind turbine through the gear is not only in higher efficiency and reliability but also in lower capital cost.

The considered generator with inner stator offers additional advantage. The wind turbine can be directly combined with the generator rotor as a one aggregate. Such a construction of the generator of 1 kW, proposed for small household can be mounted in horizontal (Fig. 5.41 a) and vertical (Fig. 5.41 b) positions on the roof of a house. To meet the need for greater power more aggregates can be used (Fig. 5.42).

a)

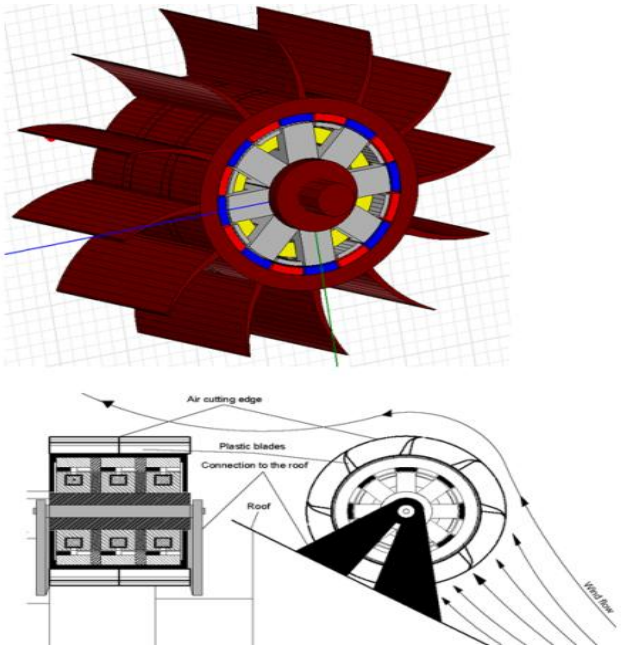

Figure 5.41 Generator aggregates: a) at horizontal position, b) at vertical position

Figure 5.41 (cont.)

b)

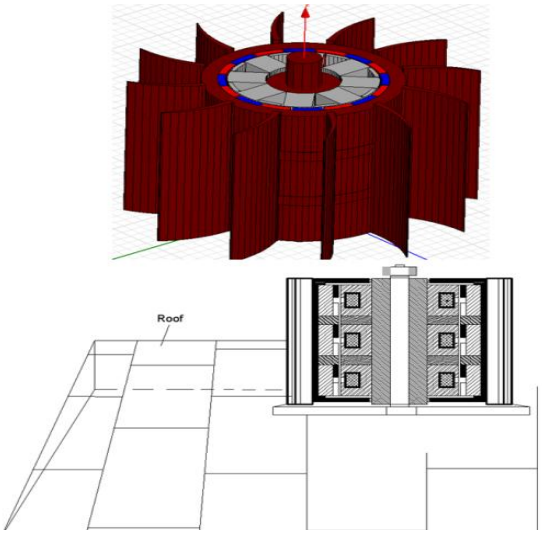

Figure 5.41 Generator aggregates: a) at horizontal position, b) at vertical position

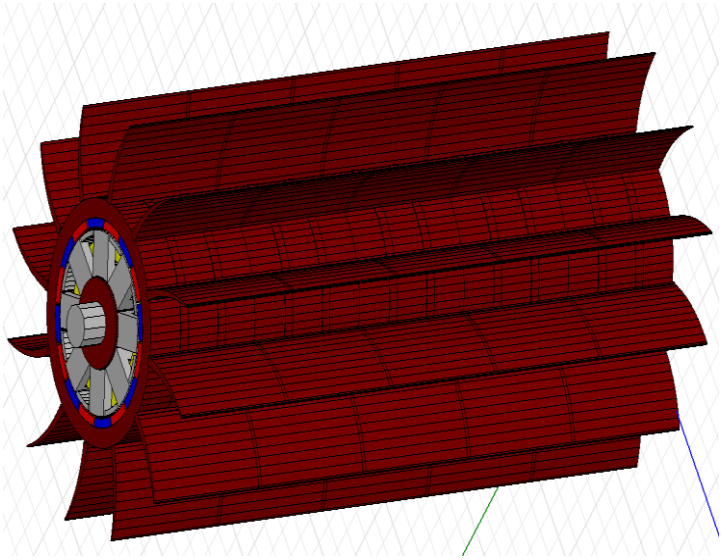

Figure 5.42 5 generators combined into one aggregate

Considered generator, can be combined with rotating half-cylinder which is shown in Fig. 5.43. The cylinder is attached to the generator shaft with help of mechanical systems which allows its

rotating. The direction of the half-cylinder's rotation is achieved by the governor blade which is always in parallel with wind flow.

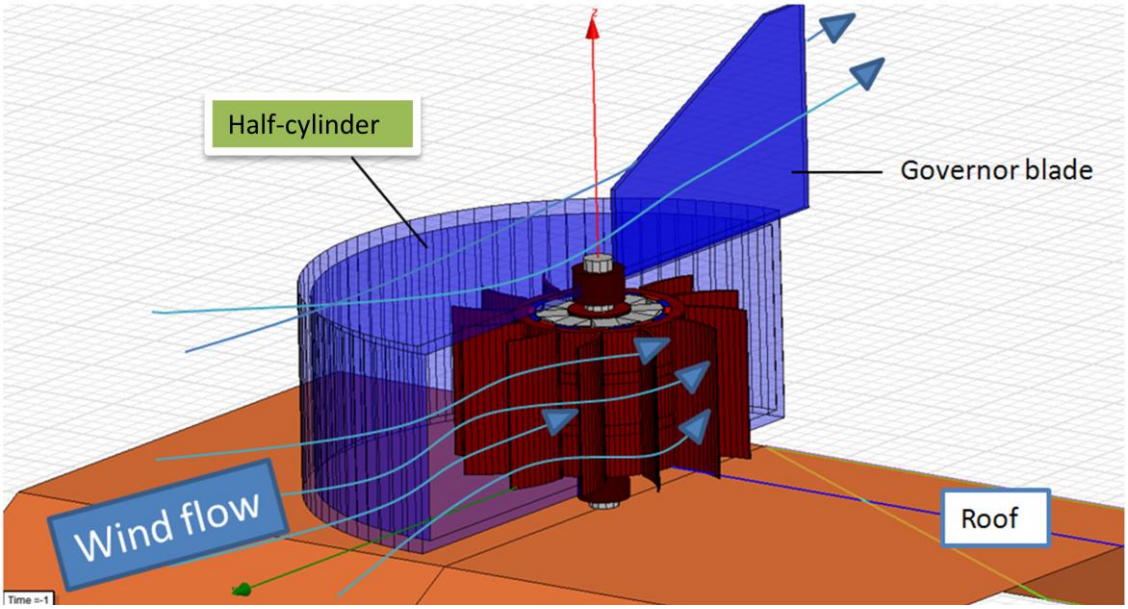

Figure 5.43 Turbine system for the generator mounted on the roof

CHAPTER 6: PMTF GENERATOR WITH DOUBLE ARMATURE

6.1 General Description of the Generator Construction

Based on the improved topology of 2010 discused in Chapter 5 a new PMTF machine design with double winding is proposed. The machine consits of two PMTF generators combined into one structure which have common rotor with permanent magnets on it (Fig. 6.1).

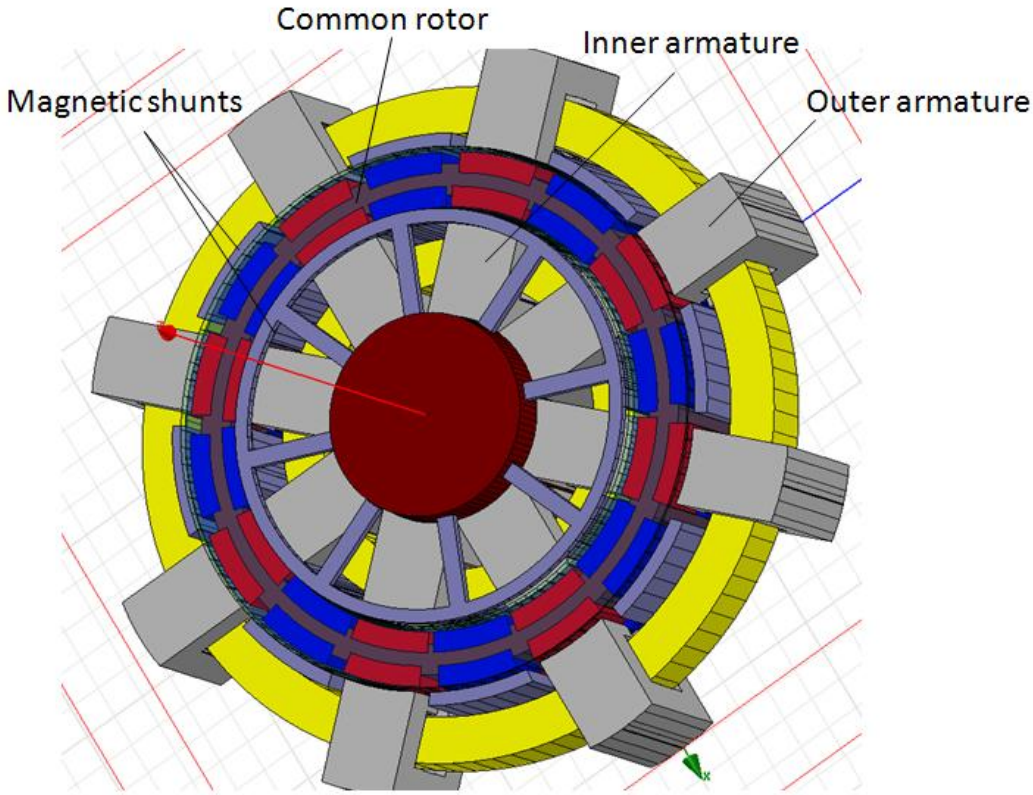

Figure 6.1 Single-phase PMTF machine with outer winding

The dimensions of the stator poles of outer and inner armatures, as well as all PMs are the same as those calculated for the generator discussed in Chapter 5. The difference is only in outer diameter

of the machine since the outer winding with corresponding magnetic poles was added. The rotor consists of an iron ring which holds the magnets. The ring is shown separately in Fig.6.2.

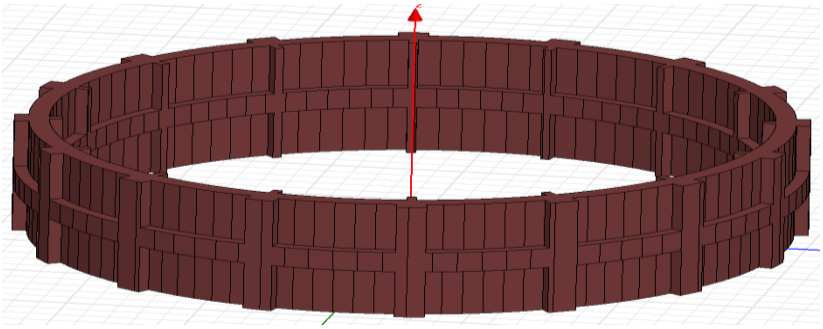

Figure 6.2 Rotor ring for holding PMs

Inner and outer stator poles face each other, so that magnetic circuit with flux Φ circulates in the the outer and inner poles as it shown in Fig. 5.35.

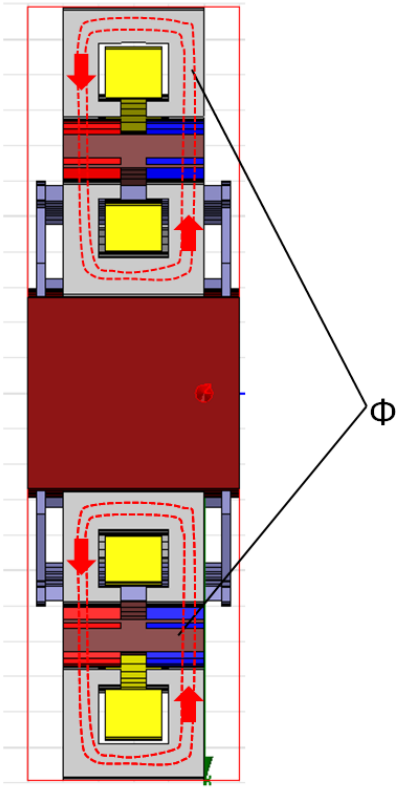

Figure 6.3 Magnetic circuit of the machine

The number of turns in each of the coils are the same.

6.2 Performance of the Generator in Steady-State Condition

6.2.1 Analysis of Induced Voltage

Induced voltage of the machine with double winding at rated speed 600 rpm is shown in Fig. 6.4 where two voltages are shown when the windings are not connected.

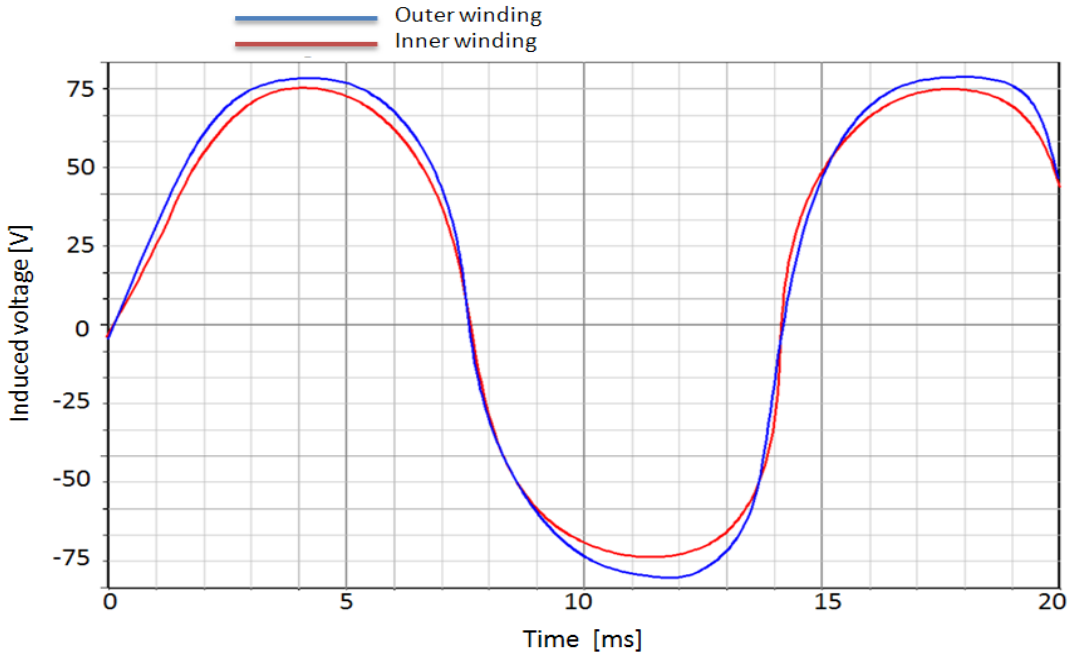

Figure 6.4 Induced phase voltages in both windings

The induced voltage in outer winding is slightly higher than the voltage of inner winding. This can be expalined by the fact, that the PMs' square of surface facing the outer armature poles are larger than that of the inner armature PMs. This difference between voltages in both windings can play negative role if the windings are connected in paralel like it is shown in Fig. 6.5 a. Current I_h circulating in the circuit between different voltage potentials will lead to winding heating even if there is no load connected. To avoid that, two windings are connected in series (Fig. 6.5 b).

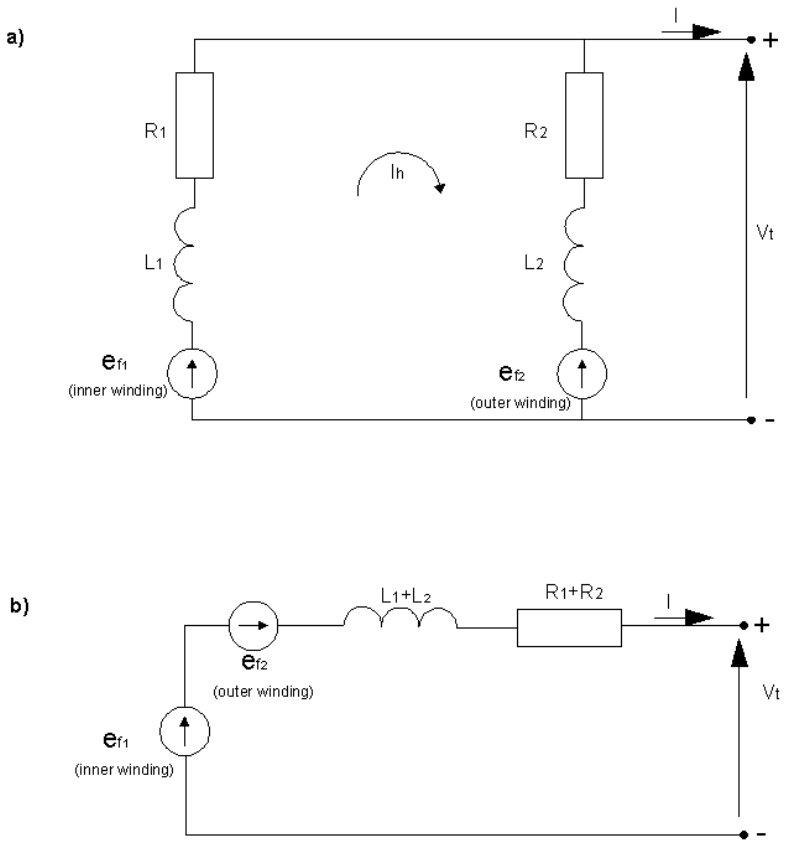

Figure 6.5 Equivalent circuit of the generator with double armature, a) windings are connected in parallel, b) windings are connected in series

Induced voltage of the generator is changing with turbine speed. The relationship between induced phase voltage and turbine speed of the machine with double stator for connected in series windings is shown in Fig. 6.6. Comparing it to the generator discussed in Chapter 5, it can be concluded that the machine with double armature promises two times higher induced voltage over the whole range of turbine speed.

The slight distortion of the voltage graph (Fig. 6.4) points on presence high order harmonics which were discussed in Chapter 5. Harmonics are caused mainly by the nonsinusoidally distributed magnetic field in the air-gap.

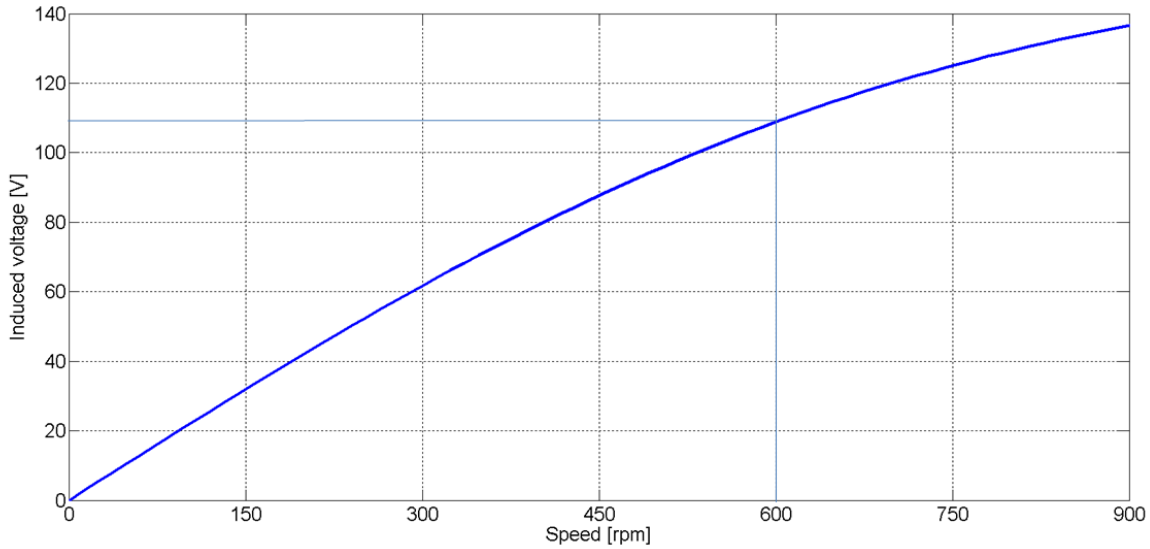

Figure 6.6 Induced voltage of the generator with different rotor speeds

6.2.2 Analysis of Torque Developed by the Generator

The importance of torque analysis for electric machines was underlined in Chapter 5 where 1 kW generator with single armature was represented. The major difference between torque curves of the machines with one armature (Chapter 5) and double armatures (presented in this Chapter) is in the fact, that the last one has a common rotor where PM's interact at the same time with outer and inner magnetic stator poles. This should produce two times higher torque than that obtained from the generator with one armature. Also, cogging torque curve is different which will have an influence on the resultant torque produced by the generator. Cogging and resultant torques of the machine with double armature for one phase ring (Fig. 6.1) are shown in Fig. 6.6. As it was discussed in Chapter 5, cogging torque of PMTF generator is high for one-phase ring structure. However, due to presence of magnetic shunts (discussed in Chapter 5), it is much smaller. Resultant average torque of the machine for one phase ring at rated phase current equal to 11.55 A is 14 N·m.

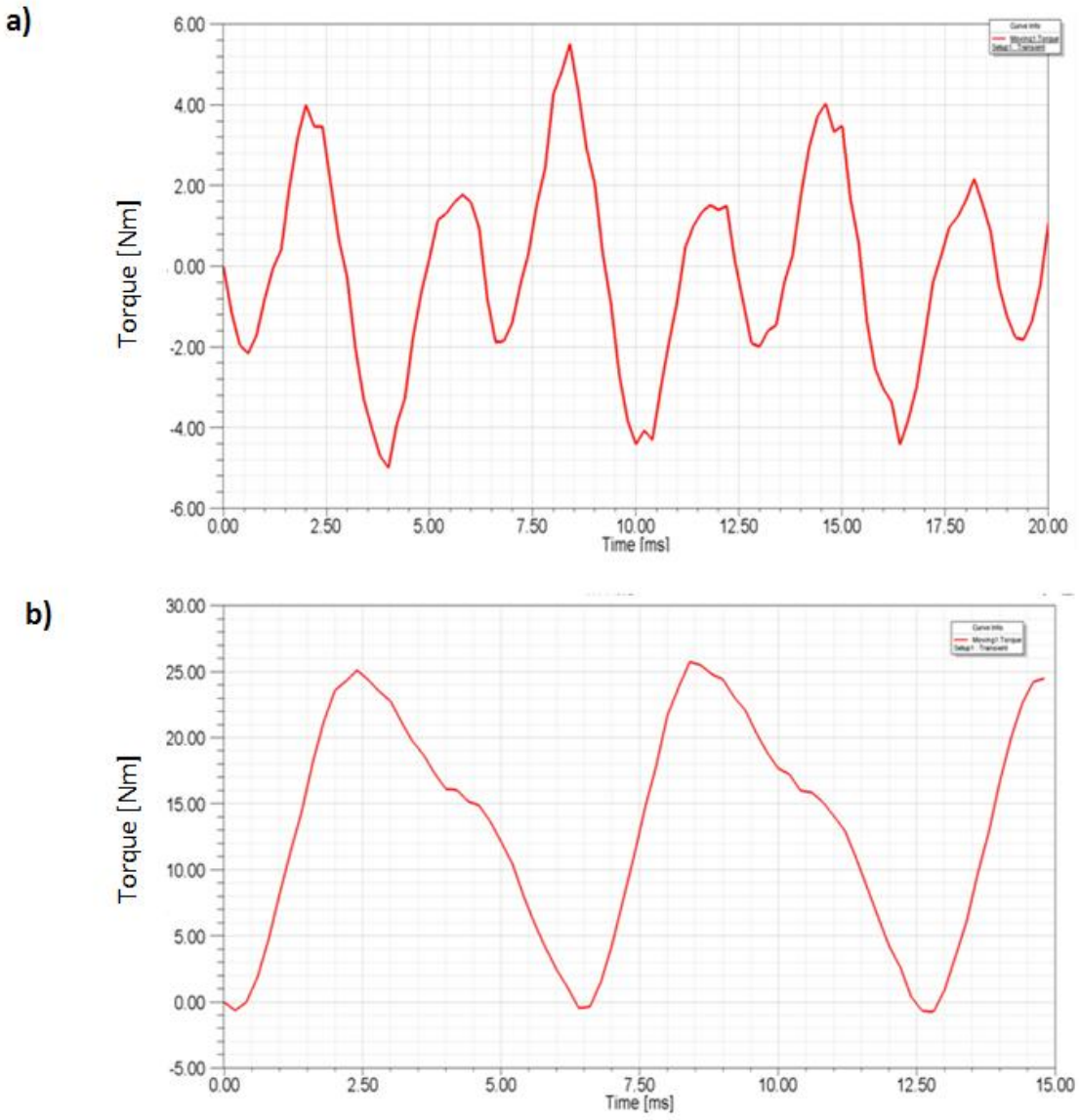

Figure 6.7 a) Cogging torque of the generator with double armature (one phase ring), b) resultant torque of the generator with double armature (one phase ring) with phase current of 11.55 A

When all 3-phase rings are considered as it shown in Fig. 6.7, the cogging torque of the generator will be lowered by the magnet skew between each of the phases (see Chapter 5). Hence, the resultant torque, which is 3 times higher than the torque for one-phase ring, is not rippled that much.

Cogging torque of the generator with double armature for 3-phase rings is shown in Fig. 6.7 a,

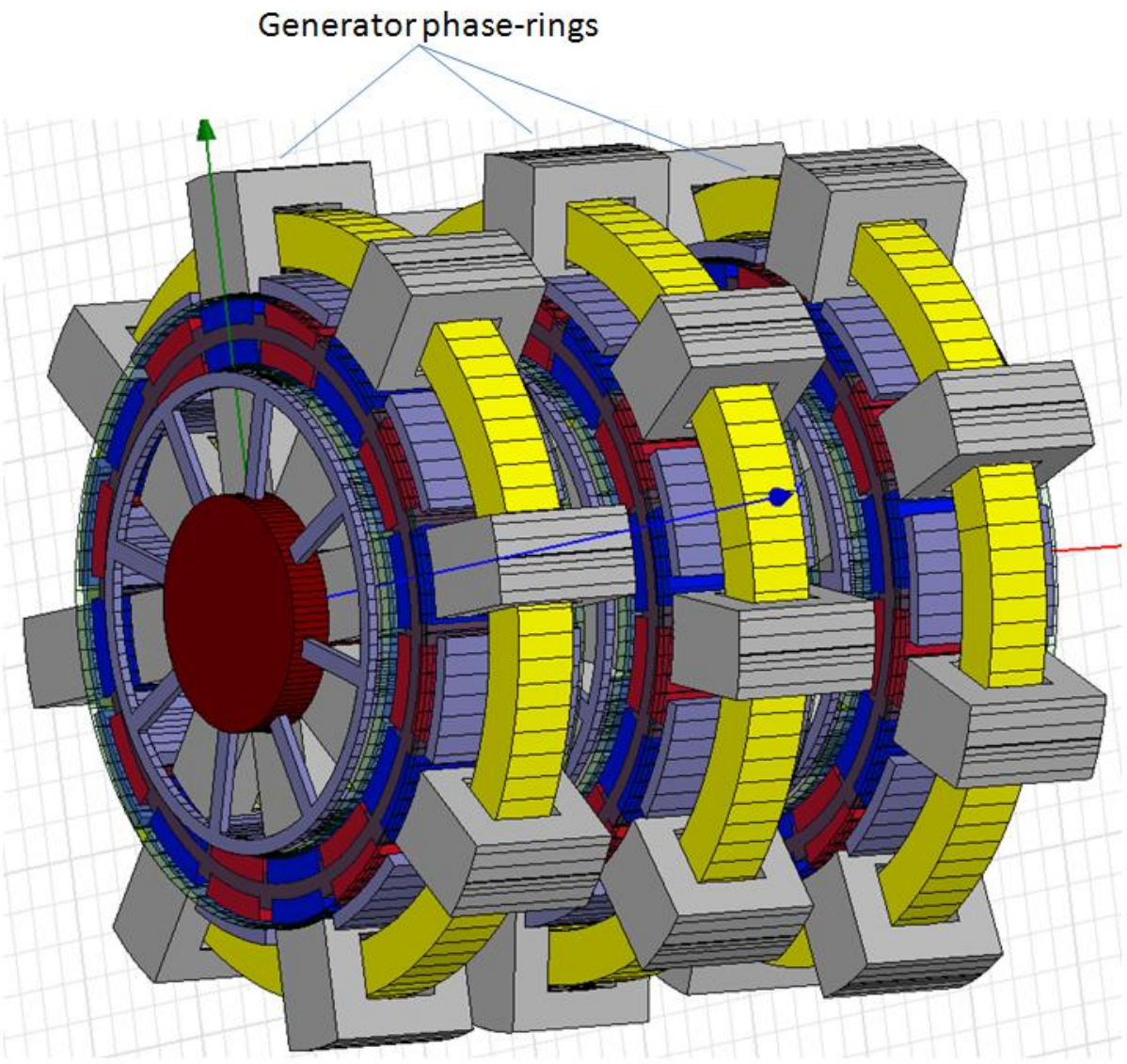

Figure 6.8 3-phase PMTF machine with outer winding

and the resultant torque is shown in Fig. 6.7 b. The average value of the resultant torque is 42.5 N·m which is two times higher than the torque of the machine with one armature discussed in Chapter 5. Torque ripple is 5% which is relatively small for PMTF machines class.

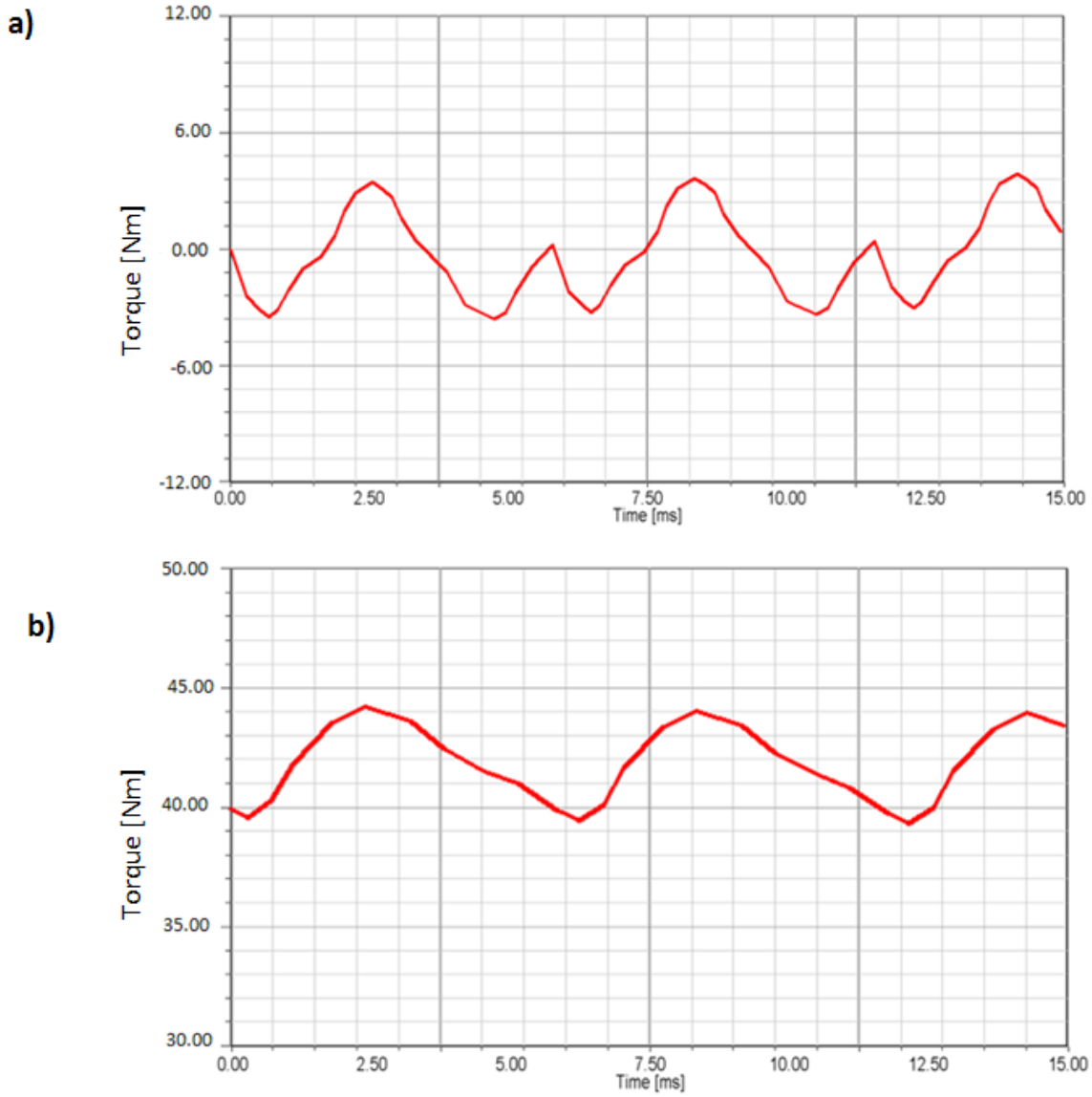

Figure 6.9 a) Cogging torque of the generator with double armature (3 phase-rings), b) resultant torque of the generator with double armature (3 phase-rings) with phase current of 11.55 A

6.2.2 Analysis of Output Power

Output power of the generator was described in section 5.3.3. In case of the generator with double winding, terminal voltage: $V_t = V_1 + V_2$. This gives the output power of the machine with

double stator to be almost two times higher than that of the machine with one armature described in Chapter 5. The terminal voltage vs. speed at load phase resistance of 3.5 Ω is shown in Fig. 6.10. The load resistance was determined using formula 5.46, and the result of calculation is shown in Fig. 5.18.

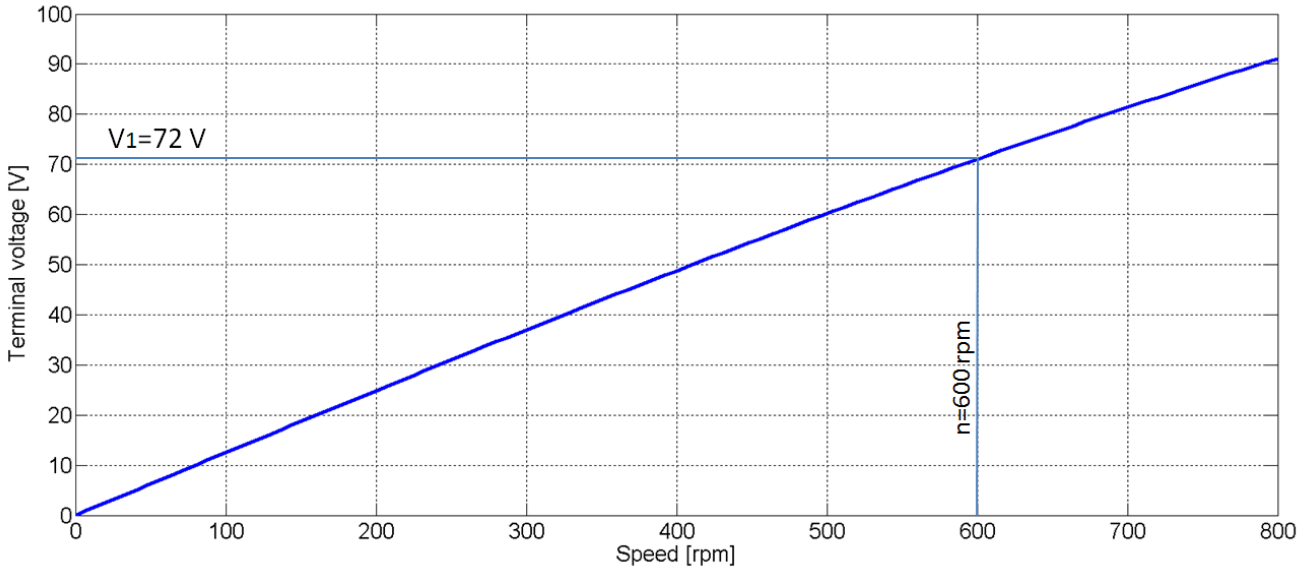

Figure 6.10 Terminal voltage of the generator with different rotor speeds

Output power of the machine with double stator for 3 phases is shown in Fig. 6.11 and equals to 2200 W at rated speed.

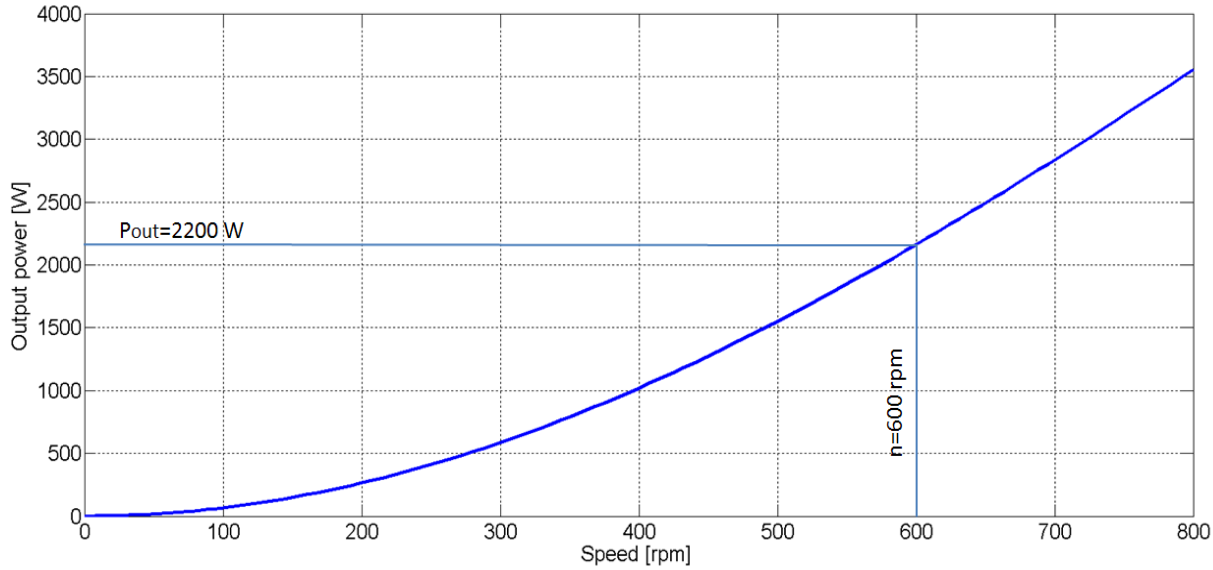

Figure 6.11 Output power of the generator with different rotor speeds

The rated parameters of the generator with double armature are enclosed in Table 6.1.

Table 6.1 Rated parameter of the generator with double armature

PARAMETER	VALUE
1. Rated current 2. Rated speed 3. Rated phase voltage (amplitude) 3. Rated power 4. Number of rotor poles	11.55 A 600 rpm 100 V 2,2 kW 16

6.4 Comparison of Different Designs of PMTF Machines Studied in the Dissertation

Three types of machines that were studied in the dissertation are shown in Fig. 6.3 a-c.

a)

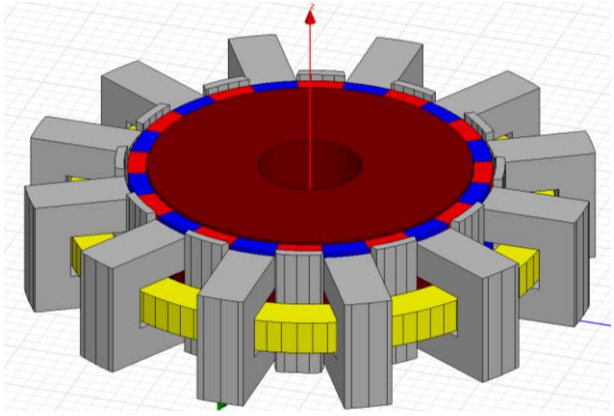

b)

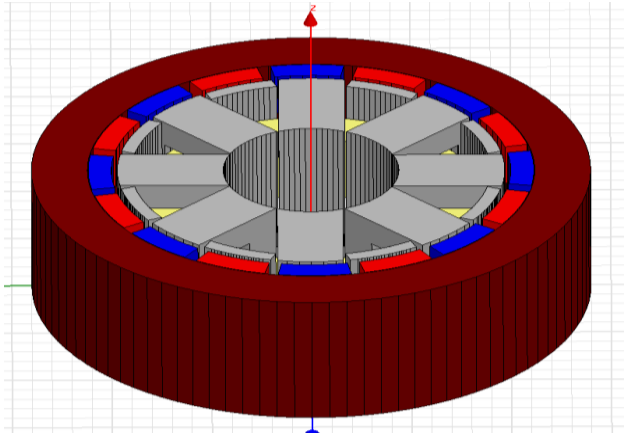

Figure 6.12 Single phase rings of PMTF machine designs studied in the dissertation: a) with internal rotor, b) with external rotor, c) with double armature

Figure 6.12 (cont.)

c)

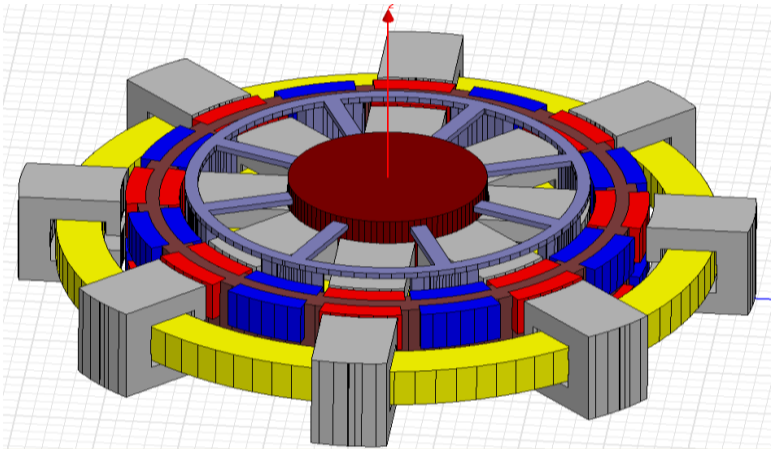

Figure 6.12 Single phase rings of PMTF machine designs studied in the dissertation: a) with internal rotor, b) with external rotor, c) with double armature

These are: PMTF machine with internal rotor (according to F. Giearas' patent), with external rotor and the machine with double armature. In order to compare three different designs, output power to volume ratios for each of them were found. They are as follows:

- Generator with external stator : 290 KW/m^3
- Generator with internal stator : 368 KW/m^3
- Generator with double armature : 512 KW/m^3

It means that PMTF machine studied in this dissertation with external rotor was modified to the design which offers higher power to volume ratio than that with internal rotor.

In case of the machine with double armature, the power of the machine was increased in two times, but machine outer diameter only by 30%, which gave the highest power to volume ratio among all the designs studied in the dissertation.

CHAPTER 7: CONCLUSIONS AND FUTURE SCOPE OF STUDY

A main goal of this dissertation was to study a PMTF generator in order to improve its performance. The interest to PM AC generators has been increased recently because they bring following benefits comparing to conventional generators:

- no electrical energy is absorbed by the field excitation system, and thus there are no excitation losses which means an increase in the efficiency.
- higher torque and output power per volume than when using electromagnetic excitation.
- better dynamic performance than generators with electromagnetic excitation (higher magnetic flux density in the air gap).
- low maintenance requirements.

Because of this, PM machines are used widely nowadays. They can be met in drives for electric cars, ship propulsion mechanisms, and various industrial applications. PM generators are applied more and more to generate electricity from wind and ocean energy.

The dissertation began with studying the newest topology of PMTF machine patented by G. F. Gieras in 2010. Machine prototype which was built and implemented significant part of this idea showed certain disadvantages of the machine design. The output power of the machine appeared to be two times lower than that what was expected [29].

With help of 3D FEM modeling, the main problems of the machine design were identified and sloved. The most serious problem was that magnetic flux density in the stator poles was drastically weakened by the magnetic field of “inactive” magnets. Necessary steps for improving machine performance were undertaken and implemented into its design. Chapter 5 discusses the modified topology of PMTF machine with outer rotor, where magnetic field coming from “inactive” magnets was blocked by magnetic shunts embedded into stator structure. In this case, magnetic field density in

the stator poles was no longer seriously affected by inactive magnets and the output power of the generator was 70% higher than that of the machine without shunts. However, when these shunts are made of solid iron, due to high eddy currents induced on their surface, power losses of the generator are very high. Temperature analysis which was done in the dissertation shows that iron magnetic shunts are one of the most significant sources of heat in the machine. When the shunts are made of laminated steel, the power losses in the shunts are negligible, and shunts are not overheated.

Proposed design of the PMTF machine with outer rotor allowed combining the generator with direct drive turbine. Such a wind turbine can be mounted on the house roof to satisfy household needs in electricity for a small house.

To maximize power to volume ratio of the PMTF machine, new design of the machine with double coil was introduced. In this case, machine volume to power ratio was 30% higher than it was in the previous designs studied in the dissertation.

Summarizing all of the results achieved by this study, the following conclusions can be formulated:

1. The given original PMTF generator of topology 2010 has around 60% of its predicted power mainly due to the large negative flux linkage that comes from “inactive” permanent magnets.

3. The magnetic shunts implementation into the generator structure almost eliminated the negative flux linkage giving rise to induced voltage and power by 70%.

3. Magnetic shunts significantly reduced cogging torque of the generator.

4. The generator structure with internal stator gives higher power to volume ratio and allows combining it with the wind turbine as a compact aggregate that was proposed.

5. Laboratory test of the prototype which was built according to the design discussed in Chapter 5 proves that magnetic shunts block 70% of negative magnetic flux coming from inactive PMs.

6. Laboratory test also shows that if the shunts are made of pure iron, there are power losses caused by eddy currents induced on the magnetic shunts' surface. To eliminate this problem, magnetic shunts have to be made whether of laminated steel or magnetic powder.

8. The new topology of PMTF machine with double stator which was proposed allows increasing the power density (power to volume ratio) by 30%.

Future scope of study can include building a computer model of the generator connected to the battery for providing power for a small electric grid which can be a house. Control system has to be developed to prevent the generator from rotating at high speeds when there is no need in power, or weather is extremely severe.

3D FEM model of the generator with shunts made of magnetic powder has to be verified for performance. Stress analysis of the model has to be done to make sure that shunts are not displaced during generator operation because of high attraction force of the PMs. Future scope of study also has to be directed on making manufacturing process for the machine easier.

BIBLIOGRAPHY

[1] J. F. Gieras, "Transverse Flux Machine", Patent Application Publication, Pub. No.: US 2010/005, March 4, 2010.

[2] H. Weh, "Machine with Transverse Flux", Patent Application Publication, Pub. No.: 5,633,551, May 27, 1997.

[3] A. Lange, "Transverse Flux Machine", Patent Application Publication, Pub. No.: 5,773,910, June 30, 1998.

[4] D. Bang, H. Polinder, G. Shrestha, and J.A. Ferreira, "Comparative design of radial and transverse flux PM generators for direct-drive wind turbines", in Proc. 2008 International Conference on Electrical Machines, Vilamoura, Portugal, September 6-9, 2008.

[5] W. Hill, "Transverse Flux Machine", Patent Application Publication, Pub. No.: 5,942,828, August 24, 1999.

[6] A. Detela, "Hybrid Synchronous Machine with Transverse Magnetic Flux", Patent Application Publication, Pub. No.: 5,712,521, January 27, 1998.

[7] H. Polinder, F.F.A. van der Pijl, G.J. de Vilder, P. Tavner, "Comparison of direct-drive and geared generator concepts for wind turbines", IEEE Trans. Energy Conversion, Vol. 21, pp. 725-733, September 2006.

[8] M. Dubois, "Optimized permanent magnet generator topologies for direct drive wind turbines", Ph.D. dissertation, Delft University of Technology, Delft, The Netherlands, 2004.

[9] P. Lampola, "Directly driven, low-speed permanent-magnet generators for wind power applications", Ph.D. dissertation, Helsinki University of Technology, Finland, 2000.

[10] A.S. McDonald, M.A. Mueller and H. Polinder, "Comparison of generator topologies for direct-drive wind turbines including structural mass", in Proc. of the International Conference on Electrical Machines(ICEM), pp. 360.1-7, September 2006.

[11] A. Grauers, "Design of direct-driven permanent-magnet generators for wind turbines", Ph.D. dissertation, Chalmers University of Technology, Göteborg, Sweden, 1996.

[12] D. Bang, H. Polinder, G. Shrestha, and J.A. Ferreira, "Design of a lightweight transverse flux permanent magnet machine for direct-drive wind turbines", 2008 IEEE Industry Applications Society Annual Meeting, Edmonton, Canada, October 5-9 2008.

[13] B.E. Hasubek and E.P. Nowicki, "Design limitations of reduced magnet material passive rotor transverse flux motors investigated using 3D finite element analysis", in Proc. 2000 IEEE Canadian Conf. Elec. and Computer Engineering, Vol. 1, pp. 365-369.

[14] D.H. Kang, D.J. Bang, J.M. Kim, Y.H. Jeong, M.H. Kim, "A Study on the design of PM exited transverse flux linear motor for ropeless elevator", Trans. KIEE(The rean stitute of Electrical Engineers). Vol. 49B. No. 3, Mar, 2000.

[15] D. Bang, H. Polinder, G. Shrestha, and J.A. Ferreira, "Comparative design of radial and transverse flux PM generators for direct-drive wind turbines", in Proc. 2008 International Conference on Electrical Machines, Vilamoura, Portugal, September 6-9, 2008.

[16] D. Svechkarenko, Juliette Soulard, Chandur Sadarangani, "Parametric study of a transverse flux wind generator at no-load using three-dimensional finite element analysis", ICEMS 2009. International Conference on Electrical Machines and Systems, 2009. Publication Year: 2009 , Page(s): 1 – 6.

[17] D. Bang , Henk Polinder, Ghanshyam Shrestha, Jan Abraham Ferreira, "Ring-shaped transverse flux PM generator for large direct-drive dind turbines ", International Conference on Power Electronics and Drive Systems, 2009. PEDS 2009, Page(s): 61 – 66.

[18] D. Bang, H. Polinder, G. Shrestha, and J.A. Ferreira, "Comparative design of radial and transverse flux PM generators for direct-drive wind turbines", in Proc. 2008 International Conference on Electrical Machines, Vilamoura, Portugal, September 6-9, 2008.

[19] O. Dobzhanskyi, E. Mendrela, and A. Trzynadlowski, "Analysis of leakage flux losses in transverse flux PM synchronous generator", IEEE Green Technology Conference, Baton Rouge, Louisiana, April 2011.

[20] M. R. Dubois, H. Polinder, J. A. Ferreira, "Transverse-flux permanent magnet (TFPM) machine with toothed rotor", IEEE Transaction on Power Electronics, Conference Publication No: 487, April 16-18, 2002.

[21] M. R. Harris, B. C. Mercow, 1993, "Variable reluctance permanent magnet motors for high specific output", IEE Conf. on Elec. Machines and Drives, 437-442.

[22] H. Weh, 1988, "Permanentmagneterregte synchronmaschinen hoher Kraftdichte nach dem Transversalflusskonzept", etzArchiv, 10, 143-149.

[23] G. R. Liu and S. S. Quek, "Finite Element Method", A practical course, Linacre House, Jordan Hill, Oxford OX 8DP, 2003, pp.3-9.

[24] D. Meeker, "Finite Element Method Magnetics – Version 4.0", *User's Manual, January 8, 2006.*

[25] Maxwell 3D v12, Getting Started Guide, ANSOFT, February 2008.

[26] ePhysics v12, Getting Started Guide, ANSOFT, February 2008.

[27] Simplorer v7, Getting Started Guide, ANSOFT, February 2008.

[28] MathWorks Corporation website: http://www.mathworks.com/

[29] J. Green, “Development of a high performance generator for wind turbines”, Stage II, The Prototype, National Wind Technology Center, National Renewable Energy Laboratory, 2010.

[30] W. Fengxiang, Hou Qingming, Bo Jianlon, Pan Jian, “Study on control system of low speed PM generator direct driven by wind turbine”, Proceedings of the Eighth International Conference on Electrical Machines and Systems, 2005. ICEMS 2005.

[31] L. L. Freris, Wind energy conversion system: Prentice Hall, 1990.

[32] E. Muljadi, S. Drouilhet, R. Holz and V. Gevorgian, "Analysis of permanent magnet generator for wind power battery charging", IEEE-IAS Annual Meeting, vol.1 , Oct. 1996, pp.541-548.

[33] A. J. G. Westlake, J. R. Bumby, and E. Spooner, "Damping the power-angle oscillations of a permanent-magnet synchronous generator with particular reference to wind applications," IEE Proc.-Electr. Power Appl, Vol. 143, No. 3, May 1996, pp. 269-280.

[34] E. Muljadi and C.P. Butterfield, "Pitch-controlled variable-speed wind turbine generation," IEEE Trans. on Industry Applications, vol.37, Jan./Feb. 2001, pp. 240-246.

[35] P. Lampola, "Directly driven, low-speed permanent-magnet generators for wind power applications," Laboratory of Electromechanics, Helsinki University of Technology, May 2000.

[36] N. Vilsboll etc., "The experience of designing and testing a 20 kW multi-pole permanent magnet generator for wind turbines. DEWI Magazine, no.9, August 1996

[37] H. Polinder, F.F.A. van der Pijl, G.J. de Vilder, P. Tavner, “Comparison of direct-drive and geared generator concepts for wind turbines”, IEEE Trans. Energy Conversion, Vol. 21, pp. 725-733, September 2006.

[38] A.S. McDonald, M.A. Mueller and H. Polinder, “Comparison of generator topologies for direct-drive wind turbines including structural mass”, in Proc. Of the International Conference on Electrical Machines (ICEM), pp. 360.1-7, September 2006.

[39] D. Bang, H. Polinder, G. Shrestha, and J.A. Ferreira, “Promising direct-drive generator system for large wind turbines”, EPE Journal, Vol. 13, pp. 7-13, September 2008.

[40] M. Dubois, “Optimized permanent magnet generator topologies for direct drive wind turbines”, Ph.D. dissertation, Delft University of Technology, Delft, The Netherlands, 2004.

[41] D. Bang, H. Polinder, G. Shrestha, and J.A. Ferreira, “Design of a lightweight transverse flux permanent magnet machine for direct-drive wind turbines”, 2008 IEEE Industry pplications Society Annual Meeting, Edmonton, Canada, October 5-9 2008.

[42] B.E. Hasubek and E.P. Nowicki, “Design limitations of reduced magnet material passive rotor transverse flux motors investigated using 3D finite element analysis”, in Proc. 2000 IEEE Canadian Conf. Elec. and Computer Engineering, Vol. 1, pp. 365-369.

[43] D.H. Kang, D.J. Bang, J.M. Kim, Y.H. Jeong, M.H. Kim, "A Study on the design of PM exited transverse flux linear motor for ropeless elevator", Trans. KIEE(The Korean Institute of Electrical Engineers). Vol. 49B. No. 3, Mar, 2000 *(in Korean).*

[44] D. Bang, H. Polinder, G. Shrestha, and J.A. Ferreira, "Comparative design of radial and transverse flux PM generators for direct-drive wind turbines", in Proc. 2008 International Conference on Electrical Machines, Vilamoura, Portugal, September 6-9 2008.
PEDS2009.

[45] S. Blumberg, "Windmill Accelerator", United States Patent, Patent No: 5.457.346, October. 10, 1995

[46] L. R. O'Hare, "Wind Tower Turbine", United States Patent, Patent No: 4.288.200, September. 8, 1981

[47] Etap software, http://etap.com/

[48] J. F. Gieras, Mitchell Wing, "Permanent magnet motor technology design".

[49] D. Meeker, "Finite Element Method Magnetics", Version 4.2, User's Manual, November 26, 2009.

[50] W. M. Arshad, T. Basckstrom, C. Sadarangani, "Analytical design and analysis procedure for a transverse flux machine", Division of Electrical Machines and Power Electronics, Royal Institute of Technology, Sweden.

[51] P. Anpalaham, Design of transverse flux machines using analytical calculations & finite element analysis, Tech. Licentiate Thesis, Royal Institute of Technology, Stockholm, 2001.

[52] W. M. Arshad, Application of SMC iron powder materials in electrical machines, Masters thesis, Royal Institute of Technology (KTH), Stockholm, Dec. 1998.

[53] T. Bäckström, Integrated energy transducer drive for hybrid electric vehicles, Ph.D. Thesis, SBN 91-7170-571-6, Royal Institute of Technology, Stockholm, 2000.

[54] D. K. Cheng, Field and wave electromagnetics, Addison-Wesley Publ. Comp. New York, 1989.

[55] E. R. Laithwaite, J. F. Eastham, H. R. Bolton & T. G. Fellows, "Linear motors with transverse flux," IEE Proceedings vol. 118, pp. 1761-1767, December 1971.

[56] A. Masmoudi and A. Elantably, "An approach to sizing high power density TFPM intended for hybrid bus electric propulsion," Electric machines and power systems, 28:341-354, 2000.

[57] G. H. Pajooman, Performance assessment and design optimization of VRPM (transverse flux) machines by finite element computation, Ph.D. Thesis, Southampton University, England, 1997.

[58] C. Sadarangani, Electrical Machines, Electrical Power Engineering Department Publication, Royal Institute of Technology (KTH), Stockholm, Sweden 2000.

[59] K. Schoepp & P. Zielinski, "Low-speed synchronous generator for wind-plant application", ICEM 98 Proceedings, pp. 1699-1704 Istanbul, Turkey, 1998.

[60] H. Weh & H. May, "Achievable force densities for permanent magnet excited machines in new configurations, " ICEM'86, Munich, 1986.

[61] J. S. D. Garcia, Mauricio V. Ferreira da Luz, "Transverse flux machines: what for?", IEEE Multidisciplinary Engineering Education Magazine, Vol. 2, No. 1, March 2007.

[62] D. Svecharenko, "On design analysis of a novel transverse flux generator for direct-driven wind application", Dissertation, Royal Institute of Technology, Sweden, 2010.

[63] E. Mendrela, "Advanced electric machines", Course pack, Louisiana State University, Baton Rouge, 2010.

[64] E. S. Hamdi, "Design of small electric machines", University of Wales, College of Cardiff, UK, 1994.

[65] S. R. Trout, "Spontaneous materials" International Magnetics Association Permanent Magnet Tutorial Indianapolis, IN October 24, 2005.

[66] T. Saitou, 'Reluctance type motor apparatus and driving method capable of reducing ripples in Motor Output Torque' US patent US 6232741, May 15, 2001.

APPENDIX A: COMPLETE DRAWINGS OF THE GENERATOR WITH CALCULATED DIMENSIONS

In this appendix included the drawings which were sent to manufacturer “Komel”. All these dimensions were optimized during 3D FEM analysis to satisfy the requirements of manufacturer. In more details the optimization process is described in Apendix B.

The last drawing (A.9) which is included in this Apendix, is an axial crossection sketch of the generator, where some differences in geometry and dimensions introduced by the manufacturer can be seen.

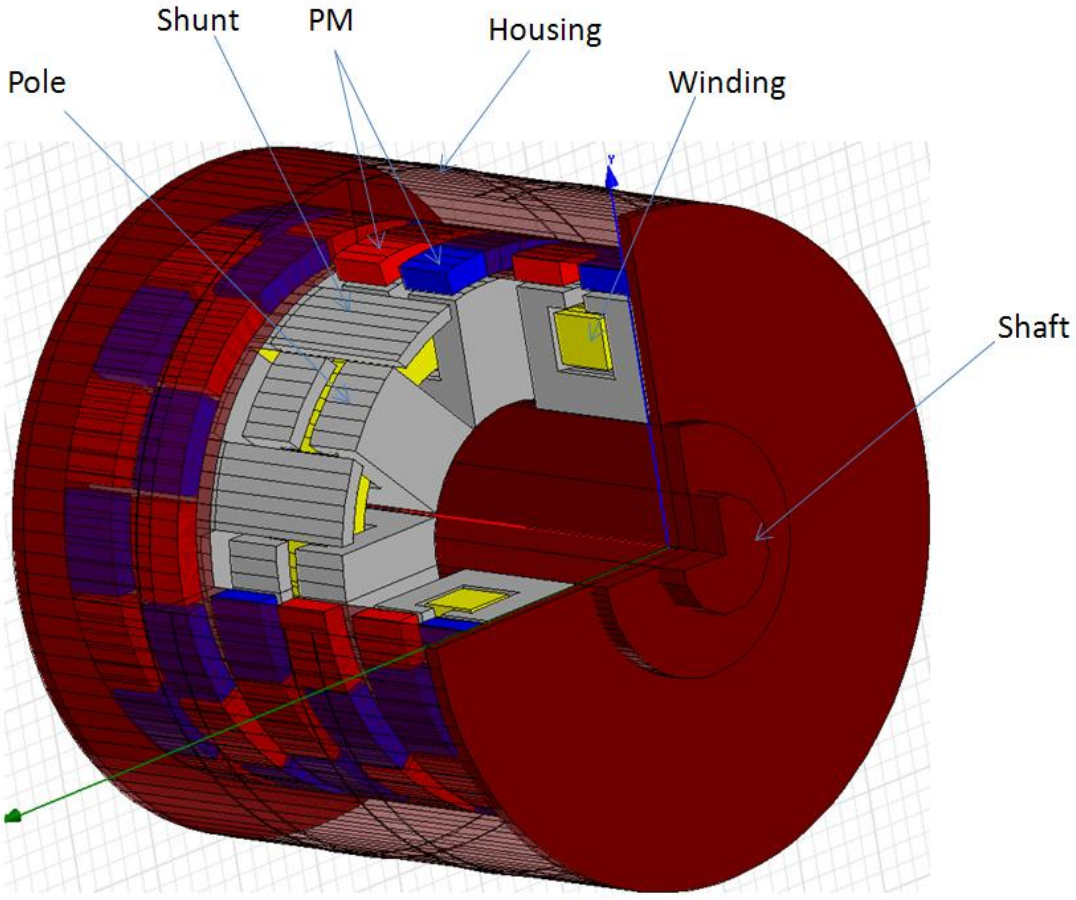

Figure A.1 General view of the machine design

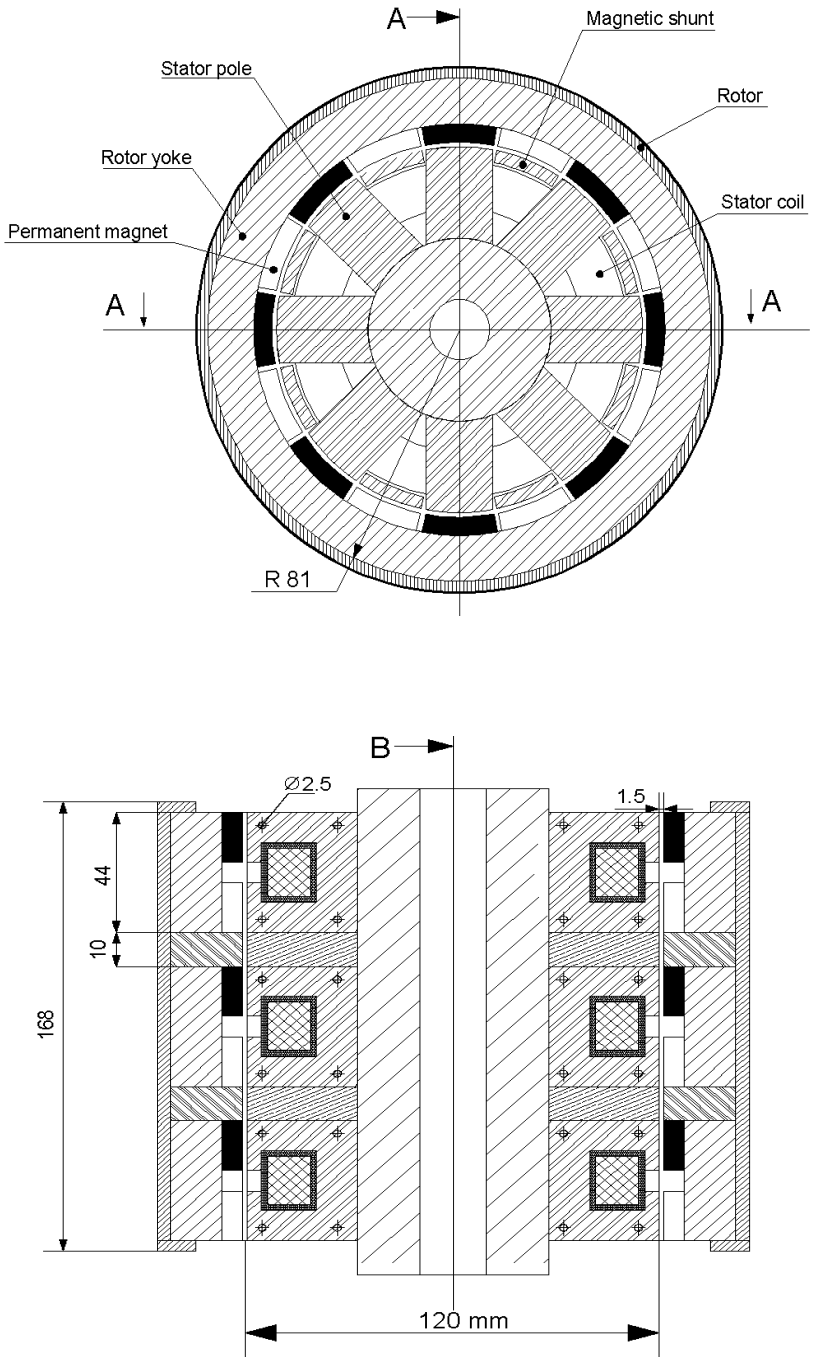

Figure A.2 Vertical and horizontal cross-section of the machine with basic dimensions

a)

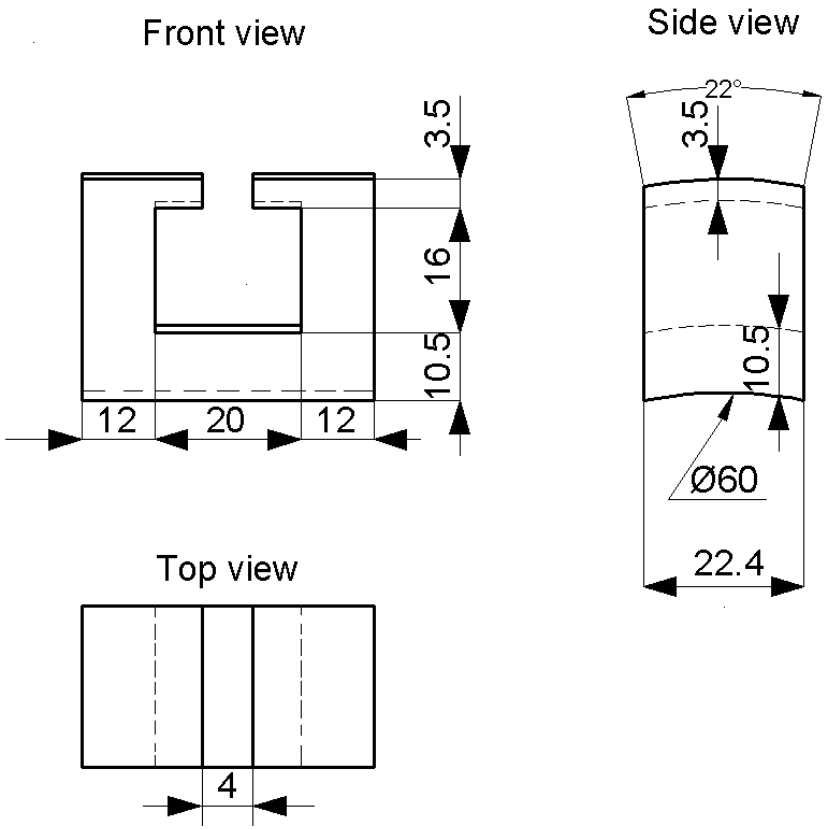

b)

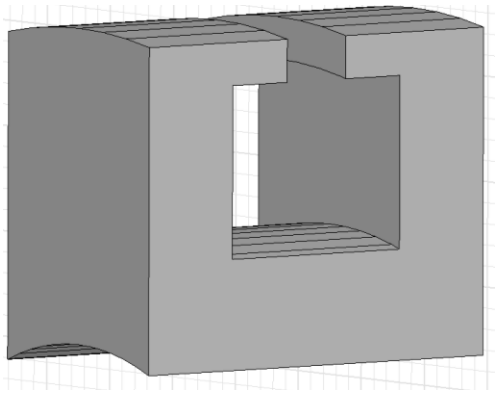

Figure A.3 a) Dimensions of the pole shoe, b) 3D view of the pole shoe

a)

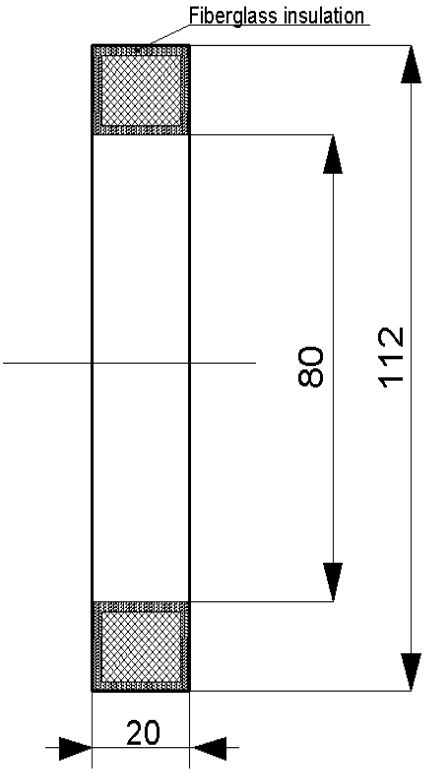

b)

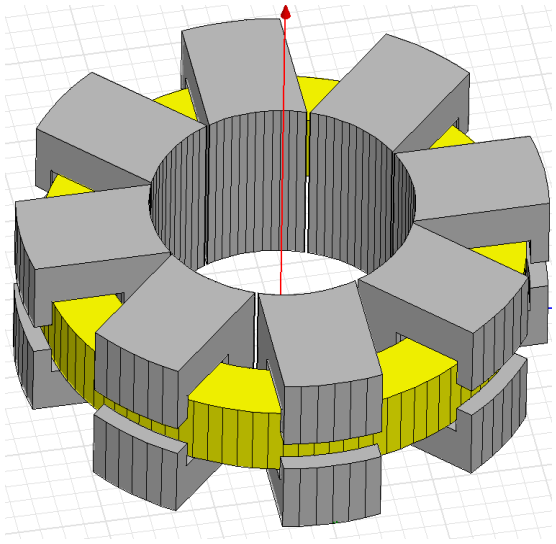

Figure A.4 a) Dimensions of the coil, b) 3D view of the coil inside of magnetic circuit

a)

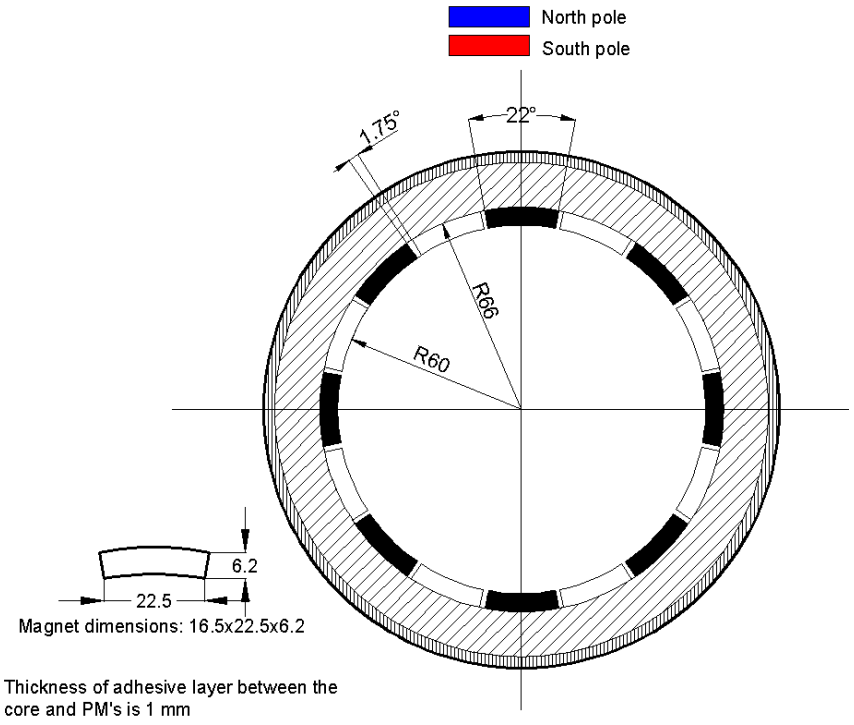

b)

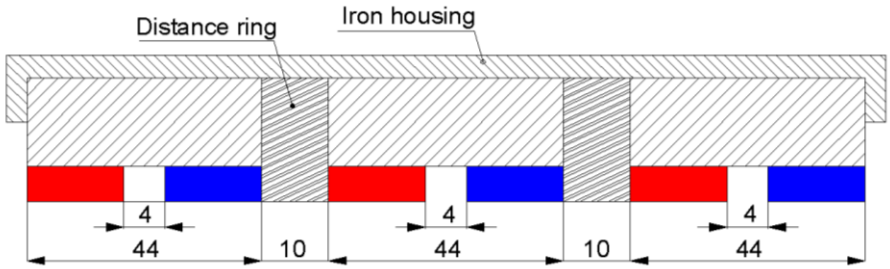

c)

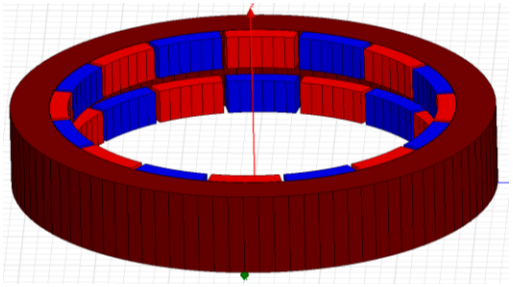

Figure A.5 a) Dimensions of rotor assembly (front cross-section), b) dimensions of magnet assembly (side cross-section), c) 3D view of the rotor yoke with PMs

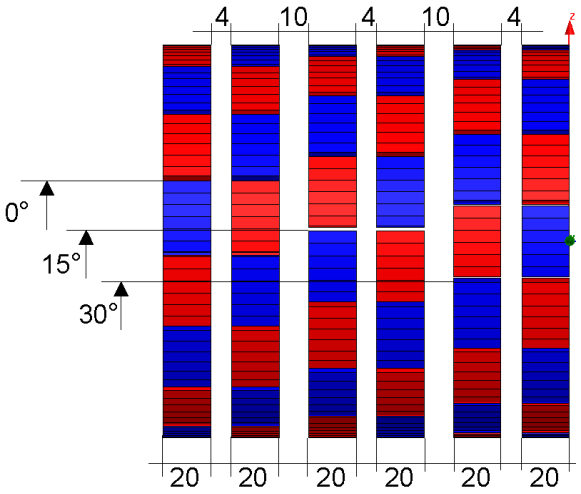

Figure A.6 Dimensions of magnets' axial layouts

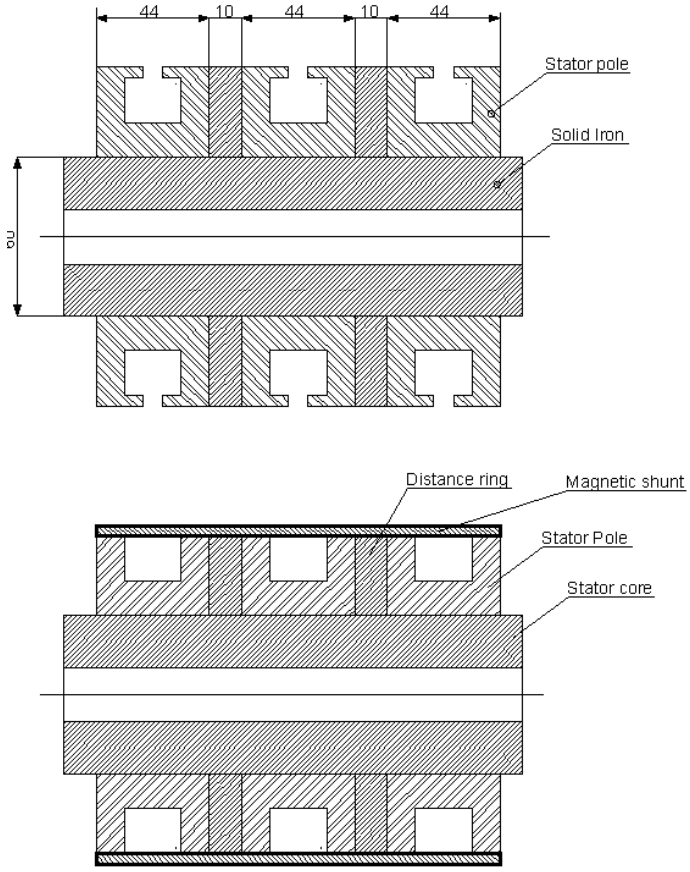

Figure A.7 Stator assembly dimensions

Figure A.7 (cont.)

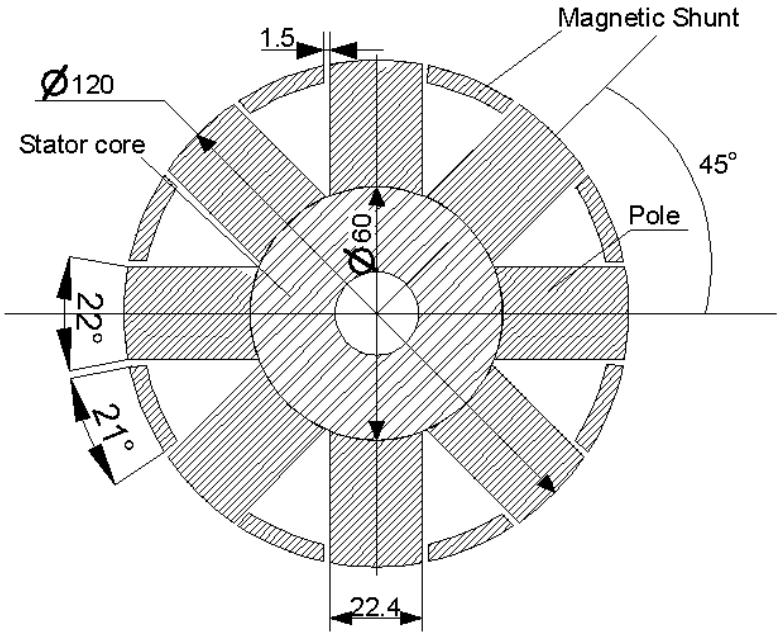

Figure A.7 Stator assembly dimensions

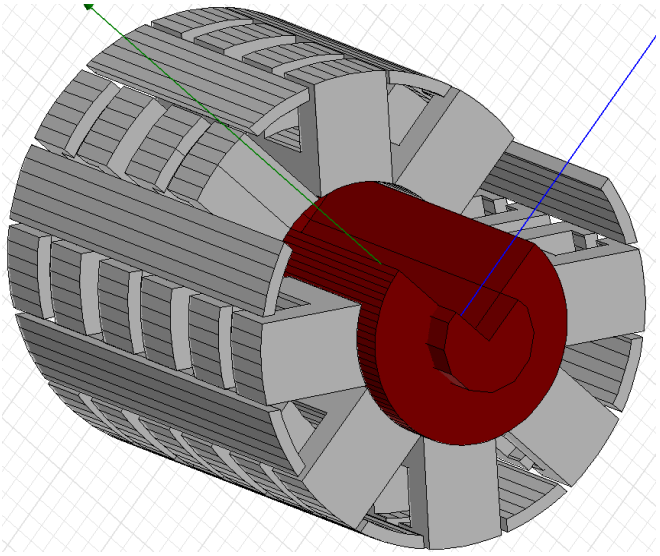

Figure A.8 Stator assembly with magnetic shunts in 3D view

APPENDIX B: OPTIMIZATION OF GENERATOR DIMENSIONS

This appendix contains information about how magnetic circuit dimensions were optimized to satisfy a request of manufacturer. Polish manufacturer "KOMEL" which built the prototype of the machine, suggested to connect the lamination of magnetic poles with iron bolts with the diameter of 3 mm. as it shown in Fig. B1.

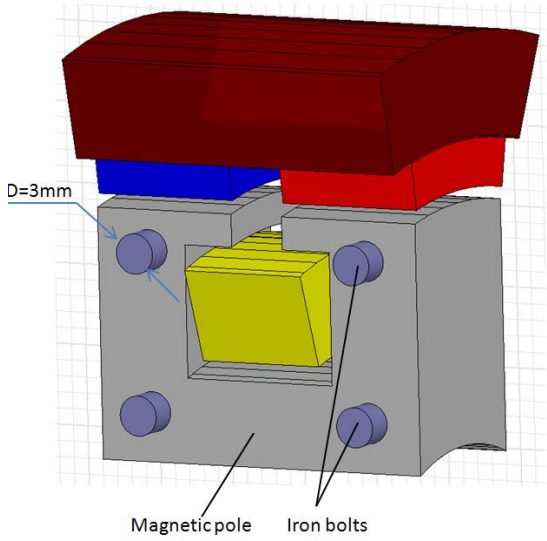

Figure B.1 Magnetic pole with connecting bolts

The bolts which go through the magnetic pole cause saturations of magnetic flux circulating in the poles. This saturation significantly drops magnetic flux density in the pole and consequently the flux linkage. Magnetic field distribution of the pole without and with bolts is shown in Figs. A.2 a, b. The magnetic flux density is equally distributed in the pole without bolts (Fig. A.2 a) and its value is 1.6 T. The flux linkage corresponding to the part of the coil shown on the picture is 0.7 mWb. In case of the pole with iron bolts (Fig. A.2 b), the average magnetic density in the pole is 40-45% lower as it is in the pole without bolts. The flux linkage is also dropped to 0.5 mWb. This is caused by the saturations along the bolts where magnetic field produced by the PMs cannot go through the pole. In total 25% of output power of the generator is lost when the poles connected with bolts as it shown in

Fig. A.2 b. To eliminate this problem, magnetic poles have to be widened in both ways for 2 mm to create more pass for magnetic flux in the pole. The new pole width W is now 44 mm. The magnetic flux density of the widened pole is shown in Fig. A.3 and its value is 1.6 T which gives the same flux linkage as the pole indicated in Fig. A.2 a.

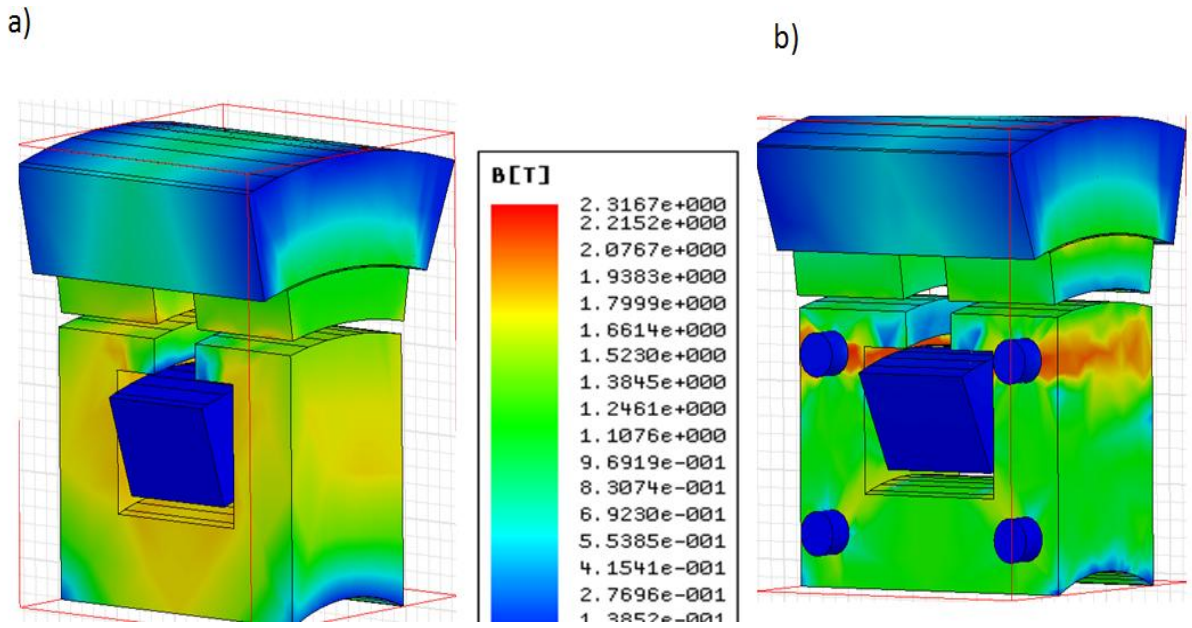

Figure B.2 Magnetic field density and flux linkage for: a) magnetic pole without bolts, b) magnetic pole with bolts

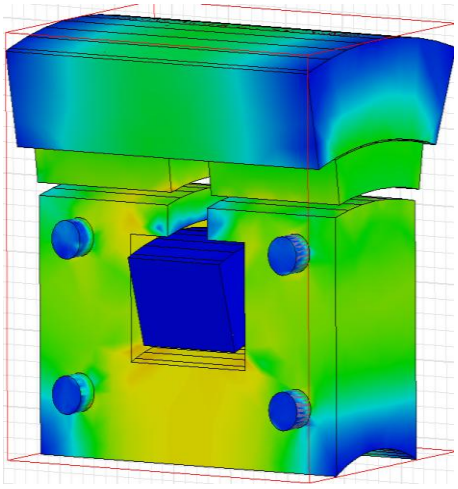

Figure B.3 Magnetic field density in the widened magnetic pole

APPENDIX C: M-FILE FOR CALCULATING LOAD RESISTANCE OF THE GENERATOR DISCUSSED IN CHAPTER 5

```
N=66;                          % Number of turns
p=16;                          % Number of poles
R=0.047;                       % Radius of the coil (m)
Nc=1;                          % Number of coils
Ls=0.0037;                     % Coil Inductance (H)
q=0.13;                        % Flux linkage of the generator with shunts(Wb*turns)
Ra=0.101;                      % Reisistance of the coil (Ohms)
n=600;                         % Rated speed (rpm)
Lc=2*pi*R;                     % Average lenght of the coil (m)
Ef=4.44*n.*p/120*q ;           % Induced voltage (V)
RL=0:12/100:12;                % Load resistance range (Ohms)
Xl=2*pi*n.*p/120*Ls;           % Inductive reactance (Ohms)
Z=sqrt((RL+Ra).^2+Xl^2);       % Impedance (Ohms)
Ia=Ef./Z;                      % Output current

CLF
figure(1)
plot (RL, Ia), xlabel ('Load resistance [Ohms]'), grid
ylabel ('Output current [A]')
```

APPENDIX D: M-FILE FOR CALCULATING STEADY-STATE CHARACTERISTICS OF THE GENERATOR DISCUSSED IN CHAPTER 5

```
N=66;                                % Number of turns
p=16;                                % Number of poles
R=0.047;                             % Radius of the coil (m)
Nc=1;                                % Number of coils
Ls=0.0037                            % Coil Inductance (H)
q=0.13;                              % Flux linkage of the generator with
shunts(Wb*turns)
q1=0.075                             % Flux linkage of the generator without shunts
(Wb*turns)
Ra=0.101;                            % Reisistance of the wire (Ohms)
RL=3.5;                              % Load resistance (Ohms)
Lc=2*pi*R;                           % Average lenght of the coil (m)
n=0:800/100:800;                     % Speed range (rpm)
Ef=4.44*n.*p/120*q ;                 % Induced voltage of the generator with shunts (V)
Ef1=4.44*n.*p/120*q1                 % Induced voltage of the generator without shunts
(V)
Xl=2*pi*n.*p/120*Ls;                 % Inductive reactance (Ohms)
Z=sqrt((RL+Ra)^2+Xl.^2)              % Impedance (Ohms)
Ia=Ef./Z;                            % Output current of the machine with shunts (A)
Ia1=Ef1./Z;                          % Output current of the machine without shunts (A)
Vph=Ia*RL;                           % Terminal voltage of the machine with shunts (V)
Vph1=Ia1*RL;                         % Terminal voltage of the machine without shunts
(V)
Pout=3*RL*Ia.^2                      % Output power of the generator with shunts (W)
Pout1=3*RL*Ia1.^2;                   % Output power of the generator without shunts (W)

CLF
figure(1)
plot(n,Pout, n, Pout1),xlabel('Speed [rpm]'), grid
ylabel('Output power [W]')
figure (2)
plot (n, Vph, n, Vph1), xlabel ('Speed [rpm]'), grid
ylabel('Terminal voltage [V]')
```

APPENDIX E: M-FILE FOR ANALYTICAL CALCULATION DIMENSIONS OF THE MACHINE DISCUSSED IN CHAPTER 5

```
% designing of transverse-flux generator
%Data
Sout=1200;          %output power (W)
Vp=60/sqrt(3);      %phase voltage (V)
n=600;              %rotary speed (rpm)
f=80;               %frequency (Hz)
p=120*f/n           %number of magnetic poles
Bav=0.9;            %average flux density in the air-gap (T)
Cm=0.9;             %coefficient for air-gap flux density: Cm=Bav/Bm
Bm=Bav/Cm;          %air-gap flux density under magnets (T)
g=0.0015;           %air-gap (m)
hM=input('permanent magnet thickness='), %permanent magnet thickness from B-H
curve =0.0061 m
BsFe=1.6;           %flux density in the stator core (T)
BrFe=1.2;           %flux density in the rotor core (T)
J=19000;            %current loading (linear current density of the stator (A/m)
Jw=4;               %wire current density (A/mm^2)
KE=0.87;            %KE=Vp/E
Kn=1;               %negative flux linkage coefficient
Km=0.8;             %ratio of axial stator pole width/total magnet width
Kcu=0.7;            %winding filling coefficient
bFe=0.004;          %width of the stator slot closing (m)

%calculation of the stator and core dimensions
DW2=Sout*60/(1.06*pi^2*p*n*Bav*J*Kn*KE); %active surface of the generator (m^2)
Do=input('stator ring outer diameter=') %mm
tau=Do*pi/p   %pole-pitch of the stator poles at outer diameter (mm)
Prin=tau*p/2        %stator inner periferry (mm)
Din=Prin/pi         %inner diameter of the stator (mm)
hs=(Do-Din)/2       %stator pole hight (mm)
W=sqrt(DW2/Din);  %stator ring width (mm)
W=input('width of stator ring W=')%(mm)
S=1.06*pi^2*p/2*n/60*Bav*J*Kn*KE*Din*W^2*10^-9  %power at actual stator
dimensions (W)
WM=Km*W/2           %magnet axial width (mm)
dsFe=Bav/BsFe*W/2 %width of the stator core (mm)
dc=W-2*dsFe         %width of the coil (mm)
drFe=Bav/BrFe*W/2 %thickness of the rotor core (mm)
Dor=Do+2*g*10^3+2*hM+2*drFe %outer rotor diameter (mm)

%calculation of the winding parameters
E=Vp/KE              %electromotive force (V)
N=E/(0.058*n*p/2*Din*W*Bav*Kn)*10^6  %number of coil turns
Np=input('The number of turns of coil N=')
Ep=0.058*n*p/2*Din*W*Bav*Np*Kn/10^6  %phase emf for given turn number (V)
I=Sout/3/Vp         %phase current (A)
Dw=2*sqrt(I/pi/Jw) %wire diameter (mm)
Dw=input('wire diameter Dw=')
Rwpkm=input('resistance per 1km Rw/m=')
Ac=pi*(0.001*Dw/2)^2*Np/Kcu*10^6  %coil cros-section area (mm^2)
hc=Ac/dc             %hight of the coil (mm)
```

```
hc=input('height of the coil hc=') %(mm)
hFe=bFe*1000+hc+dsFe %actual hight of the stator pole (mm)
Lc=pi*(Do-2*bFe*1000-hc)%average length of the coil (mm)
Rp=Rwpkm*0.001*Lc*Np %coil resistance (Ohms)
Sin=3*Ep*I           %input power (VA)

%summary of the motor parameters
%stator dimensions
Din_Do_p_tau_W_hFe_dsFe_bFe=[Din Do p tau W hFe dsFe bFe]

%Rotor dimensions
Dor_hM_WM_drFe_g=[Dor hM WM drFe g]

%Winding parameters
Np_Dw_hc_Kcu_Jw_Rp=[Np Dw hc Kcu Jw Rp]

%Electromechanical parameters
Sout_Sin_Vp_I_Ep_n_f=[Sout Sin Vp I Ep n f]
```

APPENDIX F: M-FILE FOR CALCULATION OF VOLTAGE HARMONIC CONTENT

```
X = Time;
Y = Voltage;
N = length(X*0.001);
delta_t = mean(diff(X*0.001));
f_max = 1/delta_t;              % max frequency (Sampling theory)

% frequency scale
f_scale = linspace(0,f_max/2,floor(N/2));
spectrum=fftn(Y)/(N)

subplot (2,1,1)
plot(X,Y)
xlabel('Time, ms')
ylabel('Voltage RMS, V')
subplot (2,1,2)
bar(f_scale,abs(spectrum(1:length(f_scale))));
xlabel('Harmonics')
ylabel('Voltage RMS, V')
```

APPENDIX G: M-FILE FOR PLOTTING GENERATOR CHARACTERISTICS IN DYNAMIC CONDITION

```
load torque Tem; load speed n; load in TwP;load voltage VE;load output Pout;load
input Pin;load Pelectrom Pem; load efficiency Eff
t=Tem(1,:);n=n(2,:);Pem=Pem(2,:);Pin=Pin(2,:);Pout=Pout(2,:);Tin=TwP(2,:);Ia=VE(4
,:);Vph=VE(3,:);Ef=VE(2,:);Eff=Eff(2,:);w=TwP(4,:);

CLF
figure (1)
plot(t,Pout, t, n, t, Tem*10),xlabel('time [s]'),
ylabel(' Pout [W], Tem [W], speed [rpm] '),grid

figure (2)
plot(t, Ef,t,Vph, t, Ia/10),xlabel('time [s]'),
ylabel(' Ef [V], Vph [V], Iph [A] '),grid
```

APPENDIX H: M-FILE FOR CALCULATING STEADY STATE CHARACTERISTICS OF THE MACHINE WITH DOUBLE STATOR DISCUSSED IN CHAPTER 6

```
N=132;                              % Number of turns
p=16;                               % Number of poles
R=0.047;                            % Radius of the coil (m)
Nc=1;                               % Number of coils
Ls=0.0037*2                         % Coil Inductance (H)
q=0.18;                             % Flux linkage of the inner coil (Wb*turns)
q1=0.15                             % Flux linkage of the outer coil (Wb*turns)
Rr=0.101;                           % Resistance of the wire (Ohms)
RL=7;                               % Load resistance (Ohms)
Lc=2*pi*R;                          % Average length of the coil (m)
Ra=Lc*N*Nc*Rr                       % Armature resistance (Ohms)
n=0:800/100:800;                    % Speed range (rpm)
Ef=4.44*n.*p/120*(q+q1);            % Induced voltage of the generator with shunts
(V)
Xl=2*pi*n.*p/120*Ls;                % Inductive reactance (Ohms)
Z=sqrt((RL+Ra)^2+Xl.^2)             % Impedance (Ohms)
Ia=Ef./Z;                           % Output current of the machine with shunts (A)
Vph=Ia*RL;                          % Terminal voltage of the machine with shunts
(V)
Pout=3*RL*Ia.^2                     % Output power of the generator with shunts (W)


figure(1)
plot(n,Pout), xlabel('Speed [rpm]'), grid
ylabel('Output power [W]')
figure (2)
plot (n, Vph), xlabel ('Speed [rpm]'), grid
ylabel('Terminal voltage [V]')
```

VITA

Dobzhanskyi Oleksandr, was born in Kiev (Ukraine) in July, 1985. He completed his schooling at Chernyatyn Secondary School.

He graduated with distinction from Kiev National University of Construction and Architecture with a degree of Master in Industrial Engineering in 2007. He joined the Department of Electrical and Computer Engineering at Louisiana State University in August 2009 to pursue his doctoral studies. He will be awarded the degree of Doctor of Philosophy in Electrical Engineering in May 2012.